Protein Engineering Studies on Structure and Function of Thermolysin, Matriptase, and Hepatocyte Growth Factor Activator Inhibitor Type 1

Kenji Kojima

2014

Contents

Abbreviations

BEK	bovine enterokinase
Boc	*t*-butyloxycarbonyl
CBB	Coomassie Brilliant Blue
CC	correlation coefficient
CD	circular dichroism
CHO	Chinese hamster ovary
CUB domain	complement factor 1R-urchin embryonic growth factor-bone morphogenetic protein domain
DA	degree of activation
EA	expression amount
FAAFA	*N*-[3-(2-furyl)acryloyl]-L-alanyl-L-phenylalanine amide
FAGLA	*N*-[3-(2-furyl)acryloyl]-glycyl-L-leucine amide
HAI-1	hepatocyte growth factor activator inhibitor type 1
HC	α-helix content
HEPES	2-[4-(2-hydroxyethyl)-1-piperazinyl] ethanesulfonic acid
HGF	hepatocyte growth factor
HRP	horseradish peroxidase
LDLRA domain	low-density lipoprotein receptor class A module domain
MCA	4-methylcoumaryl-7-amide
MT-SP1	membrane-type serine protease 1
PU	proteolytic unit
REA	relative expression amount

r-EK	recombinant enterokinase
RHC	relative α-helix content
sc-uPA	single-chain urokinase-type plasminogen activator
SDS-PAGE	sodium dodecyl sulfate polyacrylamide gel electrophoresis
SEA domain	sea-urchin sperm protein-enterokinase-agrin domain
Sp-tPA	spectrozyme tPA®
tc-uPA	two-chain urokinase-type plasminogen activator
Tris	tris(hydroxymethyl)aminomethane
ZDFM	*N*-carbobenzoxy-L-asparatyl-L-phenylalanine methyl ester

E_a	activation energy
IC_{50}	half maximal (50%) inhibitory concentration
k_{cat}	catalytic constant
k_{cat}/K_m	specificity constant
k_{off}	dissociation rate constant
k_{on}	association rate constant
K_i	inhibitor constant
K_m	Michaelis constant
T_{50}	temperature at which half of enzyme is inactivated

Introduction

Protein engineering method is widely applied in enzyme studies to generate novel enzymes and improve the properties of enzymes, such as optimal pH, substrate specificity, thermostability, pH-stability, and catalytic activity, using recombinant DNA technology. This method is also exploited to investigate structure-function relationships of enzymes and related protein inhibitors.

In this thesis, protein engineering method was applied to two proteases and a related protein inhibitor. One of the two proteases is matriptase, which is a serine protease expressed abundantly in epithelial cells and keratinocyte and plays a key role in the maintenance of epithelial integrity and homeostasis. The other is thermolysin, which is a metalloproteinase from *Bacillus thermoproteolyticus* and one of the most representative industrial enzymes. It has been widely utilized to synthesis of peptides such as a precursor of an artificial sweetener aspartame.

Matriptase (also known as membrane-type serine protease 1, epithin, suppression of tumorigenecity 14, *etc*.) is a type II transmembrane serine protease consisting of catalytic domain and non-catalytic stem domain (Fig. 1A) (*1*–*5*). This protease has trypsin-like activity, and is known to cleave to activate a variety of proteins, including single-chain urokinase-type plasminogen activator (sc-uPA) (*6*–*8*), pro-hepatocyte growth factor (HGF) (*7, 9*), and the precursor form of prostasin, a glycosyl-phosphatidylinositol-linked serine protease (*3, 10*). These characteristics, together with the abundant expression in surface-lining epithelial cells such as enterocytes (*8, 11*), lead to a proposal that matriptase is a key upstream regulator of the epithelial-cell turnover, including proliferation, migration, differentiation, and exfoliation. The activity

of matriptase is strictly regulated through the inhibition by a cognate Kunitz-type inhibitor, hepatocyte growth factor activator inhibitior type 1 (HAI-1).

HAI-1 is an epithelial-derived, serine protease inhibitor with multiple domains including two protease-inhibiting Kunitz domains (Fig. 1B) (*12, 13*). HAI-1 was isolated originally from the conditioned medium of a human stomach carcinoma MKN45 cell line as a potent inhibitor of HGF activator, a 53-kDa serine protease responsible for proteolytic activation of the inactive single chain precursor of HGF (pro-HGF) (*12, 14*). HAI-1 is believed to play a crucial role in growth factor-mediated biological processes such as tissue regeneration by counteracting the HGF activator activity (*13, 15*). The primary translation product of HAI-1 predicted from the cDNA sequence comprises 513 amino acid residues, including a putative N-terminal signal peptide sequence and a hydrophobic region at the C-terminal region. This suggests that HAI-1 is produced first as a type I membrane protein (*12*). Indeed, the transmembrane form of HAI-1, which has a molecular mass of 66 kDa, was detected in extracts of MKN45 cells (*16*) and monkey kidney COS-1 cells transiently transfected with a rat HAI-1 cDNA (*17*). The extracellular domain can be released by cleavage with certain proteases (*16*). At least two HAI-1 species of 58 and 40 kDa are found in conditioned media of MKN45cells (*12, 16*) and transfected COS-1 cells (*17*). The 58-kDa species (58-kDa HAI-1) has all of the HAI-1 extracellular region and comprises the N-terminal domain with eight cysteine residues, followed by the internal domain rich in acidic amino acid residues, the first Kunitz domain (Kunitz domain I), the low-density lipoprotein receptor A module (LDLRA)-like domain (LDLRA domain), and the second Kunitz domain (Kunitz domain II) (Fig. 1B). The 40-kDa species (40-kDa HAI-1) lacks Kunitz domain II (*16, 18*), but is thought to be responsible for inhibiting target proteases

in vivo because it exhibits higher inhibitory activity against HGF activator than does 58-kDa HAI-1 (*16, 18*). The ratio in the amounts of matriptase and HAI-1 has been shown to increase in late-stage tumors (*19, 20*). This imbalance might lead to the excessive activity of matriptase and would be significant for the development of advanced disease. Elucidation of the mechanism by which HAI-1 inhibits matriptase is considered important for obtaining strategy to retard cancer progression. In Chapter 1, the roles of the functional and structural domains of HAI-1 in the inhibition of matriptase were investigated by producing HAI-1 mutants made up with various combinations of domains and comparing their inhibitory activity against matriptase. In Chapter 2, the roles of the stem domain of matriptase in the interaction with HAI-1 were addressed by producing matriptase variants lacking the stem domain.

Thermolysin [EC 3.4.24.27] is a thermophilic and halophilic neutral metalloproteinase produced in the culture broth of *Bacillus thermoproteolyticus* (*21–23*). Its amino acid sequence (*24*) and crystal structures (*25–27*) have been determined. It has been widely utilized to synthesis of peptides such as a precursor of an artificial sweetener aspartame (*22, 23*), and thus is one of the most representative industrial enzymes. The improvement of its activity and stability are important subjects. In Chapter 3, to further stabilize thermolysin, the effect of the amino acid residue located at its C-terminal domain on the stability of thermolysin was examined by producing fourteen Val315 variants. In Chapter 4, to understand the structural determinants of substrate specificity of thermolysin, the role of the amino acid residue located in the S_1' subsite was examined by producing nineteen Leu202 variants.

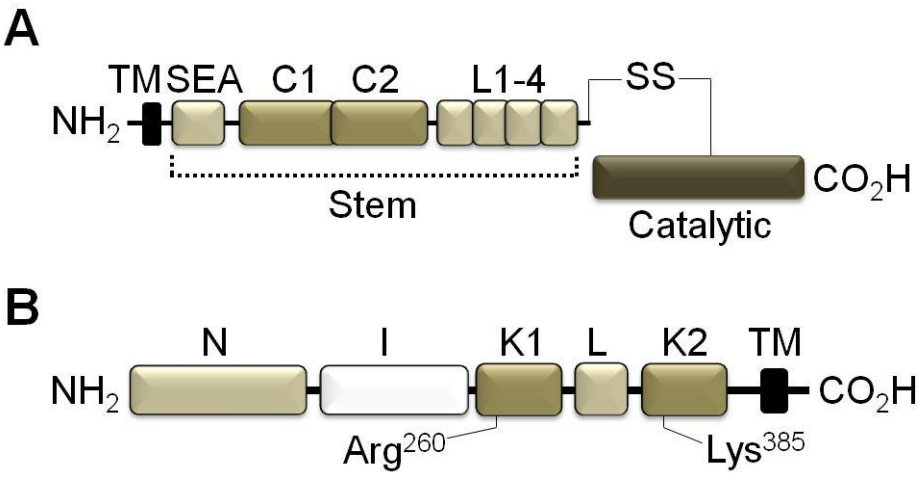

Fig. 1. Schematic domain structure of matriptase (A) and HAI-1 (B). TM, transmembrane domain; SEA, SEA domain; C1 and C2, the first and second CUB domain; L1–4, four LDLRA repeats; Stem, stem domain; Catalytic, catalytic domain; N, N-terminal domain; I, internal domain; K1, Kunitz domain I; L, LDLRA domain; K2, Kunitz domain II. The amino acid residues Arg^{260} and Lys^{385} are considered essential for the potential inhibitory activities of the respective Kunitz domains.

Chapter 1

Roles of Functional and Structural Domains of Hepatocyte Growth Factor Activator Inhibitor Type 1 in the Inhibition of Matriptase

Introduction

The primary translation product of HAI-1 predicted from the cDNA sequence comprises 513 amino acid residues, including a putative N-terminal signal peptide sequence and a hydrophobic region at the C-terminal region (Fig. 1A). This suggests that HAI-1 is produced first as a type I membrane protein (*12*). Indeed, the transmembrane form of HAI-1, which has a molecular mass of 66 kDa, was detected in extracts of MKN45 cells (*16*) and monkey kidney COS-1 cells transiently transfected with a rat HAI-1 cDNA (*17*). The extracellular domain can be released by cleavage with certain proteases (*16*). At least two HAI-1 species of 58 and 40 kDa are found in conditioned media of MKN45 cells (*12, 16*) and transfected COS-1 cells (*17*). The 58-kDa species (58-kDa HAI-1) has all of the HAI-1 extracellular region and comprises the N-terminal domain with eight cysteine residues, followed by the internal domain rich in acidic amino acid residues, the first Kunitz domain (Kunitz domain I), the low-density lipoprotein receptor A module (LDLRA)-like domain (LDLRA domain), and the second Kunitz domain (Kunitz domain II) (Fig. 1A). The 40-kDa species (40-kDa HAI-1) lacks Kunitz domain II, but is thought to be responsible for inhibiting target proteases *in vivo* because it exhibits higher inhibitory activity against HGF activator than does 58-kDa HAI-1 (*16, 18*).

Soluble HAI-1 species with molecular masses of 40 and 25 kDa are found as complexes with matriptase (also known as membrane-type serine protease 1 or MT-SP1) in biological fluids such as human milk (*28*). Matriptase is produced first as a membrane-bound form (type II transmembrane serine protease) (*29*), which comprises multiple domains in the extracellular region, including a trypsin-like serine protease domain at the C-terminus (Fig. 2A), and the ectodomain is then released by an unknown mechanism (*17, 28, 30*). This protease is expressed by epithelial elements of almost all organs examined so far (*8, 11*), and because it digests various potential substrates, including pro-HGF (*7, 9*) and single-chain urokinase-type plasminogen activator (sc-uPA) (*6–8*), is thought to play broad roles in the physiology of epithelial cells. The cellular sites of matriptase production are consistent with those of HAI-1 (*11, 13*). Importantly, matriptase activity is inhibited *in vitro* by HAI-1 (*9, 31*), but not (or poorly) by other endogenous serine protease inhibitors such as α1-antitrypsin (*32*). These observations suggest that HAI-1 functions as a physiological inhibitor of matriptase. The biological importance of the inhibition is supported by evidence showing that the ratio of matriptase to HAI-1 increases with increasing malignancy in cancers such as ovarian cancer (*19, 20*). This might be explained by overproduction of active HGF, two-chain uPA, and active matrix metalloproteinases, which are characteristic of malignant tissues (*33–37*). Furthermore, matriptase zymogen occurs in a single-chain form, and one zymogen molecule is converted into an active two-chain form by another zymogen molecule in an activation mechanism known as transactivation. This may allow matriptase to act as an initiator protease for cancer invasion and metastasis (*38*). Therefore, inhibition of matriptase activity by exogenous HAI-1 could be one strategy to retard cancer progression.

Little is known about the mechanism by which HAI-1 inhibits matriptase. Kirchhofer *et al.* (*9*) previously reported the existence of an alternative splicing variant of HAI-1 which contains an extra 16-amino acid sequence adjacent to the C-terminus of Kunitz domain I and designated it as HAI-1B. Using soluble HAI-1B mutants that comprise all extracellular region, they showed that Kunitz domain I but not Kunitz domain II is responsible for the inhibition of matriptase and HGF activator (*9*). However, there is a possibility that the availability of Kunitz domain II in HAI-1B for enzymatic inhibition is impaired because of the additional amino acid residues. Indeed, Kunitz domain II in 58-kDa HAI-1 inhibits HGF activator (*18*). Therefore, the ability of Kunitz domain II to inhibit matriptase is not understood fully. In addition, the occurrence of 25-kDa HAI-1 lacking the N-terminal domain in complex with matriptase in human milk suggests that the structural domains can also affect the inhibitory activity of HAI-1 against matriptase.

In this chapter, the roles of the functional and structural domains of HAI-1 in the inhibition of matriptase were exmained. For this, soluble recombinant rat HAI-1 mutants made of various combinations of domains were prepared, and their inhibitory activities against a soluble recombinant species of rat matriptase were characterized.

Materials and Methods

Materials – A Chinese hamster ovary cell line (CHO-K1) was obtained from Health Science Research Resources Bank (Osaka, Japan). All synthetic deoxyribonucleotides, pSecTag2/Hygro vector, and mouse anti-*Myc* epitope antibody conjugated with horseradish peroxidase (HRP) were purchased from Invitrogen

(Carlsbad, CA). PT7blue-2 vector, recombinant bovine enterokinase, immobilized S-protein, S-protein conjugated with HRP, and Perfect Protein Marker™ were purchased from Novagen (Madison, WI). Goat anti-rabbit IgG secondary antibody was from Dako Japan (Tokyo). Prestained protein markers (broad range) and restriction endonucleases were purchased from New England BioLabs (Beverly, MA). KOD_{-plus-}DNA polymerase used for polymerase chain reaction (PCR), T4 polynucleotide kinase, and a DNA ligation kit were from Toyobo (Osaka, Japan). Various peptidyl-4-methylcoumaryl-7-amide (MCA) substrates were purchased from Peptide Institute (Osaka, Japan). Spectrozyme tPA® (Sp-tPA, methylsulfonyl-D-cyclohexyltyrosyl-glycyl-arginine-*p*-nitroaniline acetate) was purchased from American Diagnostica (Stanford, CT), and bovine trypsin (type III) was from Sigma. All other reagents were of analytical grade and were purchased from Nacalai Tesque (Kyoto, Japan).

Construction of Expression Plasmids – Expression plasmids for the production of soluble recombinant rat HAI-1 mutants were created by a PCR-based technique with an expression plasmid containing the sequence of rat HAI-1 (Pro41–Leu513) with an S-tag at the N terminus in pSecTag2/Hygro B (designated as pSecHAI-1) as the template (the amino acid numbering of HAI-1 starts from the putative N terminus of the protein) (*17*). An expression plasmid ($pSecNIK^1LK^2$) for the production of a recombinant HAI-1 mutant designated HAI-1 NIK^1LK^2 (Pro41–Ser441) was constructed as follows. In the designation of the HAI-1 mutants, the abbreviations of the domains were placed according to their order in the mutants from the N terminus to C terminus (Fig. 1A). A DNA fragment amplified with 5′-TAATACGACTCACTATAGGGAGACC-3′ as a

forward primer and 5′-GCTCTAGAGCTTTCCCTCCGAAGA-3′ as a reverse primer was digested with KpnI and XbaI; and the resulting fragment was ligated into pSecHAI-1 in which the KpnI and XbaI fragment had been removed. Expression plasmids for the HAI-1 NIK^{1}L (Pro41–Ser370) and NIK^1 (Pro41–Ser307) mutants were made using the same method except that 5′-GCTCTAGAGAGGAAGTGGATACTCT-GAG-3′ and 5′-GCTCTAGAGATTCCTTTTACATCCTTGCA-3′, respectively, were used as reverse primers. Plasmids for the HAI-1 IK^{1}LK^2 (Thr154–Ser441), IK^{1}L (Thr154–Ser370), IK^1 (Thr154–Ser307), K^{1}LK^2 (Gln245–Ser441), K^{1}L (Gln245–Ser370), K^1 (Gln245–Ser307), and K^2 (Ser370–Ser441) mutants were made as follows. DNA fragments were amplified with appropriate forward primers phosphorylated at their 5′-ends, including 5′-AACTCGAGGCTTTGGAGGTTCC-3′, 5′-GCAGACGGAAGATTATTGC-3′, and 5′-CAGTGACAAAGGGTACTGT-3′, and with the appropriate reverse primers as described above. The PCR products were digested with XbaI, and the resulting fragments were ligated once into the PT7blue-2 vector predigested with SmaI and XbaI; fragments of these plasmids digested with KpnI and XbaI were ligated into pSecHAI-1 as described above. Plasmids for the HAI-1 NK^{1}LK^2 (Leu152–Ala243-truncated NIK^{1}LK^2) and NIK^{1}K^2 (Pro308–Ser370-truncated NIK^{1}LK^2) mutants were created with pSecNIK^{1}LK^2 as the template. To create pSecNK^{1}LK^2, forward primers used to create pSecK^{1}LK^2 and 5′-TCGCGGTAGGAGTTGTAAG-3′ were used as the forward and reverse primers, respectively. For pSecNIK^{1}K^2, forward primers for pSecK2 and 5′-ATTCCTTTTACATCCTTGCAGG-3′ were used as the forward and reverse primers, respectively. The amplified DNA fragments were self-ligated. Plasmids for the HAI-1 R260A, D349Y, and K385A mutants were made as follows. A restriction fragment of

pSecNIK^{1}LK^{2} produced by XhoI and XbaI was ligated into pBluescriptSK (Stratagene, La Jolla, CA) that had been predigested with the same sets of enzymes. Using this plasmid as the template, DNA fragments of about 3.8 kbp were amplified with the following sequences (the nucleotides underlined indicate the introduced mutations): 5′-CGGGCTCCTTCCCACCG-3′ and 5′-CGCAGCGGCCCACCTT-3′, 5′-ATGAGGC-CACTTGTGAAAAATATAG-3′ and 5′-AGGAGCCATCAGGGCA-3′, and 5′-CGGAG-AACATCCCACGCTG-3′ and 5′-CGCAAAATCCAGTGTCTGGCAG-3′ to introduce appropriate mutations. These PCR products were phosphorylated with T4 nucleotide kinase and then self-ligated. The plasmids were digested with XhoI and XbaI, and the resulting fragments were ligated into pSecNIK^{1}LK^{2} from which the XhoI and XbaI fragment had been removed.

Establishment of Stable Clones for the Production of Soluble Recombinant Rat Matriptase and Its Purification and Activation – CHO-K1 cells were maintained in Ham's F12 medium containing 5% fetal bovine serum. An expression plasmid, designated as pSec-ekMT-SP1s, for the production of soluble recombinant rat pro-matriptase (Fig. 2A) (*32*) was transfected into the cell line using Lipofectamine 2000^{TM} (Invitrogen) (*17*). Clones resistant to Ham's F12 medium containing 400 μg/ml hygromycin B were obtained, and the expression level in the conditioned media by each clone was determined by Western blotting using S-protein conjugated with HRP as the probe. T3245, a clone with the highest expression of soluble recombinant pro-matriptase, was propagated and stored in liquid nitrogen until use. Aliquots of the frozen cells were thawed and cultured in 75-cm^{2} flasks until reaching confluence. Cells were washed three times with ice-cold phosphate-buffered saline (8 mM Na_2HPO_4, 1.5

mM KH_2PO_4, 136 mM NaCl, and 2.7 mM KCl, pH 7.4), and 10 ml of serum-free Ham's F12 was added to each flask. After 48 h, the conditioned medium was collected, and fresh serum-free medium was added. This was repeated until half of the cells were peeled off. The collected media were centrifuged immediately at 3,000 × *g* for 10 min at 4°C, and the resulting supernatants were stored at –70°C until use. The conditioned medium was concentrated by ultrafiltration (Amicon® Ultra-15, 50,000 MWCO, Millipore, Cork, Ireland), and then desalted by gel filration on a PD-10 column. The samples were diluted with 25 mM HEPES buffer (pH 7.5) containing 145 mM NaCl and 0.1% Triton X-100 (hereinafter, called HEPES buffer) and S-protein agarose resin (Novagen) was added and incubated at room temperature on an orbital shaker for 30 min. Resin was washed with HEPES buffer for three times and recombinant matriptase was eluted and activated by adding 3.4 units/ml of recombinant enterokinase. The concentration of the activated form of recombinant matriptase was determined as described previously (*17*). Briefly, a part of the activated recombinant matriptase was incubated with 500 μM of *t*-butyloxycarbonyl (Boc)–L-Gln–L-Ala–L-Arg–MCA in HEPES buffer for 10 min at 37°C in a final volume of 80 μl. The reaction was terminated by adding 350 μl of 0.1 M sodium acetate buffer, pH 4.0, containing 100 mM monochloroacetic acid, and the absorbance at 370 nm was measured. The hydrolysis of other peptidyl-MCA substrates by recombinant matriptase was measured as described above.

Production of HAI-1 Mutants Using CHO-K1 Cells – CHO-K1 cells transfected with an expression plasmid for the production of the HAI-1 K^2 and R260 mutants were cultured in Ham's F12 medium containing 5% fetal bovine serum and 400 μg/ml

hygromycin B. The cells resistant to the antibiotic were pooled, propagated, and stored. The procedures for harvest of conditioned media (serum-free media), concentrating the media, and gel filtration in HEPES buffer were the same as used in the production of recombinant matriptase.

Production of HAI-1 Mutants in COS-1 Cells – COS-1 monkey kidney cells were transfected with the plasmid by Lipofectamin 2000™. The transfected cells were cultured in Dulbecco's modified Eagle Medium with 10% fetal calf serum for 36 h (*8*, *32*). The procedures for transient expression in COS-1 cells, harvest of conditioned media (serum-free media), and gel filtration in HEPES buffer were were the same as used in the production of recombinant matriptase (*17*).

Preparation of HAI-1 Mutants and Determination of Their Concentrations – Preparation of HAI-1 mutants from gel filtrates was performed using Ni^{2+}-charged resin (HisLink™ resin, Promega, Madison, WI) (*17*). Because of possible occurrence of cleavage between Kunitz domain I and Kunitz domain II during production in COS-1 cells (*32*), HAI-1 $NIK^{1}LK^{2}$ was subsequently treated with an immobilized S-protein. The HAI-1 mutant bound to the immobilized S-protein was eluted with 0.2 M sodium citrate buffer, pH 2.0, and the eluate was immediately neutralized with 2 M Tris solution. All HAI-1 mutants were subjected finally to gel filtration in HEPES buffer. Various amounts of HAI-1 mutants and Perfect Protein Marker™ protein size marker, in which each protein is fused to an S-tag and the concentration of each marker was known, were subjected to sodium dodecyl sulfate polyacrylamide gel electrophoresis (SDS-PAGE) followed by Western transfer. The blots were probed with S-protein conjugated with

HRP. The x-ray films were scanned digitally, and the signal intensities of protein bands were analyzed by densitometry (*17*). The concentrations of the HAI-1 NIK^{1}LK^2, NIK^{1}L, IK^{1}LK^2, NK^{1}LK^2, NIK^{1}K^2, R260A, D349Y, and K385A mutants were calculated by comparing the signal density of the bands of interest with the 50-kDa protein contained in the protein marker. The HAI-1 NIK^1, IK^{1}L, and K^{1}LK^2 mutants were compared with the 35-kDa protein, the HAI-1 IK^1 and K^{1}L mutants with the 25-kDa protein, and the HAI-1 K^1 and K^2 mutants with the 15-kDa protein (Fig. 1C).

Kinetic Studies with the Chromogenic Substrate, Sp-tPA – All enzyme and inhibitor assays using Sp-tPA were carried out in HEPES buffer at 25°C in a final volume of 100 μl in 96-well plates. Sp-tPA was dissolved in the same buffer just before each experiment. In steady-state kinetic studies, various concentrations of HAI-1 mutants were preincubated for 2 h in the assay mixture (90 μl) containing 0.12 nM recombinant matriptase. After the preincubation, hydrolysis was initiated by adding 10 μl of 5 mM Sp-tPA (500 μM) to the assay solution. The hydrolysis was followed by monitoring the increase in absorbance at 405 nm resulting from the liberation of the product *p*-nitroaniline at 30 s^{-1} intervals for 20 min with a plate reader (Powerscan HT, Dainippon Pharmaceutical, Tokyo, Japan). The initial rate of hydrolysis was determined using the molar absorption coefficient ε_{405} of 9,650 M^{-1} cm^{-1} for *p*-nitroaniline. Inhibition of trypsin (0.05 nM) by HAI-1 NIK^{1}LK^2, K^2, and R260A mutants was analyzed under the same conditions. In pre-steady-state kinetic studies, various concentrations of the HAI-1 mutants were incubated for 5 min in the assay mixture (90 μl) containing 555 μM Sp-tPA, and the hydrolysis was initiated by adding 10 μl of 1.2 nM recombinant matriptase (0.12 nM). The kinetic analysis was also performed with

various concentrations of Sp-tPA at a fixed concentration of the HAI-1 mutants. Absorbance at 405 nm was monitored at 30 s^{-1} intervals for 90 min with a plate reader, and the rate of hydrolysis was determined, as described above.

Analysis of Progress Curves – The apparent first-order rate constant (k_{obs}) for the transition of the initial rate (v_0) to the steady-state rate (v_s) observed in the matriptase-catalyzed hydrolysis of Sp-tPA in the presence of the HAI-1 mutants was determined by nonlinear regression analysis of the progress curve using Equation 1 (*39, 40*),

$$[P] = v_s t + (v_0 - v_s)[1 - \exp(-k_{obs} t)] / k_{obs} \qquad \text{(Eq. 1)}$$

where [P] is the concentration of *p*-nitroaniline at time *t*, v_s is the reaction rate at the steady state, and v_0 is the initial reaction rate. The values of k_{obs}, v_s, and v_0 were determined by fitting the progress curve to the theoretical curve using Equation 1 with the aid of commercially available software (KaleidaGraph, Synergy Software, Reading, PA). Equations 2 and 3 (*39–41*) can be used to calculate the rate constant (k_{on}) for association of the enzyme and inhibitor, the rate constant (k_{off}) for dissociation of the enzyme-inhibitor complex, and dissociation constant of the complex or the inhibitor constant (K_i) when k_{obs} increases linearly with increases inhibitor concentration and diminishes hyperbolically with increasing substrate concentration,

$$k_{obs} = k_{off} + k_{on}[I]/(1 + [S]/K_m) \qquad \text{(Eq. 2)}$$

$$K_i = k_{off} / k_{on} \qquad \text{(Eq. 3)}$$

where [I] and [S] are the concentrations of the inhibitor and substrate, respectively, and K_m is the Michaelis constant. K_m for Sp-tPA was determined separately by fitting the initial rate data to the Michaelis-Menten equation. The value of k_{off} can also be calculated using Equation 4 (*41, 42*) as follows.

$$k_{off} = k_{obs} v_s / v_0 \qquad \text{(Eq. 4)}$$

Binding of Recombinant Matriptase to the Immobilized HAI-1 Mutants – One hundred pmol of the HAI-1 K^1, K^2, R260A, or K385A mutants dissolved in 200 μl of HEPES buffer was retreated with a 20-μl slurry of Ni^{2+}-charged resin in a microcentrifuge tube as described previously (*17*). The resin was washed several times with buffer, and 1 pmol of recombinant matriptase dissolved in 300 μl of the buffer was added. The mixture was incubated for 2 h at 25°C with rocking. The proteins bound to the resin were eluted by boiling and analyzed by SDS-PAGE and Western blotting with Spr992 or anti-*Myc* antibody as described previously (*17*).

Statistical Analysis – Differences in the k_{on} and k_{off} values between any two HAI-1 mutants were determined by the two-tailed unpaired Student's *t*-test using Instat statistical software (GraphPad, San Diego, CA), $p < 0.05$ was considered significant.

Results

Design of the HAI-1 Mutants – The domain structures of the HAI-1 mutants produced in this study are illustrated in Fig. 1A. The largest HAI-1 mutant, NIK^1LK^2,

comprises the N-terminal domain, internal domain, Kunitz domain I, LDLRA domain, and Kunitz domain II. This mutant corresponds to 58-kDa HAI-1 released into the conditioned medium of the cultured cells (*12, 16, 17*). To examine the roles of the structural domains and functional domains in the inhibition of matriptase, deletion mutants were produced and designated according to the domains comprised. For instance, the role of the N-terminal domain in matriptase inhibition could be predicted by comparing kinetic parameters between HAI-1 NIK^1LK^2 and IK^1LK^2. Three HAI-1 mutants were produced by site-directed mutagenesis in the context of HAI-1 NIK^1LK^2, which were designated HAI-1 R260A, D349Y, and K385A. HAI-1 R260A and K385A are mutants in which Arg260 (in Kunitz domain I) and Lys385 (in Kunitz domain II) are replaced with Ala (*9, 18*). These residues are considered essential for the potential inhibitory activities of the respective Kunitz domains, so these mutants are expected to be impaired with respect to the inhibitory activities of Kunitz domains I and II, respectively. The HAI-1 R260A and K385A mutants may be useful for examining the ability of all HAI-1 domains to bind with and inhibit matriptase. In HAI-1 D349Y, Asp349 (in the LDLRA domain) is replaced with Tyr. This position of HAI-1 corresponds to the Asp206 residue in the fifth LDLRA domain of the LDL receptor (*43, 44*). Replacing Asp206 in the LDL receptor with Tyr strongly inhibits the binding of LDL to the receptor (*45*). Accordingly, the mutation in the LDLRA domain of HAI-1 might affect the interaction of HAI-1 with matriptase. All HAI-1 mutants were produced as fusion proteins with an S-tag at their N termini. The fusion proteins were convenient for purification of the resin-immobilized S-protein and for measuring their concentrations using HRP conjugated S-protein. The HAI-1 mutants were also fused to

the *Myc* epitope and hexahistidine tag at their C termini for convenient detection with an anti-*Myc* antibody and for purification with Ni^{2+}-charged resin.

Characterization of the HAI-1 Mutants Produced in COS-1 or CHO-K1 Cells – In this study, HAI-1 mutants except for HAI-1 K^2 and R260A were produced by a transient expression system using COS-1 cells. The cell line secreted at least 10 μg of the respective HAI-1 mutants into the cultivation medium for 2 weeks. Because HAI-1 K^2 and R260A mutants were produced poorly in the COS-1 system, we prepared them in a stable expression system using CHO-K1 cells.

All HAI-1 mutants were prepared from the conditioned media by means of single-step affinity chromatography using Ni^{2+}-charged resin. An unidentified protein with a mass of 40 kDa was mostly evident in each HAI-1 mutant preparation using this resin (the silver staining result of HAI-1 NIK^1LK^2 is shown in Fig. 1B, lane 1). Subsequent treatment of the HAI-1 NIK^1LK^2 preparation with an immobilized S-protein resulted in the removal of this and other minor contaminating proteins (a 59-kDa band of HAI-1 NIK^1LK^2 is only visible) (Fig. 1B, lane 2). Preliminary experiments revealed that there was no difference in the inhibitory activities against matriptase between an aliquot of the HAI-1 NIK^1LK^2 preparation using Ni^{2+}-charged resin alone and that using Ni^{2+}-charged resin and immobilized S-protein. The contaminating proteins included if any in the preparation with Ni^{2+}-charged resin alone could neither affect the enzyme-inhibitor interaction nor hydrolyze Sp-tPA. Because of the low recovery of HAI-1 NIK^1LK^2 and the other mutants after treatment with the immobilized S-protein, the preparations with Ni^{2+}-charged resin alone were used for the kinetic studies.

SDS-PAGE and Western blotting with the S-protein conjugated with HRP were also performed to confirm the absence of degraded products in the preparations and to measure the concentrations of the HAI-1 mutants (Fig. 1C). The preparations of HAI-1 mutants produced signals at the following positions: HAI-1 NIK^1LK^2, 59 kDa; NIK^1L, 46 kDa; NIK^1, 41 kDa; IK^1LK^2, 47 kDa; IK^1L, 38 kDa; IK^1, 26 kDa; K^1L, 22 kDa; K^1, 16 kDa; K^2, 17 kDa; NK^1LK^2, 45 kDa; NIK^1K^2, 49 kDa; R260A, 59 kDa; D349Y, 59 kDa; and K385A, 59 kDa. The HAI-1 K^1LK^2 preparation gave a signal at the position of 34 kDa with an extra 80-kDa band. Similar results were obtained when the blots were probed with anti-*Myc* antibody (the Western blot results of HAI-1 K^1, K^2, R260A, and K385A are shown in Fig. 4, bottom panel). When the mass of a sugar chain on the Asn235 residue in internal domain (5 kDa) was taken into consideration, the sizes of the respective HAI-1 mutants evaluated from SDS-PAGE were similar to the calculated masses. This indicates the absence of degraded products in each HAI-1 preparation. The absence of degraded products in the NIK^1LK^2 preparation also suggests that an HAI-1 species of 40 kDa found in the conditioned media of transfected COS-1 cells (*17*) is generated from the membrane-bound HAI-1 but not from 58-kDa HAI-1 (*16, 18*).

It was confirmed that the N- and C-terminal tags do not affect the inhibitory activities of the HAI-1 mutants. The IC_{50} value for the inhibitory activity of HAI-1 NIK^1LK^2 against trypsin is 1.5 nM, which is similar to that of 58-kDa HAI-1 purified from the conditioned medium of MKN45 cells (*18*).

Characterization of Soluble Recombinant Matriptase Produced in CHO-K1 Cells – A secreted soluble form of recombinant rat pro-matriptase has been produced using COS-1 cells (*32*). This recombinant protein is cleaved artificially *in vitro* before Val615

by recombinant enterokinase to form a disulfide-linked form (Fig. 2A). This disulfide-linked form exhibits proteolytic activity, and the activity agreed with that of soluble matriptase purified from human milk (*7, 32*). A stable CHO-K1 cell line that strongly expresses the soluble form of recombinant pro-matriptase was raised, and the procedures for its purification and activation were established. The expression product was analyzed on Western blots probed with an antibody designated Spr992 (*17*). The antibody recognizes the serine protease domain of rat matriptase (Val615–Val855) that migrates at the position corresponding to 28 kDa on SDS-PAGE under reducing conditions (*8, 17*). The recombinant matriptase produced in CHO-K1 cells produced signals at 95 kDa and 28 kDa before and after recombinant enterokinase treatment, respectively (Fig. 2B). The recombinant matriptase after recombinant enterokinase treatment hydrolyzed peptidyl-MCA substrates having an Arg residue at the P_1 position. The order of the substrates from the highest to lowest activity was Boc-L-Gln-L-Ala-L-Arg-MCA, Boc-benzyl-L-Asp-L-Pro-L-Arg-MCA, Boc-benzyl-L-Glu-L-Ala-L-Arg-MCA, Boc-benzyl-L-Glu-Gly-L-Arg-MCA, Boc-L-Leu-Gly-L-Arg-MCA, Boc-L-Phe-L-Ser-L-Arg-MCA, and Boc-L-Val-L-Pro-L-Arg-MCA. The relative activity for these substrates was similar to that of the recombinant matriptase preparation produced in COS-1 cells (*32*). The K_m value of recombinant matriptase for Sp-tPA substrate (*30*) was determined to be 221 ± 40 μM (mean ± S.D. of triplicate sample) by an initial rate method.

Steady-state Kinetic Analysis – The HAI-1 mutants except for HAI-1 K^2 and R260A inhibited the recombinant matriptase catalyzed hydrolysis of Sp-tPA substrate, and the steady-state kinetic studies were done to overview their inhibitory activities.

The order of their inhibitory activities evaluated by the IC_{50} values was HAI-1 IK^1L (IC_{50} = 0.065 nM) > D349Y (0.18 nM) > NIK^1 (0.23 nM) = IK^1LK^2 (0.25 nM) > NIK^1L (0.32 nM) = IK^1 (0.32 nM) > K^1LK^2 (0.52 nM) > K^1L (0.65 nM) > NIK^1K^2 (0.75 nM) > K385A (1.2 nM) > NIK^1LK^2 (1.5 nM) = K^1 (1.6 nM) > NK^1LK^2 (16 nM). The steady-state fractional rates (v_i/v, where v_i and v are the initial reaction rates in the presence and absence of the HAI-1 mutant, respectively) of the representative HAI-1 mutants, NIK^1LK^2, NIK^1L, IK^1L, and R260A, were plotted against their concentrations (Fig. 3). Mixing recombinant matriptase with these HAI-1 mutants inhibited matriptase activity strongly at the inhibitor concentration equal to that of the enzyme. Thus, these HAI-1 mutants appear to be tight binding inhibitors. In contrast, the lack of inhibitory activity of HAI-1 K^2 and R260A may not arise from their misfolding because they inhibited trypsin with IC_{50} values of 0.25 and 4.0 nM, respectively. Consequently, Kunitz domain I must be solely responsible for the matriptase inhibition by HAI-1, but Kunitz domain II is not directly involved in the inhibition.

Involvement of Kunitz Domain I in the Interaction of HAI-1 with Matriptase –The author examined whether the contribution of domains other than Kunitz domain I to the matriptase inhibition by HAI-1. Recombinant matriptase was precipitated with the respective resins attached to HAI-1 K385A and K^1, but it did not precipitate with resins attached to HAI-1 R260A and K^2 (Fig. 4). No serious degradation of these HAI-1 mutants was observed (Fig. 4), suggesting that no domains other than Kunitz domain I interact with matriptase and that Arg260 in Kunitz domain I is critical for both the inhibition and interaction.

Pre-steady-state Kinetic Analysis – Pre-steady-state kinetics for the interaction of recombinant matriptase with HAI-1 mutants was examined by measuring the inhibition of the matriptase-catalyzed hydrolysis of Sp-tPA. The hydrolysis was initiated by the addition of enzyme to a mixture of the HAI-1 mutant and substrate. The kinetic parameters, the association rate constants (k_{on}) of recombinant matriptase with the HAI-1 mutants, the dissociation rate constant (k_{off}) of the matriptase-HAI-1 mutant complexes, and the inhibitor constants (K_i) of the HAI-1 mutants for the inhibition of matriptase were determined (Table 1). Preliminary experiments revealed that the HAI-1 K^2, NK^1LK^2, and R260A mutants showed no inhibition under the conditions examined.

Progress curves for the recombinant matriptase-catalyzed hydrolysis of Sp-tPA in the presence of increasing concentrations of the HAI-1 NIK^1LK^2 and IK^1L mutants are shown in Fig. 5A. The degree of inhibition increased in a manner related to the reaction time and inhibitor concentration. Nonlinear regression analysis of the curves using Equation 1 revealed that k_{obs} increased linearly with increasing concentrations of HAI-1 NIK^1LK^2 or IK^1L (Fig. 5B). k_{obs} diminished hyperbolically with increasing Sp-tPA concentration at fixed concentrations of HAI-1 NIK^1LK^2 and IK^1L (Fig. 5C), indicating that the interaction of these two HAI-1 mutants with recombinant matriptase is competitive with respect to the substrate (*41*). All the other HAI-1 mutants that exhibited inhibitory activity also showed reaction time- and inhibitor concentration-dependent competitive inhibition (data not shown). Therefore, the k_{on} values for the interaction of recombinant matriptase with the HAI-1 mutants can be determined according to Equation 2. In contrast, the intercepts on the vertical axis in the plots of k_{obs} *versus* [HAI-1 mutant] for all HAI-1 mutants examined were too small to estimate the k_{off} values correctly (Fig. 5B). Instead, the k_{off} values were calculated

according to Equation 4. Linear correlation analysis revealed that the order of the inhibitory activities of HAI-1 mutants (which are expressed by the $1/K_i$ values determined according to Equation 3) were consistent with that under steady-state conditions (p = 0.0002, r = 0.874). This strongly suggests the validity of the k_{off} values determined by Equation 4. The kinetic parameters for the interaction of recombinant matriptase with HAI-1 mutants are summarized in Table 1. It is noteworthy that the inhibitory activity assessed by $1/K_i$ of HAI-1 IK[1]L is 400 times higher than that of HAI-1 NIK[1]LK[2], whereas the inhibitory activity of HAI-1 K[1] is similar to that of HAI-1 NIK[1]LK[2]. Table 1 also shows that any two HAI-1 mutants with similar inhibitory activity do not necessarily give similar k_{on} and k_{off} values. For instance, the K_i values of HAI-1 NIK[1]L and IK[1] are similar, but their k_{on} and k_{off} values differ considerably.

Roles of N-terminal Domain, Internal Domain, LDLRA Domain, and Kunitz Domain II in the Inhibition of Matriptase – The k_{on}, k_{off}, and K_i values (Table 1) were compared between any two HAI-1 mutants to evaluate the roles of the respective domains. The differences in these values, described below, were significant.

The k_{on} value was 6.6 times higher in HAI-1 NIK[1]L than in HAI-1 NIK[1]LK[2], whereas k_{off} was similar in HAI-1 NIK[1]L and NIK[1]LK[2], suggesting that Kunitz domain II decreases the rate of association between Kunitz domain I and matriptase. Lys385 is unlikely to be essential for the effect of Kunitz domain II because there was no difference in the k_{on} values between HAI-1 K385A and NIK[1]LK[2]. In the absence of the N-terminal domain, the deletion effect of Kunitz domain II was still observed, although slightly weaker. The k_{on} value was 3.4 times higher in HAI-1 IK[1]L than in HAI-1 IK[1]LK[2]. In the absence of both the N-terminal and internal domains, the deletion effect

of Kunitz domain II was not so evident, and the k_{on} was 2.6 times higher in HAI-1 K^1L than in HAI-1 K^1LK^2.

The k_{on} value was 18 times higher in HAI-1 IK^1LK^2 than in HAI-1 NIK^1LK^2, whereas their k_{off} values were similar, suggesting that the N-terminal domain as well as Kunitz domain II decreases the association rate without affecting the dissociation rate. In the absence of Kunitz domain II, the deletion effect of the N-terminal domain was still observed, although weaker, and the k_{on} was 9.4 times higher in HAI-1 IK^1L than in HAI-1 NIK^1L. In the absence of the LDLRA domain and Kunitz domain II, the N-terminal domain did not severely decrease the association rate, and the difference in k_{on} between HAI-1 NIK^1 and IK^1 was only 2.2 times.

The k_{on} values of HAI-1 IK^1LK^2, IK^1L, and IK^1 were 4.0, 5.3, and 4.7 times higher than those of HAI-1 K^1LK^2, K^1L, and K^1, respectively. The k_{off} was 4.9 times lower in HAI-1 IK^1L than in K^1L, and 1.6 times lower in HAI-1 IK^1 than in K^1. These results suggest that the internal domain increase the rate of association between Kunitz domain I and matriptase, and decreases the dissociation rate of the Kunitz domain I-matriptase contact in the enzyme-inhibitor complex. These association and dissociation rates show that the internal domain contributes to the stability of the interaction between Kunitz domain I and matriptase. However, the k_{off} values did not differ between HAI-1 K^1LK^2 and IK^1LK^2, indicating that the internal domain decreases effectively the dissociation of the Kunitz domain I-matriptase complex only in the absence of Kunitz domain II.

The k_{on} values were 10 times higher in HAI-1 NIK^1K^2 and 4.9 times higher in D349Y than in HAI-1 NIK^1LK^2. The k_{on} value was 3.3 times higher in HAI-1 NIK^1 than in HAI-1 NIK^1L. This shows that the LDLRA domain decreases the association rate between Kunitz domain I and matriptase, and that Asp349 in the LDLRA domain is

critical to this effect. However, the k_{on} value was similar in HAI-1 K^1L and K^1, suggesting that the LDLRA domain exhibits its effect only when it is accompanied by the N-terminal domain or Kunitz domain II. The k_{off} values were 3.3 times lower in HAI-1 NIK^1L than in HAI-1 NIK^1, 17 times lower in IK^1L than in IK^1, and 6.3 times lower in K^1L than in K^1. These results suggest that the LDLRA domain decreases the dissociation rate of the Kunitz domain I-matriptase complex and that the effect of the LDLRA domain is maximized when the domain is accompanied by the internal domain in the absence of the N-terminal domain and Kunitz domain II.

Discussion

Slow- and Tight-Binding Inhibition of HAI-1 – The HAI-1 mutants exhibited time-dependent inhibition of matriptase (Fig. 5A), and some of them, such as HAI-1 IK^1L, interacted very tightly with the enzyme (Fig. 3). Some Kunitz-type inhibitors interact with their target proteases in a time-dependent manner. Tissue factor protease inhibitor, an anti-factor Xa, is one type of such inhibitors, and acts through a mechanism involving the rapid interaction between the inhibitor and enzyme to form an initial collision complex with a low affinity, followed by a slow isomerization to a tightened enzyme-inhibitor complex (*41, 46*). In such cases, the plots of k_{obs} *versus* [I] give hyperbolic curves, and this type of inhibitors is defined as a slow-binding inhibitor. In the interaction of recombinant matriptase with HAI-1 mutants, however, the plots of k_{obs} *versus* [I] were linear, although the kinetics of inhibition was slow in all cases examined (Fig. 5B). No evidence supporting the formation of an initial low-affinity complex was observed. Such time-dependent reactions have been described in the inhibition of blood

coagulation factors XIa and Xa by protease nexin-2 and a tick anticoagulant peptide, respectively, each of which has a Kunitz-like domain (*47*, *48*). The physiological significance of the time-dependent binding process of protease inhibitors is unclear. Matriptase and HAI-1 might be coexpressed in tissues (*11*, *13*). If so, the enzyme is hardly active if the inhibitor binds with the enzyme rapidly to form the tight and stable complex. On the other hand, prolonged matriptase activity might be harmful to the cells (*49*). Therefore, the time-dependent process associated with the binding between matriptase and HAI-1 may allow the enzyme to be active temporarily.

The Role of Kunitz Domains of HAI-1 – The precise roles of the Kunitz domains in the matriptase inhibition remain to be determined (*9*). This study demonstrated that Kunitz domain I has inhibitory activity against the enzyme, but Kunitz domain II does not. The inhibitory activity of the Kunitz domains is characterized by their sequences from the P_4 to P_1 positions in the protease-binding site. The sequences of Kunitz domains I and II are Gly-Arg-Cys-Arg260 and Gly-Phe-Cys-Lys385, respectively. Kunitz domain I is preferred by matriptase (*6*). Another important finding regarding Kunitz domain II is that the deletion of the domain from HAI-1 NIK^1LK^2 enhanced the rate of association between Kunitz domain I and the enzyme. Kunitz domain II may obstruct the protease-binding site of Kunitz domain I (Fig. 6). This idea is supported by the observation that HGF activator binding of each Kunitz domain is affected by the presence of other Kunitz domain (*18*). Because Kunitz domain II has inhibitory activity against HGF activator and trypsin (*18*), the occurrence of soluble HAI-1 species lacking Kunitz domain II may be more important for the inhibition of matriptase than for that of HGF activator (*12*, *17*, *18*, *28*).

The Role of N-terminal Domain of HAI-1 – The deletion of the N-terminal domain, like that of Kunitz domain II, increased the association rate between Kunitz domain I and matriptase. Because the N-terminal domain does not bind specifically to matriptase (Fig. 4), this effect of the N-terminal domain may also be caused by obstruction of the protease-binding site of Kunitz domain I (Fig. 6). A synergistic effect was observed when both N-terminal domain and Kunitz domain II were deleted: the k_{on} values were 18 and 6.6 times higher in HAI-1 IK^1LK^2 and NIK^1L than in HAI-1 NIK^1LK^2, respectively, and the values were 62 times higher in HAI-1 IK^1L than in HAI-1 NIK^1LK^2. This suggests that the N-terminal domain and Kunitz domain II act cooperatively to obstruct enzyme activity (Fig. 6). It is suggested that 58-kDa HAI-1 may not inhibit matriptase *in vivo* because the corresponding HAI-1 mutant NIK^1LK^2 had low inhibitor activity (Table 1). This suggestion is supported by the fact that 58-kDa HAI-1 is not found as a complex with the enzyme in human milk. Thus, the 40- and 25-kDa HAI-1 species may be responsible for the matriptase inhibition *in vivo*.

The Role of Internal Domain of HAI-1 – No reports have described the occurrence of HAI-1 variants lacking the internal domain, which suggests the importance of the domain. The effect of the internal domain on the inhibitory activities of HAI-1 IK^1LK^2, IK^1L, and IK^1 was examined. The internal domain increased the association rate k_{on}, suggesting that the domain improves the availability of Kunitz domain I for the enzyme inhibition. Unexpectedly, however, HAI-1 NK^1LK^2 showed inhibitory activity too weak to evaluate the k_{on} value, and this result cannot be accounted for only by the lack of this putative effect of the internal domain. The most probable explanation is that the N-terminal domain moves closer to Kunitz domain I by the deletion of the internal

domain, thereby severely suppressing the association between Kunitz domain I and the enzyme.

The Role of LDLRA Domain of HAI-1 – The cysteine-rich LDLRA domain is about 40 amino acids, is biologically ubiquitous, and is found in more than 100 proteins. This domain is thought to be involved in protein-protein interaction (*50*). However, no apparent role of the LDLRA domain has been implicated in the inhibition of HGF activator and trypsin by HAI-1 (*18*). Dual effects of this domain on the matriptase inhibition were found; the domain decreased both the association rate and the dissociation rate. A crystallographic study of the fifth LDLRA domain in the LDL receptor showed that this domain contains six amino acids that coordinate a Ca^{2+} ion in an octahedral arrangement, termed the calcium cage (*43, 44*). Site-directed mutagenesis at Asp206, one of the six amino acid residues comprising the cage, strongly suppresses the LDL binding to this domain (*45*), suggesting that the three-dimensional structure essential for LDL binding involves the binding of Ca^{2+} to it. In this study, HAI-1 D349Y showed a higher association rate than did HAI-1 NIK^1LK^2. This suggests that the Ca^{2+} binding to the LDLRA domain may be important in HAI-1 to maintain the correct protein conformation and that the conformation is critical for suppressing the association between Kunitz domain I and matriptase. However, the LDLRA domain *per se* is unlikely to suppress the association. The conformation may be essential for the correct positioning and orientation of Kunitz domain II in 58-kDa HAI-1 (Fig. 6). The higher association rate of HAI-1 D349Y than NIK^1LK^2 can be explained by the altered position of Kunitz domain II in HAI-1 D349Y. In contrast, the correct conformation of the LDLRA domain is probably not essential for its effect on the dissociation, because

the k_{off} value is lower than in HAI-1 D349Y that in HAI-1 NIK^{1}LK^2. The reason for the decrease in the dissociation rate of Kunitz domain I-matriptase complex caused by the presence of the LDLRA domain in HAI-1 (*i.e.* the considerably lower dissociation rate of HAI-1 IK^{1}L-matriptase complex than HAI-1 IK^1-matriptase complex) is unclear. It seems unlikely that a specific interaction, which stabilizes the Kunitz domain I-matriptase complex, occurs between the LDLRA domain and enzyme (Figs. 4 and 5B). One explanation is that the LDLRA domain in HAI-1 mutants such as HAI-1 IK^{1}L and K^{1}L is positioned so that it can obstruct the dissociation of matriptase from the Kunitz domain I.

In summary, these results demonstrate that Kunitz domain I is responsible for the inhibition of matriptase and that domains other than Kunitz domain I affect the inhibitory activity considerably. Together with evidence of the occurrence of soluble HAI-1 species *in vivo*, these data suggest that the domain structure of HAI-1 is organized in a way that allows HAI-1 to flexibly control the activity of matriptase, possibly in relation to the protease activity in tissues. Another striking finding of this study is that HAI-1 IK^{1}L showed potent inhibitory activity. It remains unknown whether 25-kDa HAI-1 in human milk corresponds to the HAI-1 IK^{1}L mutant and whether the inhibitory activity is stronger in 25-kDa HAI-1 than in 40-kDa HAI-1. Regardless, HAI-1 IK^{1}L could be a powerful tool for suppressing cancer invasion and metastasis, for which matriptase is responsible.

Table 1. Kinetic parameters for reaction of recombinant matriptase with HAI-1 mutants[a]

[a]Assays were performed as described in "Materials and Methods". NIK^{1}LK^2 and IK^{1}L were included in the reaction mixture over the concentration range as described in the legend for Fig. 5A: K385A, 20–80 nM, the other HAI-1 mutants, 4–20 nM. The values of k_{on} were determined by fitting the data to Equations 1 and 2. The value of k_{off} was determined from each progress curve according to Equation 4. The mean of the seven k_{off} values obtained in a separate experiment was taken as the k_{off} value. The values of K_i were calculated according to Equation 3. The values shown are means ± S.D. of 3–4 separate experiments.

HAI-1 mutants	k_{on} ($\times 10^4$ M^{-1} s^{-1})	k_{off} ($\times 10^{-6}$ s^{-1})	K_i (pM)
NIK^{1}LK^2	3.5 ± 2.0	23 ± 14	647 ± 62
NIK^{1}L	23 ± 3	12 ± 3	53 ± 18
NIK^1	75 ± 9	40 ± 10	45 ± 11
IK^{1}LK^2	64 ± 6	15 ± 4	24 ± 7
IK^{1}L	217 ± 10	3.5 ± 2.1	1.6 ± 1.0
IK^1	168 ± 37	61 ± 8	38 ± 3
K^{1}LK^2	16 ± 3	18 ± 10	42 ± 17
K^{1}L	41 ± 30	17 ± 2	54 ± 27
K^1	36 ± 9	107 ± 37	328 ± 181
K^2	ND	ND	ND
NK^{1}LK^2	ND	ND	ND
NIK^{1}K^2	35 ± 15	28 ± 7	86 ± 28
R260A	ND	ND	ND
D349Y	17 ± 1	5.9 ± 2.0	37 ± 11
K385A	6.3 ± 0.7	18 ± 5	278 ± 93

ND, kinetic parameters cannot be determined.

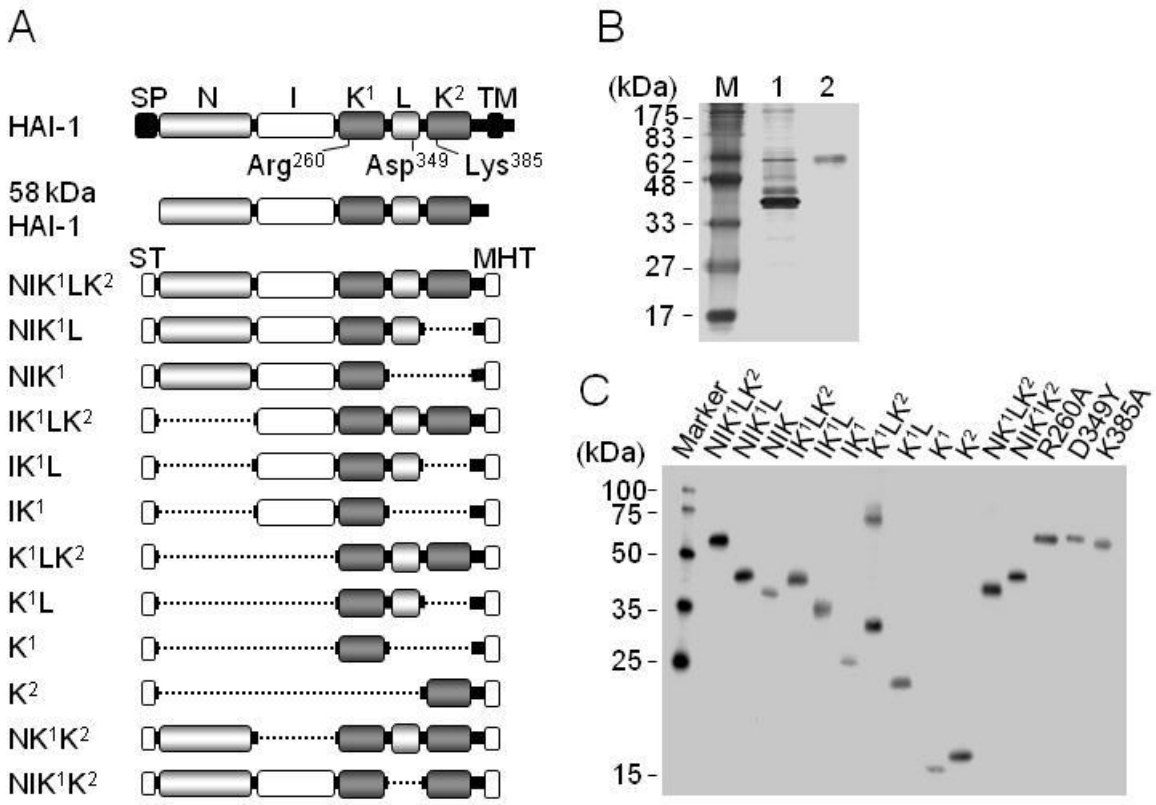

Fig. 1. Schematic domain construction of rat HAI-1 variants and their characterization. (A) Schematic representation of the structure of rat HAI-1 and diagram of expression constructs. Domain structure of the primary translation product of rat HAI-1 is indicated as *HAI-1* at the *top*. A soluble HAI-1 occurring naturally is indicated as *58-kDa HAI-1*. HAI-1 *NIK*^{1}*LK*^{2} represents a recombinant form of 58-kDa HAI-1 in which the N-terminal region containing the signal peptide (Met1–Pro40) is replaced by the human immunoglobulin κ-chain signal peptide and S-tag (*ST*) and the *Myc* epitope and hexahistidine tag (*MHT*) is fused after Ser441. The deletion mutants are shown below the HAI-1 *NIK*^{1}*LK*^{2} mutant. The truncated regions in each deletion mutant are indicated by the *dotted line*. The positions at which amino acid substitution was introduced for HAI-1 R260A, D349Y, and K385A are indicated on the *top*. *TM*, transmembrane domain; *N*, N-terminal domain; *I*, internal domain; *K*^{1}, Kunitz domain I; *L*, LDLRA domain; *K*^{2}, Kunitz domain II. (B) Silver staining of HAI-1 NIK^{1}LK^{2} preparations. The concentrated conditioned medium was treated with Ni^{2+}-charged resin, and the proteins bound to the resin were eluted (*lane 1*). The eluate was subsequently treated with an immobilized S-protein (*lane 2*). The eluates were analyzed SDS-PAGE (12% polyacrylamide) under reducing conditions and silver staining. *Lane M* shows the protein size markers with each mass indicated on the *left* in kilodaltons (kDa). Note that an unidentified protein with a mass of 40 kDa is mostly evident in the preparation with Ni^{2+}-charged resin alone. (C) Western blot analysis of all HAI-1 mutants prepared in this study. The HAI-1 mutants treated with Ni^{2+}-charged resin were separated by SDS-PAGE (12% polyacrylamide) under reducing conditions, and the Western blot was probed with S-protein conjugated with HRP. No cleaved products were evident in each HAI-1mutant preparation. *Lane Marker* shows the signals given by proteins to which S-tag was fused at their N-terminus (Perfect Protein Marker™). Note that longer exposure was required to detect the marker protein with a mass of 15 kDa.

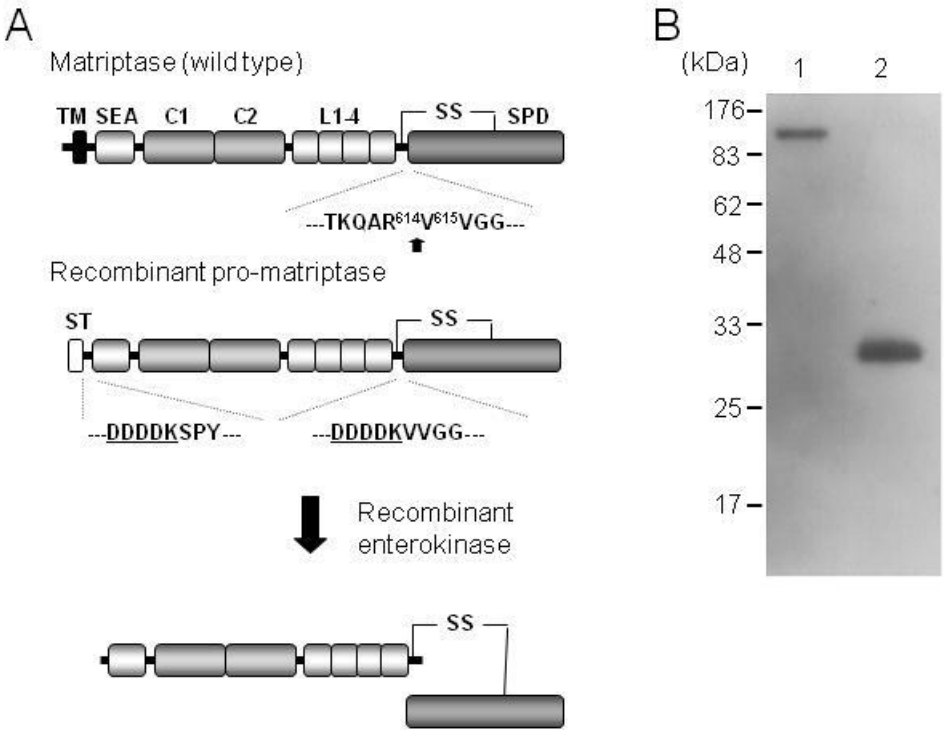

Fig. 2. Production and characterization of recombinant rat matriptase. (A) Schematic representation of the structure of rat matriptase and an expression construct. This protease comprises 855 amino acids. The amino acid numbering starts from the putative N terminus of the protein. The domain structure is indicated as *matriptase (wild type*) at the *top*. The predicted disulfide linkages are shown as *SS*. The activation cleavage site (indicated by the *arrow*) and its surrounding sequence (*single-letter code*) are shown in *matriptase (wild type). Recombinant pro-matriptase* is a secreted form of matriptase in which the cytoplasmic domain and the signal anchor (Met1–His80) are replaced with the human immunoglobulin κ-chain signal peptide, S-tag (*ST*), and the enterokinase recognition sequence (*DDDDK*, *underlined*). In addition, TKQAR615 in the wild-type enzyme was replaced with the enterokinase recognition sequence for *in vitro* cleavage before Val615 (activation cleavage). The disulfide-linked, two-chain recombinant matriptase (active recombinant matriptase) is illustrated at the *bottom*. Note that the S-tag at the N terminus can also be removed with recombinant enterokinase. *TM*, transmembrane domain; *N*, N-terminal domain; *I*, internal domain; *SEA*, sea urchin sperm protein enterokinase-agrin domain; *C1* and *C2*, the first and second complement protein subcomponents C1r/C1s-urchin embryonic growth factor-bone morphogenetic protein 1 domains, respectively; *L1–4*, four tandem repeats of LDLRA domain; *SPD*, serine protease domain. (B) Western blot analysis of recombinant matriptase produced in CHO-K1 cells. Recombinant matriptase treated with an immobilized S-protein was eluted by boiling (*lane 1*) as described previously (*17*) or eluted with enterokinase (*lane 2*) as described under "Materials and Methods" Samples were separated by SDS-PAGE (12% polyacrylamide) under reducing conditions, and the Western blot was probed with rabbit anti-rat matriptase catalytic domain antibody (*Spr992*). The molecular masses of the standards are indicated on the left in kDa.

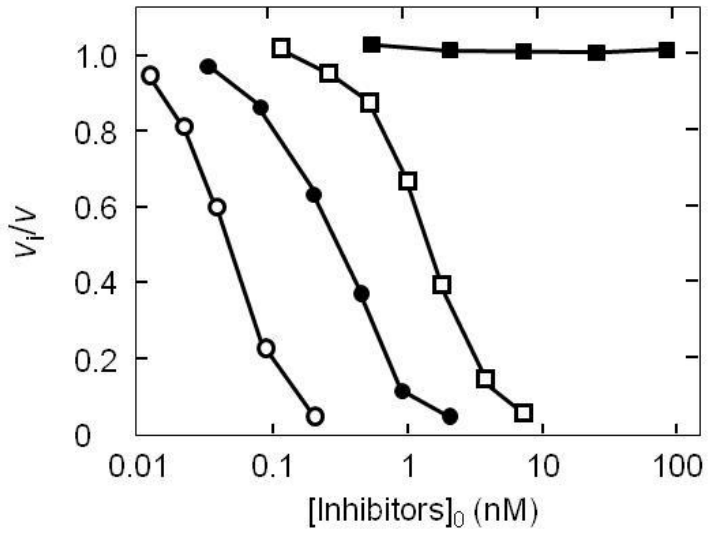

Fig. 3. Plots of the steady-state fractional rate as a function of the concentrations of HAI-1 mutants. The steady-state initial reaction rates in the presence (v_i) and absence (v) of HAI-1 mutants were measured as described under "Materials and Methods" The reaction mixtures contained various concentrations (indicated) of HAI-1 NIK^{1}LK^2 (*open squares*), HAI-1 NIK^{1}L (*closed circles*), HAI-1 IK^{1}L (*open circles*), and HAI-1 R260A (*closed squares*), and 0.12 nM recombinant matriptase. Reactions were initiated by addition of Sp-tPA at a final concentration of 500 μM.

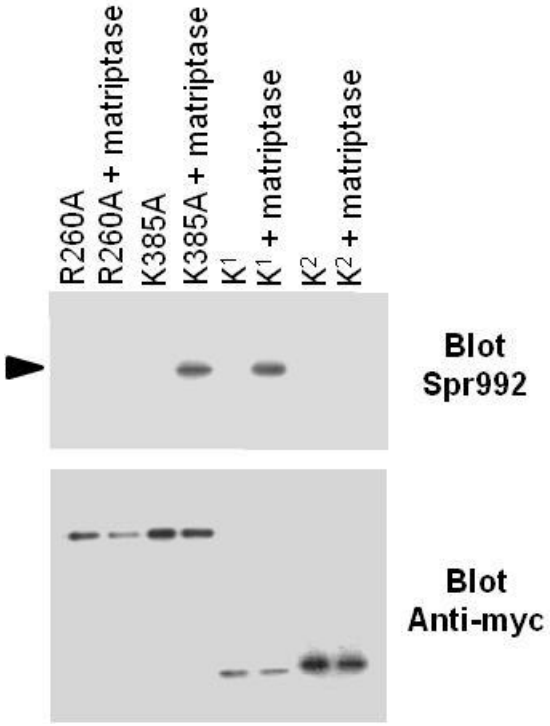

Fig. 4. Exclusive responsibility of Kunitz domain I in the interaction of HAI-1 with matriptase. The Ni^{2+}-charged resin bound to HAI-1 R260A, K385A, K^1, or K^2 was incubated with HEPES buffer alone or with HEPES buffer containing recombinant matriptase. After being washed with HEPES buffer, the precipitants were eluted by boiling. The eluates were separated by SDS-PAGE (12% polyacrylamide) under reducing conditions, blotted, and probed with rabbit anti-rat matriptase catalytic domain antibody (Spr992) (*upper panel*) or anti-*Myc* antibody (*bottom panel*). The catalytic domain of matriptase is visualized at the position corresponding to 28 kDa (indicated by *arrowhead*). The HAI-1 R260A, K385A, K^1, and K^2 mutants are visualized at the positions corresponding to 59, 59, 16, and 17 kDa, respectively.

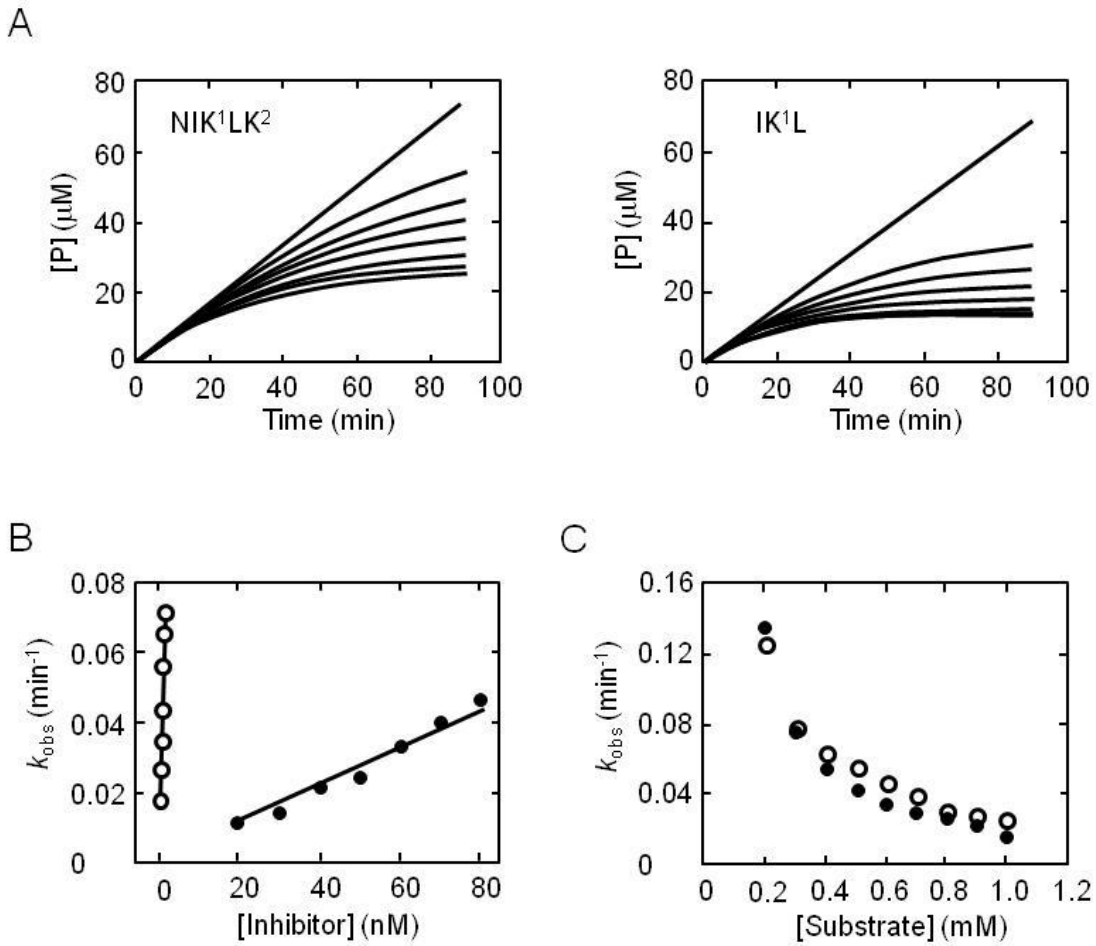

Fig. 5. Pre-steady-state kinetic analysis of the inhibition of recombinant matriptase by the HAI-1 NIK^{1}LK^2 and IK^{1}L mutants. (A) Progress curves for the reaction of recombinant matriptase in the presence of increasing concentrations of HAI-1 NIK^{1}LK^2 and IK^{1}L. The enzymatic reactions were initiated by the addition of 0.12 nM recombinant matriptase, and the product formation was monitored as detailed under "Materials and Methods." The concentrations (from *top* to *bottom*) for HAI-1 NIK^{1}LK^2 are 0, 20, 30, 40, 50, 60, 70, and 80 nM; those for HAI-1 IK^{1}L are 0, 0.4, 0.6, 0.8, 1.0, 1.2, 1.4, and 1.6 nM. (B) Dependence of k_{obs} on the concentration of inhibitor. The progress curve data were analyzed using Equation 1 to obtain k_{obs} as a function of the concentrations of HAI-1 NIK^{1}LK^2 (*closed circles*) and HAI-1 IK^{1}L (*open circles*). (C) Dependence of k_{obs} on the substrate concentration. Assays were performed under the same conditions as described under "Materials and Methods" except that the reaction mixtures contained 0.2–1.0 mM Sp-tPA and 60 nM HAI-1 NIK^{1}LK^2 (*closed circles*) or 1.0 nM HAI-1 IK^{1}L (*open circles*).

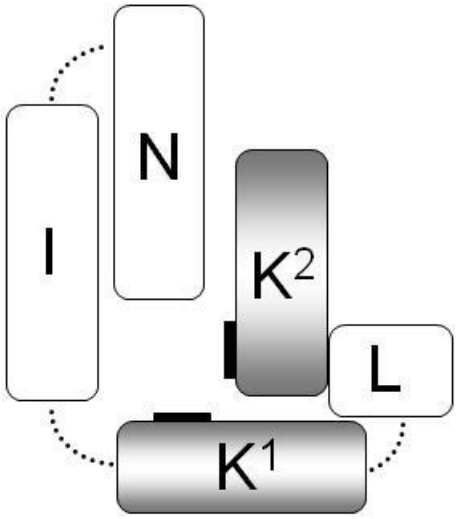

Fig. 6. Proposed domain structure of 58-kDa HAI-1. Putative sites for protease binding in Kunitz domain I and II are indicated by *small black rectangles*. Spacer regions are indicated by *dotted curves*. In 58-kDa HAI-1, HGF activator binding of each Kunitz domain is affected by the presence of other Kunitz domain, suggesting that the two protease-binding sites in the molecule are close to each other (*18*). In the interaction of HAI-1 NIK^1LK^2 with matriptase, Kunitz domain II is postulated to function only in the obstruction of the protease-binding site of Kunitz domain I. The N-terminal domain and Kunitz domain II may collaborate to severely obstruct this site. The presence of LDLRA domain appears to be critical for the correct positioning of Kunitz domain II. These can account for the low association rate of NIK^1LK^2 (58-kDa HAI-1) with matriptase. *N*, N-terminal domain; *I*, internal domain; K^1, Kunitz domain I; *L*, LDLRA domain; K^2, Kunitz domain II.

Chapter 2

Role of the Stem Domain of Matriptase in the Interaction with Its Physiological Inhibitor, Hepatocyte Growth Factor Activator Inhibitor Type 1

Introduction

Type II transmembrane serine proteases are characterized by the N-terminal cytoplasmic domain, a signal anchor transmembrane domain, and an extracellular C-terminal serine protease catalytic domain. In addition, members of this family with a few exceptions (*e.g.*, hepsin) have the extracellular non-catalytic domains (hereinafter called stem domain) consisting of various structural motifs (*51, 52*). For instance, the matriptase stem domain comprises a sea-urchin sperm protein–enterokinase–agrin (SEA) domain, two complement factor 1R–urchin embryonic growth factor–bone morphogenetic protein (CUB) domains, and four low-density lipoprotein receptor A module (LDLRA) domains (Fig. 1A). Of interest is the finding that the activity of enteropeptidase (also called enterokinase), a member of this family, is greatly dependent on the stem domain (*42*). Indeed, a secreted variant of recombinant (or r-) bovine enterokinase containing the entire extracellular domain (HL-BEK) cleaves the substrate trypsinogen with a catalytic efficiency 520 times higher than does another variant consisting only of the catalytic domain (L-BEK) (*42*). Later, the N-terminal fragment 118–465 [consisting of a mucin-like domain, a first LDLRA domain, a first CUB domain, and the N-terminal half of an MAM domain (named for motifs found in Meprin,

Xenopus laevis A5 protein, and protein tyrosine phosphatase μ)] in the stem domain was found to contain a secondary substrate-binding site that interacts directly with trypsinogen (*53*). Effects of the stem domain in matriptase on its antivity remain to be determined.

HAI-1 is a physiological inhibitor of matriptase (*1*). HAI-1 is a Kunitz-type serine protease inhibitor isolated originally from the conditioned medium of a human stomach carcinoma MKN45 cell line as a potent inhibitor of a serine protease, HGF activator (*12, 14*). The primary translation product of HAI-1 predicted from the cDNA sequence comprises 513 amino acid residues, including a putative N-terminal signal peptide sequence and a hydrophobic region at its C-terminal region, suggesting that HAI-1 is produced first as a type I transmembrane protein (*12*). An HAI-1 species with a molecular mass of 66 kDa detected in extracts of MKN45 cells and monkey kidney COS-1 cells transiently transfected with a full-length rat HAI-1 cDNA is thought to be the membrane-anchored form (hereinafter 66-kDa HAI-1) (*16, 17*). The extracellular domain of HAI-1 comprises an N-terminal domain, followed by an internal domain, first protease inhibitory domain (Kunitz domain I), an LDLRA domain, and a second Kunitz domain (Kunitz domain II) (Fig. 1B). The extracellular domain is shed by cleavage with certain proteases. At least two HAI-1 species of 58 and 40 kDa are found in conditioned media of MKN45 cells (*12, 16*). The 58-kDa species (58-kDa HAI-1) has the N-terminal domain to Kunitz domain II, whereas the 40-kDa species (40-kDa HAI-1) lacks Kunitz domain II and presumably the LDLRA domain (Fig. 1B) (*12*).

In Chapter 1, secreted variants of r-HAI-1 were produced, and Kunitz domain I was found to be responsible for the inhibition of HL-matriptase but Kunitz domain II was not. It was also found that a secreted variant of r-HAI-1 (designated sHAI-1 NIK[1]

in this study, Fig. 1B), which might correspond to 40-kDa HAI-1, inhibited HL-matriptase more efficiently than did another secreted variant (designated sHAI-1 NIK^1LK^2, Fig. 1B) corresponding to 58-kDa HAI-1. Taken together, it was suggested that the matriptase-binding site in Kunitz domain I could be obstructed by Kunitz domain II, and thus, the inhibitory activity of sHAI-1 NIK^1LK^2 was lower than that of sHAI-1 NIK^1 against HL-matriptase.

The stem domain of enterokinase was also shown to drastically affect the inhibitory interaction of this protease with macromolecule inhibitors (*42*). For instance, L-BEK was inhibited with a Kunitz-type inhibitor from soybean, whereas HL-BEK was not. This led the author to examine whether the stem domain of matriptase affects the interaction of this protease with HAI-1. In this chapter, the inhibitory activities of the r-HAI-1 variants against HL-matriptase and L-matriptase were compared, and evidence that the stem domain of matriptase can facilitate the inhibitory interaction of this protease with the HAI-1 was provided.

Materials and Methods

Materials – Peptidyl-MCA substrates, including *t*-Butyloxycarbonyl (Boc)-L-glutamyl-L-alanyl-L-arginine-MCA (Boc-QAR-MCA), acetyl-L-lysyl-L-threonyl-L-lysyl-L-glntaminyl-L-leucyl-L-arginine-MCA (Ac-KTKQLR-MCA), and Boc-[(2*S*)-2-amino-3-(benzyloxycarbonyl)propionyl]-L-prolyl-L-arginine-MCA [Boc-D(OBzl)-PR-MCA] were purchased from Peptide Institute (Osaka, Japan). All other materials were prepared as described in Chapter 1.

Cell Culture – A Chinese hamster ovary cell line (CHO-K1) was obtained from Health Science Research Resources Bank (Osaka, Japan), and were maintained in Ham's F12 medium supplemented with 5% fetal bovine serum, 100 IU/ml penicillin, and 100 IU/ml streptomycin at 37°C in 5% CO_2.

Preparation of Secreted Variants of r-Matriptase – Using CHO-K1 cells, secreted variants of rat r-matriptase consisting of the entire extracellular domains (Tyr81–Val855) (HL-matriptase) and of the catalytic domain (and its N-terminal spacer region) (Asp603–Val855) (L-matriptase) were produced (Fig. 1A). They are activated *in vitro* by r-EK. Hereinafter, the secreted variants of r-matriptase activated by incubation with r-EK are referred to as simply HL-matriptase and L-matriptase (or r-matriptase variants). The procedures for the production, purification using immobilized S-protein, and activation with r-EK were described in Chapter 2. The active sites of the r-matriptase variants were titrated in the procedures as follows: A part of them was incubated with 1 mM of Boc-QAR-MCA in 25 mM HEPES buffer (pH 7.5) containing 145 mM NaCl and 0.1% Triton X-100 (hereinafter called HEPES buffer), for 10 min at 37°C in a volume of 80 μl. The reaction was terminated by adding 350 μl of 0.1 M monochloroacetic acid in 0.1 M sodium acetate buffer, pH 4.3 (stop solution), and the absorbance at 370 nm was measured. One unit of activity was defined as the amount of the enzyme that librates 0.5 nmol of 4-methyl-coumaryl-7-amine/min from Boc-QAR-MCA, and the enzyme concentration was estimated by sodium dodecyl

sulfate-polyacrylamide electrophoresis (SDS-PAGE) followed by silver staining with bovine trypsin as the standard. One enzyme unit was given by 1 pmol enzyme.

Preparation of r-HAI-1 Variants – A plasmid for expression of an HAI-1 variant harboring the amino acid residues from Pro41 to Leu513 (the amino acid numbering of HAI-1 starts from the putative N-terminus of the protein), including those for the transmembrane and cytoplasmic domains, has already been constructed using the pSecTag/hygroB vector (Invitrogen) (*17*). In the present study, the expression plasmid and product were designated pSec-maHAI-1 and maHAI-1, respectively (Fig. 1B). Expression plasmids designated pSecNIK^{1}LK^2 and pSecNIK^1 for the respective secreted r-HAI-1 variants, sHAI-1 NIK^{1}LK^2 and sHAI-1 NIK^1, have already been constructed using this vector (*Chapter 1*). In the designation of the secreted r-HAI-1 variants, the abbreviations of the domains were placed according to their order in the variants from the N-terminus to C-terminus (Fig. 1). The plasmids were transfected into CHO-K1 cells using LipofectAMINE2000™ (*8*). Clones resistant to Ham's F12 medium containing 400 μg/ml hygromycin B were obtained, and the expression levels in the conditioned media by each clone was determined by Western blotting using HRP-conjugated S-protein as described in Chapter 1. S2125, N1403, and N1515, clones with the highest expression of maHAI-1, sHAI-1 NIK^{1}LK^2, and sHAI-1 NIK^1, respectively, were propagated and stored in liquid nitrogen until use.

maHAI-1 was prepared from Triton extracts of S2125 as follows: Cells were cultured on 100-cm^2 dishes (Asahi Techno Glass, Tokyo, Japan). After reaching

confluence, cells were washed three times with ice-cold phosphate-buffered saline (PBS; 8 mM Na_2HPO_4, 1.5 mM KH_2PO_4, 136 mM NaCl, 2.7 mM KCl, pH 7.4), and then exposed to 1 ml of ice-cold PBS containing 1% Triton X-100. After incubation for 5 min on ice, cells were scraped with Triton, transferred to a 1.5 ml microcentrifuge tube, and incubated for 1 h on ice with occasional agitation. After incubation, the mixture was centrifuged at 10,000 × *g* for 30 min at 4°C. The resulting supernatant (Triton extract) was incubated for 30 min with 30 μl of a slurry of immobilized S-protein at 25°C with rocking. After centrifugation at 5,000 × *g* for 2 s at 25°C, the resulting supernatant was incubated again with fresh immobilized S-protein as described above. After centrifugation at 5,000 × *g* for 2 s at 25°C, the resulting supernatant was discarded. Slurries were pooled, washed extensively with PBS containing 0.1% Triton X-100 (PBST), and washed once with 0.1% Triton X-100 solution. Then, maHAI-1 bound to the slurry was eluted with 375 μl of 0.2 M sodium citrate buffer (pH 2.0), and the eluate was immediately neutralized with 125 μl of 2 M Tris. The r-HAI-1 variant was subjected to gel filtration in HEPES buffer using NAP-5 column (GE Healthcare, Tokyo blanch) with an elution volume of 1.0 ml. The gel filtrate was stored at –20°C until use.

sHAI-1 NIK^1LK^2 and NIK^1 were prepared as follows: N1403 and N1515 were cultured on 75-cm^2 flasks. After reaching confluence, cells were washed three times with ice-cold PBS, and 10 ml of serum-free Ham's F12 was added to each flask. After 48 h, the conditioned medium was collected, and fresh serum-free medium was added. This was repeated until half of the cells were peeled off. The collected media were

centrifuged immediately at 3,000 × *g* for 10 min at room temperature, and the resulting supernatants were stored at –20°C until use. For purification, 120 ml of the conditioned media was collected using 2 flasks. After thawing, the media were pooled and concentrated to 2.5 ml by ultrafiltration using Amicon® Ultra-15 (10,000 MWCO, Millipore, Cork, Ireland). The concentrated medium was subjected to gel filtration in PBST using a PD-10 column (GE Healthcare) with an elution volume of 3.5 ml. sHAI-1 NIK^1LK^2 and NIK^1 were purified from 1 ml of the gel filtrates using immobilized S-protein as described above. The remainder of the gel filtrate was stored at –20°C until purification. sHAI-1 NIK^1LK^2 and NIK^1 samples eluted from the S-protein column were subjected to gel filtration in HEPES buffer and stored at –20°C until use.

Determination of Concentrations of r-HAI-1 Variants – A portion of the sample of each r-HAI-1 variant in HEPES buffer was added to an equal volume of 2×Laemmli protein sample buffer (or Laemmli buffer) [1×Laemmli buffer: 0.05 M Tris-HCl (pH 6.8), 12 mM dithiothreitol, 10% glycerol, 2% SDS, and 0.005% bromophenol blue] (*54*). Perfect Protein™ Marker, in which each protein is fused to an S-tag and the concentration of each marker was known, was diluted with 1×Laemmli buffer (1:25 dilution). After boiling for 3 min, various amounts of diluted samples were subjected to SDS-PAGE followed by Western transfer. The blots were probed with HRP-conjugate S-protein, and the X-ray films were scanned digitally, and the signal intensities of protein bands were analyzed by densitometry. The concentration of maHAI-1 was calculated by comparing the signal density of the bands of interest with the 75-kDa

protein contained in the protein marker. The sHAI-1 NIK^1LK^2 and NIK^1 were compared with the 50-kDa and 35-kDa proteins, respectively (Fig. 2).

Inhibition Assays – Peptidyl-MCA substrates used were dissolved in dimethylsulfoxide at the concentration of 40 mM and stored at –20°C until use. Inhibition assays were carried out in HEPES buffer at 37°C in a final volume of 80 μl in a 0.5 ml microcentrifuge tube. The r-matriptase variants (at 2.5 nM each) were pre-incubated with or without r-HAI-1 variants in HEPES buffer (78 μl). After pre-incubation (with various incubation time), the enzyme reaction was initiated by adding 2 μl of 40 mM peptidyl-MCA substrates to the assay mixture. After further incubation for 60 min, the reaction was terminated by adding 350 μl of stop solution. The following assay was also conducted: The r-HAI-1 variants (or HEPES buffer alone) were incubated for 2 min in 72 μl of HEPES buffer containing 1.1 mM peptidyl-MCA substrates, and the hydrolysis was initiated by adding 8 μl of 25 nM r-matriptase variants. After further incubation for 60 min, the reaction was terminated as described above. In each kinetic study, the absorbance at 370 nm of the product 4-methyl-coumaryl-7-amine was measured. The initial reaction rate (v_o) of the hydrolysis was determined using the molar absorption coefficient of 7.7 mM^{-1} cm^{-1} of 4-methyl-coumaryl-7-amine.

Results

The Effect of the Stem Domain on the Activity of Matriptase – The kinetic parameters (K_m, k_{cat}, and k_{cat}/K_m) of HL-Matriptase and L-Matriptase after treatment with r-enterokinase were characterized using Boc-QAR-MCA as follows: K_m = 590±15 and 582±20 μM; k_{cat} = 13.1±1.8 and 13.7±3.5 s^{-1}; and k_{cat}/K_m = 22.2±3.6 and 23.7 ±6.4 $mM^{-1}s^{-1}$, respectively. The activities of the two matriptase variants in the hydrolysis of the respective peptidyl-MCA substrates containing an Arg residue at P_1 site were similar (Table 1). The conversion of sc-uPA into two-chain uPA (tc-uPA) catalyzed by the matriptase variants were also examined. Preliminary experiments indicated that the hydrolysis of spectrozyme UK (sp-UK, American Diagnostica, Stanford, CT), a specific substrate for tc-uPA, by sc-uPA and the active matriptase variants was negligible. Figure 3 shows the rate of *p*NA formation after incubation of sc-uPA at the concentrations indicated with the active matriptase variants. These data, combined with previously reported data (*55*) that 1 nM tc-uPA hydrolyzes a sp-UK-like substrate, L-Pyroglu-Gly-L-Arg-*p*-nitroanilide, at a rate of 6 nM s^{-1}, give the kinetic parameters of active HL-Matriptase and active L-Matriptase in the hydrolysis of sc-uPA into tc-uPA: K_m = 3.52±0.18 and 5.99±0.58 μM; k_{cat} = 0.71±0.08 and 0.57±0.09 s^{-1}; and k_{cat}/K_m = 202±32 and 95±22 $mM^{-1}s^{-1}$, respectively (Fig. 3). On the basis of kinetic data, it is concluded that matriptase activity is dependent on the catalytic domain, that the stem domain has no significant effect on the activity, and that the role of the stem domain of matriptase is different from that of enterokinase.

Characterization of r-HAI-1 Variants Produced in CHO-K1 Cells – In this study, a cell membrane-anchored form of r-HAI-1 with S-tag at its N-terminus (maHAI-1) and

secreted variants of r-HAI-1 with S-tag and *Myc*-hexahistidine-tag at their N- and C-termini, respectively (sHAI-1 NIK^1LK^2 and sHAI-1 NIK^1) were produced in a stable expression system using CHO-K1 cells (Fig. 1B). These r-HAI-1 variants were purified by means of single-step affinity chromatography using an immobilized S-protein. The variants were purified to homogeneity (higher than 95%) as judged by SDS-PAGE and silver staining (data not shown). A representative Western blot data of the rHAI-1 variants probed with HRP-conjugated S-protein is shown in Fig. 2 (left panel). maHAI-1, sHAI-1 NIK^1LK^2, and sHAI-1 NIK^1 produced signals at the positions corresponding to 66 kDa, 59 kDa, and 41 kDa, respectively. sHAI-1 NIK^1LK^2 and NIK^1 also produced 59-kDa and 41-kDa signals, respectively, when probed with an anti-*Myc* epitope-tag antibody (Fig. 2, right panel). When the mass of a sugar chain on the Asn235 residue in the internal domain (~5 kDa) was taken into consideration, the molecular masses of the r-HAI-1 variants evaluated from SDS-PAGE were in good agreement with the calculated ones.

Inhibition of HL-Matriptase and L-Matriptase by maHAI-1 – To address the role of the stem domain of matriptase in its interaction with HAI-1, the inhibitory activities of r-HAI-1 variants against HL-matriptase and L-matriptase in the hydrolysis of peptidyl-MCA substrates were compared. Boc-QAR-MCA and Boc-D(OBzl)-PR-MCA were used as substrates, because they were preferred by the r-matriptase variants. Ac-KTKQLR-MCA, a substrate for proteases that have pro-HGF converting activity was also examined (*9, 14, 38*).

At first, the inhibition of r-matriptase variants by the purified preparation of maHAI-1 was investigated. It is known that the secreted r-HAI-1 variants inhibit HL-matriptase as slow-binding inhibitors (*Chapter 1*). To monitor inhibition evidently, the enzyme was incubated with the inhibitor prior to adding the substrate. Preliminary experiments using Boc-QAR-MCA showed that 2.5 nM HL-matriptase was inhibited 90% or more by 15 nM maHAI-1 after they were pre-incubated for 15 min. Under the kinetic conditions, HL-matriptase and L-matriptase were inhibited by maHAI-1 with a similar extent when Boc-QAR-MCA and Ac-KTKQLR-MCA were used (Fig. 4). HL-matriptase was inhibited more than 90% in the hydrolysis of Boc-D(OBzl)-PR-MCA (Fig. 4), whereas L-matriptase was not much inhibited and only (45 ± 5)% was observed (Fig. 4).

Kinetic assay where the enzyme reaction was initiated by adding enzyme to the mixture containing inhibitor and substrate was also conducted. In the hydrolysis of Boc-QAR-MCA and Ac-KTKQLR-MCA, HL-matriptase and L-matriptase were inhibited by 15 nM maHAI-1 with a similar extent (Fig. 4). However, in the hydrolysis of Boc-D(OBzl)-PR-MCA, HL-matriptase was inhibited moderately [(52 ± 3)% inhibition], and L-matriptase was hardly inhibited (10% inhibition or less) (Fig. 4). These results indicate that the stem domain of matriptase facilitates the inhibitory interaction of this protease with maHAI-1 in the specified hydrolysis of Boc-D(OBzl)-PR-MCA, although it has no effect in the hydrolysis of Boc-QAR-MCA and Ac-KTKQLR-MCA.

To validate further the difference in the inhibitory activities of maHAI-1 against

the hydrolysis of Boc-D(OBzl)-PR-MCA by HL-matriptase and L-matriptase, HL-matriptase and L-matriptase were added to the mixture containing various concentrations of maHAI-1 and a fixed concentration of the substrate. The degree of inhibition of HL-matriptase increased with increasing concentrations of the inhibitor (Fig. 5A, black circles). On the other hand, no significant inhibition of L-matriptase was observed at any inhibitor concentrations examined (Fig. 5A, white circles). Figure 5B shows inhibition as a function of pre-incubation time at fixed concentrations of the enzyme (2.5 nM) and inhibitor (15 nM). HL-matriptase was inhibited 90% or more when it was pre-incubated with maHAI-1 for 15 min. Pre-incubation for 60 min was required for the strong inhibition of L-matriptase. Results shown in Fig. 5 clearly indicate that HL-matriptase is inhibited with maHAI-1 more efficiently than L-matriptase in the hydrolysis of the Boc-D(OBzl)-PR-MCA substrate.

Inhibition of HL-Matriptase and L-Matriptase by the Secreted Variants of r-HAI-1 – The inhibitory activities of sHAI-1 $NIK^{1}LK^{2}$ and sHAI-1 NIK^{1} against r-matriptase variants were examined in the hydrolysis of Boc-D(OBzl)-PR-MCA. HL-matriptase and L-matriptase were inhibited by sHAI-1 $NIK^{1}LK^{2}$ similarly by maHAI-1 (Fig. 6, upper panel). On the other hand, there was no difference in the inhibitory activity of sHAI-1 NIK^{1} against HL-matriptase and L-matriptase (Fig. 6, bottom panel).

Discussion

Inhibitory Activity of 66-kDa HAI-1 – In Chapter 1, secreted variants of r-HAI-1 were produced using COS-1 cells and their inhibitory activities against HL-matriptase were demonstrated. However, the inhibitory activity of membrane-anchored form of HAI-1 (66-kDa HAI-1) toward matriptase has been unknown. In this study, maHAI-1 was purified from the Triton extracts of CHO-K1 cells stably transfected with pSec-maHAI-1. maHAI-1 migrated at the position corresponding to 66 kDa in SDS-PAGE (Fig. 2), suggesting that this variant corresponds to the membrane-anchored form of HAI-1. Likewise, the sHAI-1 NIK^1LK^2 and sHAI-1 NIK^1 variants produced in CHO-K1 cells might correspond to 58-kDa and 40-kDa HAI-1 species, respectively. maHAI-1 and sHAI-1 NIK^1LK^2 exhibited the similar inhibitory activity toward the r-matriptase variants (Figs. 4 and 6). These findings lead to an assumption that 66-kDa HAI-1 may behave against matriptase similarly to 58-kDa HAI-1 *in vivo*.

The Role of the Stem Domain of Matriptase in the Interaction with HAI-1 – The activation cleavage sequence of latent matriptase is P_4(Lys)-P_3(Gln)- P_2(Ala)-P_1(Arg) (Fig. 1A); and that of pro-HGF is P_4(Lys)-P_3(Gln)-P_2(Leu)-P_1(Arg). Hence, the hydrolysis of Ac-KTKQLR-MCA and Boc-QAR-MCA is expected to be as indicated by the activation cleavage of latent matriptase and pro-HGF. However, there was no difference between the inhibitory activities of maHAI-1 against HL-matriptase and L-matriptase when these substrates were used (Fig. 4). In addition, HL-matriptase and L-matriptase were inhibited with a similar extent by sHAI-1 NIK^1LK^2 in the conversion of sc-uPA into two-chain uPA (Kojima, K., Tsuzuki, S., Fushiki, T., and Inouye, K.,

unpublished observation). These results suggest that the stem domain of matriptase has no significant effect on the inhibitory interaction of this protease with HAI-1 (*e.g.*, 66-kDa and 58-kDa HAI-1 species) in the activation cleavage of some substrates, including latent matriptase, pro-HGF, and sc-uPA.

In the hydrolysis of Boc-D(OBzl)-PR-MCA, HL-matriptase was inhibited more efficiently than L-matriptase by maHAI-1 and sHAI-1 NIK^1LK^2 (Figs. 4–6). Matriptase was previously shown to cleave and activate the precursor form of prostasin, which activation cleavage sequence is P_4(Ile)-P_3(Gln)-P_2(Pro)-P_1(Arg) (*10*). Note that proline is in the P_2 position. It is, therefore, tempting to speculate that the matriptase-catalyzed hydrolysis of Boc-D(OBzl)-PR-MCA is an indicative of the activation cleavage of prostasin zymogen. It has recently been shown that HAI-1 (corresponding to our sHAI-1 NIK^1LK^2) inhibits the activation of prostasin zymogen catalyzed by a recombinant catalytic domain of matriptase (*56*). Here, the author could give a possibility that the stem domain of matriptase may facilitate the inhibitory interaction of this protease with HAI-1 in a specific cleavage of substrates, including prostasin zymogen.

In Chapter 1, it was reported that sHAI-1 NIK^1 associated with HL-matriptase faster than did sHAI-1 NIK^1LK^2, and suggested that the Kunitz domain II might obstruct the matriptase-binding site in Kunitz domain I. In this study, it was found that there is no difference in the inhibition between HL-matriptase and L-matriptase by sHAI-1 NIK^1 in the hydrolysis of Boc-D(OBzl)-PR-MCA (Fig. 6, bottom panel). Taken together, the author presents a model explaining the stronger inhibition of

HL-matriptase than L-matriptase by maHAI-1 (or sHAI-1 NIK^1LK^2) in the hydrolysis of the substrate (Fig. 7, upper). In this model, the stem domain of HL-matriptase is postulated to interact with the LDLRA domain and/or Kunitz domain II of maHAI-1, thereby alleviating the Kunitz domain II-mediated obstruction of Kunitz domain I. L-matriptase is illustrated to bind with Kunitz domain I very slowly, because of the lack of the stem domain (*i.e.*, the lack of alleviation of obstruction). On the other hand, HL-matriptase and L-matriptase are inhibited by sHAI-1 NIK^1 with a similar extent, because the HAI-1 variant lacks LDLRA domain and Kunitz domain II (Fig. 7, bottom). The reason that the stem domain has no significant effect on the interaction with maHAI-1 in the hydrolysis of Boc-QAR-MCA and Ac-KTKQLR-MCA is unclear. One explanation is that these substrates themselves alleviate the obstruction of Kunitz domain I by Kunitz domain II to an extent that matriptase catalytic domain could bind to Kunitz domain I without the aid of the stem domain.

In summary, it was found that the stem domain of matriptase facilitates the inhibitory interaction of this protease with maHAI-1 in a specific cleavage of Boc-D(OBzl)-PR-MCA. To my knowledge, this is the first report showing that the stem domain of matriptase can affect the interaction between this protease and HAI-1.

Table 1. Activities of HL-matriptase and L-Matriptase toward peptidyl-MCA substrates with an arginine residue exisiting at the P_1 site.

Substrates	HL-matriptase (%)	L-matriptase (%)	Trypsin (%)
Boc-Gln-Ala-Arg-MCA	100	100	100
Boc-Asp(OBzl)-Pro-Arg-MCA	90	93	88
Boc-Glu(OBzl)-Ala-Arg-MCA	76	85	87
Boc-Glu(OBzl)-Gly-Arg-MCA	61	71	104
Boc-Leu-Gly-Arg-MCA	31	36	74
Ac-Lys-Thr-Lys-Gln-Leu-Arg-MCA	17	16	N.T.
Boc-Phe-Ser-Arg-MCA	14	14	104
Boc-Val-Pro-Arg-MCA	7	12	42

Each MCA substrate was incubated with 3.1 nM of matriptase mutants in HEPES buffer for 60 min at 37^{o}C. The activity toward Boc-QAR-MCA was taken as 100%, and relative activities are shown. The values of the standard deviation were less than 5% of mean values. For comparison, the activity of bovine trypsin (3.1 nM) is shown on the right. The initial reaction rates of HL-matriptase, L-matriptase, and trypsin in the cleavage of Boc-QAR-MCA were 13.8 nM s^{-1}, 11.4 nM s^{-1} and 13.0 nM s^{-1}, respectively. OBzl, benzyl ester; Ac, acetyl; N.T., no tested. All amino acids are L-forms.

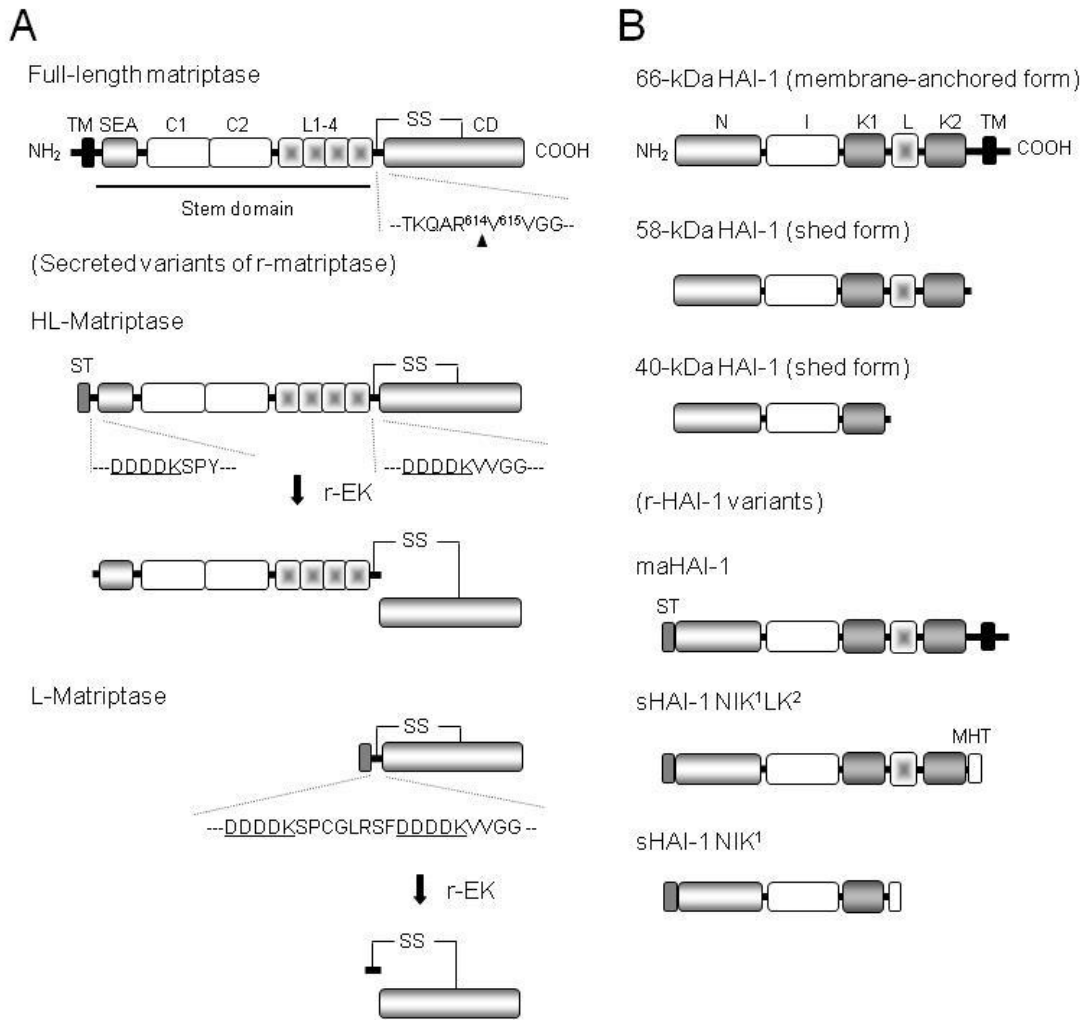

Fig. 1. Schematic illustration of the structure of naturally-occurring matriptase and HAI-1 species and their expression constructs. (A) Domain structures of full-length rat matriptase (top), HL-matriptase, and L-matriptase. The amino acid numbering starts from the putative N-terminus of the protein. The N- and C-termini are indicated by NH_2 and COOH, respectively in full-length matriptase. The predicted disulfide linkages between two cysteine residues corresponding to Cys604 and Cys731 in matriptase are shown as SS. The amino acid sequence around the matriptase activation cleavage site is indicated in the single-letter code with amino acid numbering at the N-terminal Val residue of the catalytic domain (Val615). The activation cleavage site is indicated by arrowhead. The stem domain of matriptase is indicated with underline. HL-matriptase is a secreted form of r-matriptase in which the cytosolic domain and the signal anchor (Met1–His80) are replaced with the human immunoglobulin κ-chain signal peptide and S-tag (ST). L-matriptase is another r-matriptase variant in which Tyr81–Cys602 is truncated from HL-matriptase. Enterokinase recognition sequences (DDDDK, underlined) and their surrounding sequences are shown in both r-matriptase variants. Both HL-matriptase and L-matriptase are activated *in vitro* by incubation with r-EK. Note that S-tag at the N-terminus of each variant can also be removed by incubation with r-EK. TM, transmembrane domain; SEA, SEA domain; C1 and C2, the first and second CUB domain; L1–4, four LDLRA repeats; CD, catalytic domain. (B) Domain structures of 66-kDa HAI-1, 58-kDa HAI-1, 40-kDa HAI-1, maHAI-1, sHAI-1 NIK^1LK^2, and sHAI-1 NIK^1. The N- and C-termini are indicated by NH_2 and COOH, respectively, in the 66-kDa HAI-1. maHAI-1 is a cell membrane-anchored form of r-HAI-1 in which S-tag (ST) is fused at its N-terminus. sHAI-1 NIK^1LK^2 and sHAI-1 NIK^1 are secreted variants of r-HAI-1 corresponding to 58-kDa HAI-1 and 40-kDa HAI-1, respectively. S-tag and *Myc*-hexahistidine tag (MHT) are fused at their N- and C-termini, respectively. N, N-terminal domain; I, internal domain; K1, Kunitz domain I; L, LDLRA domain; K2, Kunitz domain II; TM, transmembrane domain.

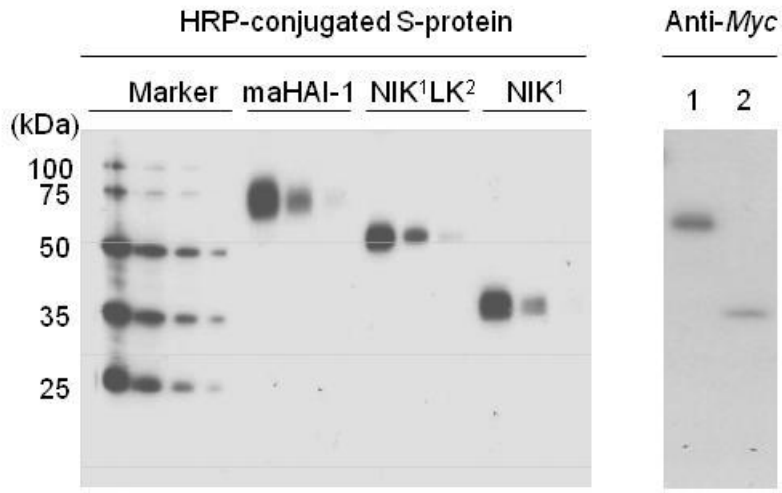

Fig. 2. Western blot analysis of r-HAI-1 variants. Various amounts of a protein size marker (Marker) diluted with Laemmli buffer (16, 8, 4, and 2 μl) and those of r-HAI-1 variants [maHAI-1, sHAI-1 NIK^1LK^2 (NIK^1LK^2), and sHAI-1 NIK^1 (NIK^1)] in 1×Laemmli buffer (20, 10, and 5 μl) were subjected to SDS-PAGE (12% polyacrylamide). After electronic transfer, the blot was probed with an HRP-conjugated S-protein (left panel). The molecular masses of the marker proteins are indicated on the left in kilodaltons (kDa). sHAI-1 NIK^1LK^2 (lane 1) and NIK^1 (lane 2) were also probed with an anti-*Myc* epitope-tag antibody (Anti-*Myc*, right panel).

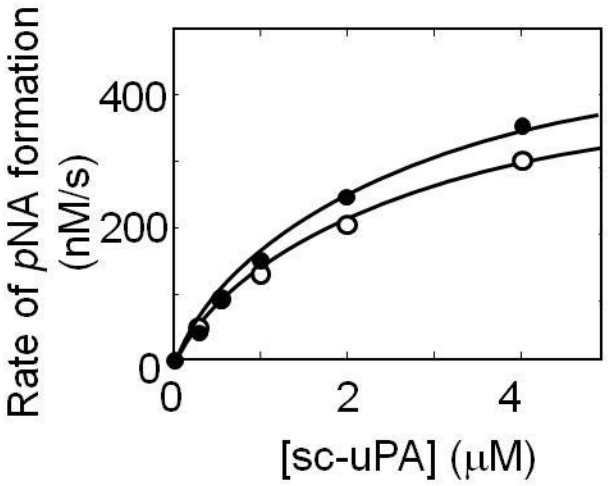

Fig. 3. Conversion of sc-uPA into tc-uPA by HL-Matriptase and L-Matriptase. The matriptase-catalayzed hydrolysis of sc-uPA was conducted as follows: The reaction was initiated by adding 15 μl of HEPES buffer (pH 7.5) containing 0.5 nM active matriptase variants to 15 μl of the buffer containing various consentrations (0.5–8.0 μM) of r-human sc-uPA (Technoclone, Vienna, Austria). After incubation for 50 min at 37°C, 10 μl of 4.0 mM spectrozyme UK (sp-UK, *N*-carbobenzoxy-L-Glu-Gly-L-Arg-*p*-nitro-anilide, American Diagnostica, Stanford, CT) dissolved in HEPES buffer was added to the mixtures. After further incubationfor 5 min at 37°C, the reaction was terminated by adding 350 μl of the stop solution, and the absorbance at 405 nm of the product, *p*-nitroaniline (*p*NA), was measured. The initial rate (v_o) of hydrolysis was determined using a molar absorption coefficient of 9.65 mM^{-1} cm^{-1}. The vertical axis shows the initial reaction rate (v_o) of *p*NA formation from sp-UK, which is catalyzed by tc-uPA generated by incubating sc-uPA with matriptase variants. The values for HL-matriptase and L-matriptase are indicated with closed and open circles, respectively.

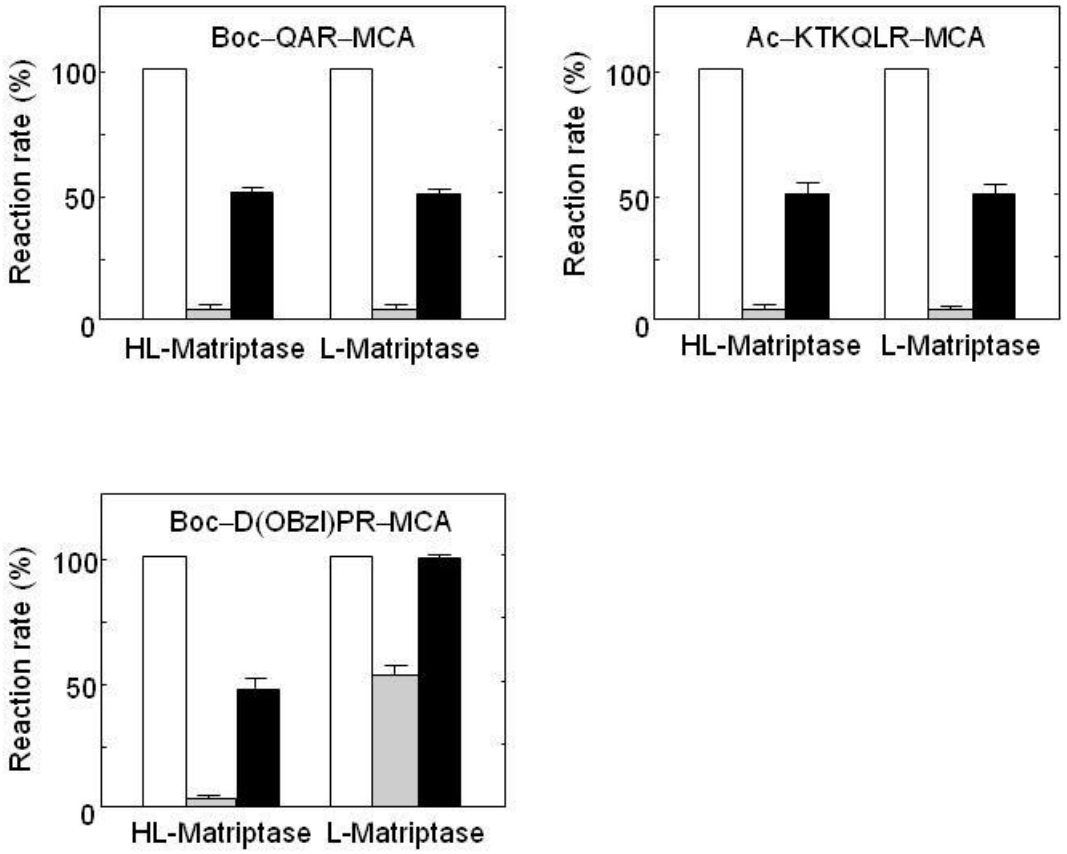

Fig. 4. Inhibition of r-matriptase variants by maHAI-1. HL-matriptase and L-matriptase (2.5 nM each) were incubated with Boc-QAR-MCA, Ac-KTKQLR-MCA, and Boc-D(OBzl)-PR-MCA (1 mM each) for 60 min. The v_0 values for the hydrolysis of Boc-QAR-MCA, Ac-KTKQLR-MCA, and Boc-D(OBzl)-PR-MCA by HL-matriptase were 12 nM s^{-1}, 2.0 nM s^{-1}, and 11 nM s^{-1}, respectively, and they were comparable to those by L-matriptase (*Table 1*). The rates (in the absence of inhibitor) were taken as 100% (white bars). HL-matriptase and L-matriptase (2.5 nM each) were incubated for 15 min with maHAI-1 (15 nM), and the reaction was initiated by adding peptidyl-MCA substrates at a final concentration of 1 mM (grey bars). Black bars indicate the reaction initiated by adding HL-matriptase and L-matriptase at a final concentration of 2.5 nM to mixture containing 17 nM maHAI-1 and 1.1 mM peptidyl–MCA substrates. All values are expressed as means ± standard deviations (SD) of at least two separate experiments.

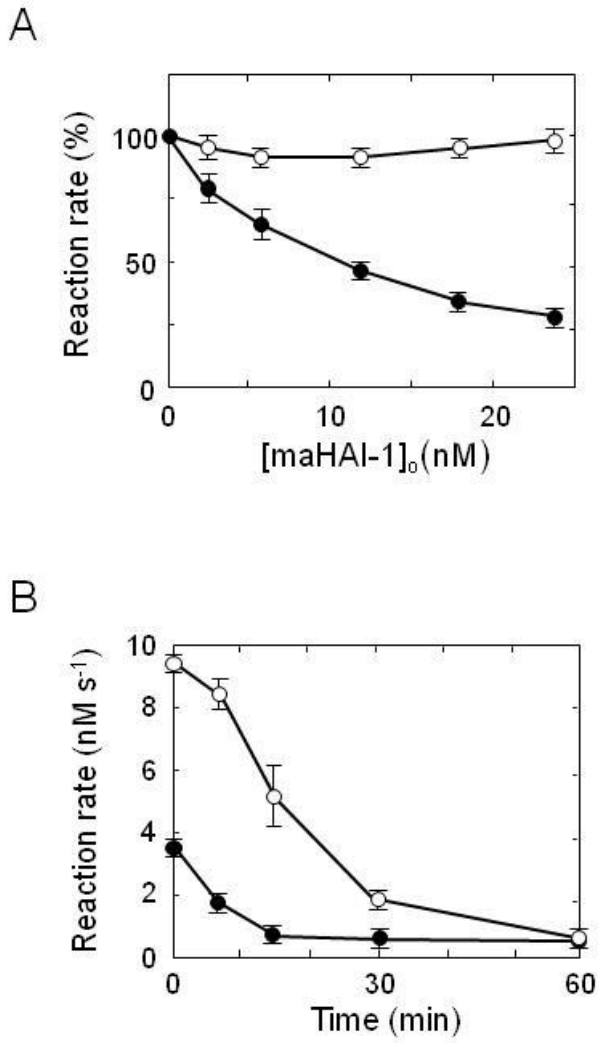

Fig. 5. Further characterization of inhibition of r-matriptase variants by maHAI-1 in the hydrolysis of Boc-D(OBzl)-PR-MCA. (A) Concentration dependency of inhibition of r-matriptase variants by maHAI-1. The reaction was initiated by the addition of 8 μl of HEPES buffer containing 25 nM matriptase variants to 72 μl of the buffer containing maHAI-1 and 1.11 mM Boc-D(OBzl)-PR-MCA. The final concentrations of maHAI-1 were 0, 3, 6, 12, 18, and 24 nM (from left to right). (B) The effect of pre-incubation on the inhibition of r-matriptase variants by maHAI-1. Each r-matriptase variant (2.5 nM) was incubated with maHAI-1 (15 nM) for the times indicated in 78 μl of HEPES buffer, and then 2 μl of 40 mM Boc-D(OBzl)-PR-MCA was added to initiate the reaction. In (A) and (B), the values for HL-matriptase and L-matriptase are indicated with closed and open circles, respectively. All values are expressed as means ± SD of at least two separate experiments.

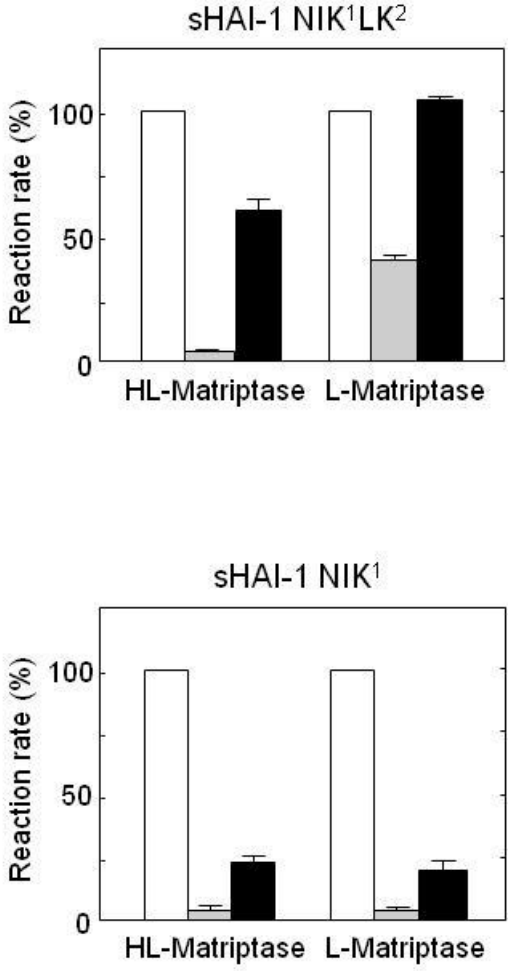

Fig. 6. Inhibition of r-matriptase variants by secreted variants of r-HAI-1 in the hydrolysis of Boc-D(OBzl)-PR-MCA. HL-matriptase and L-matriptase (2.5 nM each) were incubated with Boc-D(OBzl)-PR-MCA (1 mM) for 60 min. The initial reaction rate for the hydrolysis of the substrate (in the absence of inhibitor) was taken as 100% (white bars). HL-matriptase and L-matriptase (2.5 nM each) were incubated for 15 min with sHAI-1 NIK^1LK^2 (15 nM) or sHAI-1 NIK^1 (8 nM), and the reaction was initiated by adding the substrate at a final concentration of 1 mM (grey bars). Black bars indicate the reaction initiated by adding HL-matriptase and L-matriptase at a final concentration of 2.5 nM to HEPES buffer containing 17 nM sHAI-1 NIK^1LK^2 (or 9 nM sHAI-1 NIK^1) and 1.1 mM substrate. All values are expressed as means ± SD of at least two separate experiments.

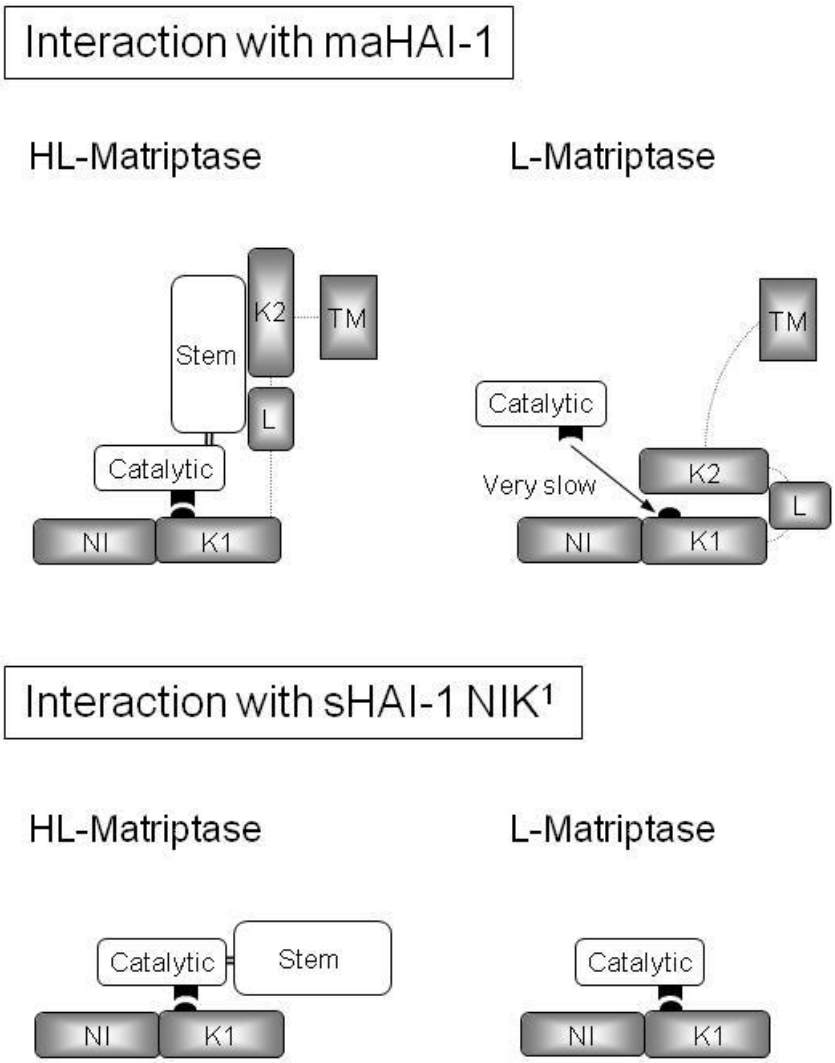

Fig. 7. A schematic model for interaction of r-matriptase variants with maHAI-1 and sHAI-1 NIK[1] in the hydrolysis of Boc-D(OBzl)-PR-MCA. Spacer regions of maHAI-1 are indicated by dashed line or curve. The disulfide bond between the stem domain and the catalytic domain of HL-matriptase is indicated by double line. The matriptase binding site in Kunitz domain I and the active site of matriptase are indicated (black). The N-terminal and internal domains of maHAI-1 are illustrated as one rectangle (NI). Catalytic, catalytic domain; K1, Kunitz domain I; K2, Kunitz domain II; L; LDLRA domain; NI, N-terminal and internal domains; Stem, stem domain; TM, transmembrane domain.

Chapter 3

Involvement of Val315 Located in the C-terminal Region of Thermolysin in Its Expression in *Escherichia coli* and Its Thermal Stability

Introduction

Thermolysin [EC 3.4.24.27] is a thermophilic and halophilic neutral metalloproteinase produced in the culture broth of *Bacillus thermoproteolyticus* (*21–23*). It has been widely utilized to the synthesis of peptides such as a precursor of an artificial sweetener aspartame (*22, 23*), and thus thermolysin is one of the most representative industrial enzymes.

It requires one zinc ion essential for enzyme activity and four calcium ions for structural stability (*57–59*). The molecular mass is 34.6 kDa based on the amino acid composition (316 amino acids) plus one zinc and four calcium atoms (*3*). It is a typical α+β protein (*59*) composed of the β-structure-rich N-terminal (residues 1–134) and α-structure-rich C-terminal (residues 135–316) domains. The majority of zinc metalloproteinases have the zinc-binding HEXXH motif. Thermolysin has the consensus motif, $H^{142}ELTH^{146}$, and His142, Glu143, and His146 are catalytically essential (*22, 25*). Its high-resolution crystal structures are available (*25*). Many variants of thermolysin and thermolysin-like proteases (TLPs) with enhanced catalytic activity and stability have been obtained using site-directed mutagenesis (*60–67*).

A TLP-ste variant, which has 4 times higher activity than the wild-type enzyme,

was constructed by the combined mutations of its four residues Asn116, Gln119, Asp150, and Gln225 (*65*), and the enzyme with enhanced stability was constructed by introducing a disulfide bond between positions 8 and 60 (the numbering of amino acid sequence of thermolysin was adopted for TLP-ste) (*66, 67*). Mutations to amino acid residues whose C_α atoms locate within 1.2 nm from the catalytic zinc atom were introduced. The variants with mutation of Asp150, Ile168, and Asn227 give remarkable stabilization (*61, 62*). It is also stabilized by mutating Leu155 located at the autodegradation site (*68*). Combination of the mutation of Ser65 to Pro and that of both Gly8 and Asn60 to Cys for introducing a disulfide bond as well as the case of TLP-ste (*66*) leads further stabilization (*62, 63*). Extensive combinations of effective mutations are more effective for increasing the catalytic activity and/or stability (*61*). For example, activity of a variant in which Leu144 is converted to Ser, Asp150 to Glu, and Ser53 to Asp is 10 times higher than that of wild-type thermolysin (WT) and the inactivation rate at 80^oC is decreased to 60% of that of WT (*61*). The stability of thermolysin is increased with stabilizing the Ca^{2+} ion (Ca3) which is located in the N-terminal domain and decreases with its destabilization (*69, 70*).

It has been shown that the stability of the N-terminal domain (or N-domain) is lower than that of C-terminal domain (C-domain); thus the stabilization of the N-domain rather than of the C-domain has been considered more effective for stabilizing thermolysin (*71*). The stabilization of the C-domain has been also effective for stabilizing variants in which N-terminal domain is already enough stabilized (*71*). Accordingly, stabilization of the C-domain is still useful for further stabilization of thermolysin. Previous studies on TLPs have shown that mutation of the C-terminus may indeed affect the stability of this type of proteases (*72*). This suggests a possibility that

some amino acid residues might have a significant role in the stability of the C-domain and the total structure of thermolysin. Stabilized mutants of TLPs were predicted using computational techniques and produced successfully (*73*).

In this Chapter, the author aimed to evaluate the effects of the C-terminal region of thermolysin on its activity and stability. It is known that proteins mutated to have lower stability have tendency to be easily digested in the host *Escherichia coli* cells (*74*) and the author intended to testify this empirical relationship in the present study. The author describes the effect of the truncation from the C-terminal end of thermolysin on its expression in the culture supernatant of the transformed *E. coli* cells and that the penultimate amino acid residue, Val315, is important for the expression of thermolysin. The expression amount of the thermolysin (EA) of the variants is in good agreement with the order of the hydrophathy index of the amino acid residue incorporated in position 315. Hydrophobic amino acids are favored at position 315 for high EA of the variant, which exhibits also high stability and activity. These findings may provide some insights into the molecular mechanism for the folding of thermolysin and techniques to design recombinant enzymes with enough EA.

Materials and Methods

Materials – Casein (Lot PEH5596) was purchased from Wako Pure Chemical (Osaka, Japan). *N*-[3-(2-Fury)acryloyl]-glycyl-L-leucine amide (FAGLA, Lot 111K1764) was from Sigma (St. Louis, MO). The concentration of FAGLA was determined spectrophotometrically using the molar absorption coefficient at 345 nm, ε_{345} = 766 M^{-1} cm^{-1} (*23*, *75*).

Expression and Purification of Thermolysin Variants – Expression and purification of thermolysin variants were performed according to the method described previously (*76*). *E. coli* K12 JM109 [*recA1, endA1, gyrA96, thi, hsdR17, supE44, relA1, Δ(lac-proAB), F'(traD36, proAB*$^{+}$ *lac*^{Iq}*, lacZΔM15*)] was used as host. An expression plasmid pTMP1 was used, which co-expresses the mature sequence combined with the pelB leader sequence at its N-terminus (as the pelB-mature sequence) and pre-prosequence in *E. coli* as separate polypeptides. Expression plasmids for thermolysin variants were constructed by polymerase chain reaction (PCR) using primers listed in Table 1 and pTMP1 as a template. Site-directed mutagenesis was carried out using a Quikchange^{TM} site-directed mutagenesis kit (Stratagene, La Jolla, CA). The nucleotide sequences of mutated thermolysin genes were verified with a Shimadzu DSQ-2000 DNA sequencer (Kyoto, Japan). Site-directed mutagenesis and production of the variants was performed as described previously (*61, 76, 77*). Briefly, the seed culture (5 ml) of the transformed JM109 cells was diluted 100 times with 500 ml of L broth in a 1-liter flask and incubated at 37^{o}C for 48 h, with 0.1% (w/v) anti-foam A (Sigma) and vigorous aeration. At the end of the culture, a 500-ml supernatant was obtained. The cell number reached the maximum at around 24 h from the start of cultivation and decreased after this gradually. The casein-hydrolysis activity increased with the cultivation time and reached the maximum at around 36 h and this activity level was almost kept even at 48 and 72 h with a slight increase (*64*). The 48-h cultivation was confirmed to be optimal for expression of thermolysin variants before starting the present study.

For the purification of thermolysin variants, three liters of the culture supernatants of *E. coli* transformants with low protein expression (Δ315–316, Δ314–316, Δ313–316,

Δ312–316, Δ298–316, V315G, V315W, V315D, V315E, V315R, and V315K) obtained by cultivation for 72 h were used, while 0.5 liters were used for the other transformants. Thermolysin variants were purified to homogeneity from the culture supernatant with hydrophobic-interaction chromatography followed by affinity chromatography with a column [10 mm (inner diameter) x 50 mm] of glycyl-D-phenylalanine (Gly-D-Phe) coupled to a Cyanogen-bromide (CNB)-activated Sepharose 4B resin (GE Healthcare, Buckingshire, UK) equilibrated with 20 mM acetate-NaOH buffer (pH 5.5) containing 10 mM $CaCl_2$ (designated as buffer A hereinafter). Thermolysin variants were eluted by buffer A added with 20% (v/v) 2-propanol and 2.5 M NaCl at a flow rate of 1 ml/min. Prior to kinetic measurements, the preparations were desalted using pre-packed PD-10 gel filtration columns (GE Healthcare) in 40 mM Tris-HCl (pH 7.5) (designated as buffer B) added with 10 mM $CaCl_2$ (which is designated as buffer B*) and stored at 4^oC.

Sodium Dodecyl Sulfate-Polyacryl Amide Gel Electrophoresis (SDS-PAGE) – SDS-PAGE was performed in a 12.5% polyacrylamide gel under reducing conditions according to the method of Laemmli (*54*). A constant current of 40 mA was applied for 40 min. Samples were reduced by treatment with 2.5% 2-mercaptoethanol at 100°C for 10 min. Proteins were stained with Coomassie Brilliant Blue (CBB) R-250. The molecular-mass marker kit consisting of rabbit muscle phosphorylase *b* (97.4 kDa), bovine serum albumin (66.4 kDa), hen egg-white ovalbumin (44.3 kDa), bovine carbonic anhydrase (29.0 kDa), soybean trypsin inhibitor (20.1 kDa), and hen egg white lysozyme (14.3 kDa) was from Takara Bio (Otsu, Japan).

Hydrolysis of Casein – The casein-hydrolysis activity of thermolysin was determined according to the methods described previously (*22, 60*). The thermolysin solution (187.5 μl) was added to 562.5 μl of 1.33% (w/v) casein and 40 mM Tris-HCl (pH 7.5) (designated as buffer B hereinafter), and incubated at 25°C for 30 min. The reaction was stopped by adding 0.75 μl of a solution containing 0.11 M trichloroacetic acid, 0.22 M sodium acetate, and 0.33 M acetic acid. After 30-min incubation at 25°C, the reaction mixture was filtered through Whatman No. 2 filter paper (70 mm in diameter), and the absorbance at 275 nm (A_{275}) was measured. One proteolytic unit (PU) of activity is defined as the amount of enzyme activity needed to liberate a quantity of acid soluble peptides corresponding to an increase in A_{275} of 0.0074 cm^{-1} min^{-1} (A_{275} of 1 μg of tyrosine per min).

Hydrolysis of FAGLA – The thermolysin-catalyzed hydrolysis of FAGLA was measured by following the decrease in absorbance (A_{345}) at 345 nm in buffer B* at 25°C (*23, 75*). The amount of FAGLA hydrolyzed was evaluated using the molar absorption difference due to hydrolysis, $\Delta\varepsilon_{345} = -310$ M^{-1} cm^{-1}. The hydrolysis was carried out under pseudo-first-order conditions, where the substrate concentration is much lower than the Michaelis constant (K_m) (>30 mM) (*23*). Under the conditions, the molecular activity (k_{cat}) and K_m could not be determined separately, and the enzyme activity was evaluated by the specificity constant (k_{cat}/K_m)

Far-UV CD Spectra – The CD spectra were measured using 0.2-cm cell with a Jasco J-820 spectropolarimeter (Tokyo, Japan) equipped with a Peltier system of cell temperature control. The measurement conditions were: spectral range, 200-250 nm;

sensitivity, 100 mdeg; resolution, 0.2 nm; response time, 4 s; scan speed, 20 nm min^{-1}; the number of accumulations, 4; and the protein concentration, 1.0 μM in buffer B*. CD spectra were processed with a Jasco software, and finally expressed in mean-residue molar ellipticity, [θ] (deg cm^2 $dmol^{-1}$). The α-helix content of was calculated from the mean-residue molar ellipticity at 222 nm ([θ]$_{222}$ (deg cm^2 $dmol^{-1}$)) (*78*).

Thermal Denaturation of Thermolysin – Thermolysin (2.5 μM) in buffer B* was incubated at 25°C for 5 min. Then the thermolysin solution (400 μl) was transferred to a 0.2-cm quartz cell, and mineral oil (50 μl) was added to avoid evaporation. Thermal denaturation was examined by monitoring the θ_{222} with increasing cell temperature from 60 to 100°C at a rate of 0.5°C min^{-1}. The fraction unfolded (F_u) was determined after normalizing θ_{222} of native and denatured thermolysin between 0 and 1, according to Eq. 1.

$$F_u = (A_o - A_N) / (A_D - A_N) \qquad \text{(Eq. 1)}$$

where A_o is the observed θ_{222} of thermolysin at a temperature and A_N and A_D are the θ_{222} values of native and denatured enzymes, respectively. The denaturation process is irreversible and is accompanied with autolysis (*71*, *72*). The temperature at which F_u is given by 0.5 is defined as the observed melting temperature (the temperature at which 50% of the thermolysin molecules is denatured), $T_{m,\,app}$.

Thermal Inactivation of Thermolysin – Thermolysin (2.5 μM) in buffer B* was incubated at a temperature ranging from 60 to 75°C for a specified time (2–32 min).

Then, it was cooled at 25°C for 5 min and the FAGLA-hydrolysis activity was determined by the method described above. It is known that the thermal inactivation of thermolysin is irreversible and consists of only one step, the first-order rate constant, k_{obs}, of the inactivation was evaluated by plotting logarithm of the residual activity (k_{cat}/K_m) against the duration time of thermal treatment (*71, 72*). The activation energy, E_a, for the thermal inactivation of thermolysin was determined accoriding to Arrhenius equation by plotting logarithm of k_{obs} against $1/T$ where T is the temperature in Kelvin.

Thermal inactivation of thermolysin was handled to obey the first-order reaction, Eq. 2:

$$\ln ([E]_t/[E]_o) = - k_{obs}t \qquad \text{(Eq. 2)}$$

where $[E]_t$ and $[E]_o$ are the enzyme concentrations at incubation time (t) at temperature T and at time zero. The temperature (T_{50}) is defined as a temperature at which the enzyme loses 50% of the activity in the incubation for 30 min. Thus T_{50} is represented as a temperature at which the k_{obs} value is given as 3.85×10^{-4} s^{-1} when the enzyme is incubated for 30 min.

Results

Expression of Truncated Thermolysin Variants – A truncated thermolysin variant, Δ298–316, lacking the C-terminal α-helix (residue 298–316) was failed to be produced in the expression system used, suggesting that amino acid residues necessary for thermolysin expression might be contained in the C-terminal α-helix. The transformants

for the variants lacking Lys316, Val315–Lys316, Gly314–Lys316, and Val313–Lys316, designated as Δ316, Δ315–316, Δ314–316, and Δ313–316, respectively, were cultivated in *E. coli* at 37°C for 48 h. The 34.6-kDa protein bands corresponding to thermolysin were detected in SDS-PAGE for the supernatants of WT and Δ316 but not those of Δ315–316, Δ314–316, and Δ313–316 (Fig. 1). The casein-hydrolysis activity in the supernatant of Δ316 was 126 ± 1 PU/ml comparable to that of WT, and not detected with Δ315–316, Δ314–316, and Δ313–316 (detection limit: 2 PU/ml). These results indicate that truncation of the C-terminal Lys316 has no effect on the thermolysin expression but the penultimate residue Val315 is critical.

Expression and Purification of Val315 Variants of Thermolysin – The expression of fourteen Val315 variants was examined (Fig. 2). The casein-hydrolysis activities observed in the culture supernatants of the variants varied but well correlated with the intensities of the 34.6-kDa protein bands corresponding to thermolysin variants. The variants were classified into four groups based on their casein-hydrolysis activities (PU/ml-supernatant) produced in the supernatants. As the volumes of the supernatants produced from all cultures for 48 h at 37°C were almost the same as 500 ml, this classification is that based on the total casein-hydrolysis activities of the supernatants: Group A, showing 104–91% activity relative to that of WT, includes Δ316, V315L, and V315I; group B, showing 77–66%, includes V315A, V315T, and V315F; group C, showing 39–21%, includes V315S, V315Q, and V315Y; and group D, showing 8–2%, includes V315G, V315W, V315D, V315E, V315K, and V315R (Table 2). All variants were purified to homogeity as judged by SDS-PAGE (Fig. 3) and showed the molecular mass of 34.6 kDa. They are produced in *E. coli* culture supernatants and purified in an

intact form without any damage.

Far-UV CD Spectra of Thermolysin Variants – CD spectra of WT and the variants were measured in buffer B* (pH 7.5) and at 25°C (Fig. 4) and the α-helix contents (HCs) were calculated from the $[\theta]_{222}$ values (Table 2). The HC of WT was 36%, consistent with that previously reported (*79*). The HCs of the variants of groups A, B, and C are 36–31%. Among them, the HCs (36–34%) of Δ316, V315L, V315Y, and V315T are in good agreement with that of WT, while those (32–31%) of V315A, V315I, V315F, and V315S are in reasonable agreement. On the other hand, the HCs of V315Q and the variants of group D are considerably low (29–22%). In other words, the relative α-helix contents (RHCs) of the variants in groups A–C and D are 100–86% and 81–61% to that of WT, respectively. This suggests that the degree of expression of the variants has some correlation with their secondary structures.

Casein- and FAGLA- Hydrolysis Activities of Thermolysin Variants – The Δ316, Δ315–316, and all Val315 variants showed casein- and FAGLA-hydrolysis activities at pH 7.5 and at 25°C (Tables 2 and 3). All variants except for V315W keep activities toward both substrates higher than 70% of those of WT. The activities of V315W are significantly low. The orders of the variants in the activities toward both substrates are almost the same. The relative activities of V315G for casein and FAGLA are 80% and 70% of those of WT. The substitution of Val315 with a charged residue decreased the activity in a complicated manner. The relative casein-hydrolysis activities of V315R and V315K were 70 and 50%, whereas those of V315D and V315E were 80 and 90%. The relative FAGLA-hydrolysis activities of both V315D and V315E were 70%, whereas

those of V315R and V315K were 90 and 80%. By taking ratios of the relative activities for casein and FAGLA of the respective variants, namely by dividing the numerals in parentheses in the column of the casein-hydrolysis activity of purified variants (Table 2) by those in the column of the (k_{cat}/K_m) values at 0 M NaCl of the FAGLA-hydrolysis activity (Table 3), substrate specificity of the variants was evaluated. The order is: V315W (1.5) >> V315E (1.3) > V315G (1.2) > Δ315–316 = V315D = Δ316 (1.1) > WT = V315L = V315I = V315Y (1.0) > V315T = V315A = V315F = V315Q (0.9) > V315S = V315R (0.8) >> V315K (0.6). This order indicates that V315W, V315E, and V315G favor casein rather than FAGLA while V315K, V315R, and V315S favor FAGLA rather than casein. The characteristics of the residue incorporated at position 315, which is 2.2 nm far from the active site are not so critical to the enzyme activity. However, some amino acid incorporated changed significantly the substrate specificity. This effect might be transferred through a long-range interaction from the C-terminal region to the active site.

Expression Amounts of Thermolysin Variants – The expression amount (EA) of the variant was defined as a weight (mg) of the variant protein produced in a 500-ml culture supernatant during the cultivation of the transformant at 37°C for 48 h. It was calculated in the division of the total casein-hydrolysis activity [proteolytic unit (PU)] contained in the supernatant by the specific activity (PU/mg) of the variant purified from the supernatant (Table 2). The EA (μg/ml) given in Table 2 is shown as the weight of the variant in one-ml of the supernatant out of 500 ml. In the case of WT, the EA was 9.3 ± 0.7 μg/ml, thus indicating that the total amount of the WT protein produced in the culture must be 4.7 ± 0.4 mg. The relative EA or REA (as shown in the parentheses of

the 3rd column in Table 2) was defined as the ratio of the EA of the variant to that of WT.

The EAs of Δ316 and V315L were almost the same as that of WT, and that of V315I was 20% higher than that of WT. Those three are the member of group A. V315F, V315A, and V315T, giving REAs of 90 to 80% are the group B members. V315Q, V315S, and V315Y, giving 40% to 20%, are the group C members. V315G, V315K, V315R, V315W, V315D, and V315E, giving <10%, are the group D members. Grouping of the variants based on the EA is in good agreement with that based on the casein-hydrolysis activity in the supernatants.

Effect of NaCl on the Catalytic Activities of Thermolysin Variants – Thermolysin is remarkably activated by high concentrations (1–5 M) of mono-valent salts such as LiCl, NaCl, KBr, etc. and the activity increases in an exponential fashion with increasing salt concentration (*23, 80, 81*). This activation is solely due to increase in k_{cat}. The effects of NaCl on the activity of the variants were examined (Table 3). The degree of activation (DA) is defined as the value obtained by dividing the FAGLA-hydrolysis activity in the presence of 4 M NaCl by that in the absence, and the value of WT was 17 (*80*). The DAs of the variants were all within the range of 15–18, indicating that the modification at Val315 and truncation of the C-terminal residues examined here give substantially no effect on the salt-induced activation of thermolysin. Relationship between the salt-induced activation, and effects of anions and cations of salts on the structures of thermolysin and bulk water have been suggested (*81, 82*). The present result suggests that Na^+ and/or Cl^- ions have no significant interaction with the C-terminal end of thermolysin. The hydrophobic interaction is stabilized with high concentration of salts,

although electrostatic and hydrogen-bonding interactions are destabilized (*83*). The variants in which Val315 was replaced with more hydrophobic residues like Leu, Ile, and Trp showed higher DAs than those with less hydrophobic ones. This suggests that the stability of the C-terminal hydrophobic cluster might be significant for the enzyme activity.

Thermal Unfolding of Thermolysin Variants – The effect of substituting Val315 with any other amino acid residues on its stability was examined by CD measurement. The CD signal at 222 nm ($[\theta]_{222}$), was continuously measured with increasing the cell temperature (Fig. 5) and the $T_{m,\ app}$ was determined for each variant (Table 2). The $T_{m,\ app}$ of WT was 88.8°C being in good agreement with that measured by differential scanning calorimetry (*84*) and the variants examined are all destabilized in comparison with WT. The order of the variants in the $T_{m,\ app}$ values: WT > (Δ316 = V315I) > (V315L = V315T = V315A) > V315F > V315S > V315Q > V315Y > V315D > V315G > V315E > V315K > V315W > V315R > Δ315–Δ316. The effect of the amino acid substitution was assessed by the difference ($\Delta T_{m,\ app}$) in the $T_{m,\ app}$ of the variant from that of WT [namely, $\Delta T_{m,\ app}$ = ($T_{m,\ app}$ of the variant) – ($T_{m,\ app}$ of WT)]. The variants classified in group A (Table 2) show relatively small $\Delta T_{m,\ app}$ values ranging from –2.2 to –1.0°C. The $\Delta T_{m,\ app}$ of Δ316 was –1.0°C and that of Δ315–316 was –12.8°C, indicating that Δ316 is the most stable and Δ315–316 is the most unstable variants among all examined. Deletion of the C-terminal Lys316 is not much effective on the stability, although additional deletion of Val315 causes extensive damage, suggesting that Val315 plays a critical role in thermolysin stability. This result is well correspondent with that observed with *B. subtilis* neutral protease (*72*). The $T_{m,\ app}$ value

of Δ315–316 is similar to those of V315E, V315K, V315W, and V315R, showing that Glu, Lys, Trp, and Arg residues at position 315 have no contribution in the stability. Good correlation is observed between the $T_{m, app}$ values of the variants in groups B, C, and D were in the ranges of –3.5 to –2.2; –8.0 to –4.0; and –12.8 to –8.0, respectively, indicating that the higher the EA of the variant is, the higher its stability is.

Thermal Inactivation of Thermolysin Variants – Thermal inactivation of variants V315I, V315T, and V315R was examined by incubating at temperatures of 60°C, 65 °C, 70°C, and 75°C. The semi-logarithmic plots of the remaining activity after thermal incubation against the incubation time gave the linear relationship, suggesting that all inactivation processes followed pseudo-first order kinetics (Fig. 6). The first-order rate constant k_{obs} (s^{-1}) values for thermal inactivation of WT, V315I, V315T, and V315R increased with increasing temperatures from 60°C to 75°C, and those at 75°C were (0.87 ± 0.10)×10^{-3}, (0.80 ± 0.10)×10^{-3}, (0.93 ± 0.10)×10^{-3}, and (1.98 ± 0.10)×10^{-3}, respectively. Linear relationship was observed in Arrhenius plot for k_{obs} to evaluate the activation energy (E_a) for thermal inactivation. The E_a values (kJ mol^{-1}) are as in the order: V315R (95 ± 3) > WT (66 ± 3) > V315I (60 ± 1) > V315T (60 ± 5). On the other hand, the T_{50} (°C) values of the variants were calculated and are in the order of WT (60.5 ± 0.1) = V315I (60.5 ± 0.7) > V315T (58.2 ± 0.9) > V315R (57.5 ± 0.6). Interestingly, V315R has the largest E_a and smallest T_{50} values among the variants examined.

Discussion

Relationship between the Activity and Stability of Val315 Variants – Group A variants show 120–100% in REAs and 95–87% in RHCs comparing with those of WT. Group B variants show 80–70% in REAs and 99–86% in RHCs, group C variants, 40–20% in REAs and 95–76% in RHCs; and group D variants, 10% or less in REAs and 80–62% in RHCs. The enzyme avtivities of the variants for both casein and FAGLA substrates decrease with decreasing REA and RHC and also decreasing the stability as given by $\Delta T_{m,\ app}$. It is noticeable that the enzyme activites are not much clearly distinguished between groups B and C, though the REA, RHC, and $\Delta T_{m,\ app}$ are distinctly different between them.

Roles of the Residue at Position 315 in the Expression of Thermolysin – The truncation of the C-terminal Lys316 as shown with the variant Δ316 has no effects on the EA, enzyme activities, $T_{m,\ app}$, and HC. This result is consistent with crystal-structural data indicating that Lys316 projects ouward from the C-terminal α-helix with no interactions with other residues. On the other hand, Val315 points toward the hydrophobic cluster formed by three α-helices together with Tyr217, Ile236, Phe281, Ser282, Arg285, Phe310, and Val313 (Fig. 7B) (*25*). TLPs from *B. stearothermophilus* and *B. cereus* bear Val315 and the C-terminal residues at position 316 of Tyr and Asn, respectively, as well as, Lys of thermolysin, and those of *B. subtilis* and *B. amyloliquefaciens* lack the residue at position 316 and Leu315 is the C-terminal end (*72*). It seems that the residue at position 316 is not always essential for TLPs. Val315 of TLPs plays an important role in forming the hydrophobic cluster (*85*). The

thermostability of *B. subtils* neutral protease was lowered by deleting Leu300 (correspondent to Val315 in thermolysin) or by replacing this by a polar amino acid, although the stability was increased upon replacing Leu300 by Phe (*72*). The Val315 variants in which Val315 is replaced with hydrophobic amino acid residues exhibited the similar EAs to that of WT (Table 2). In contrast, those replaced with hydrophilic residues, especially with charged ones, exhibited much lower EAs than that of WT.

The hydropathy index is regarded to represent the combined character of hydrophobic and hydrophilic tendencies of the side chain (*86*), and thus, should be suitable for characterizing amino acid residues in the protein structure. The REAs (%) of the Val315 variants (Table 2) were plotted against the hydropathy indexes of the amino acid residues introduced into position 315 (Fig. 8A). A positive linear correlation was observed with a correlation coefficient (CC) of 0.90 and the slope of 12, indicating that the REA increases by 12% as the increase in hydropathy of 1.0 unit.

Roles of the Residue at Position 315 in the Secondary Structure of Thermolysin – The α-helix content (HC) of WT is 36%, and those of the variants in groups A–C and D (Table 2) are 36–32% and 30–25%, respectively. Thermolysin contains seven α-helix segments (residues 67–87, 137–152, 159–180, 225–246, 260–274, 282–296, and 301–313) (*59*). Assuming that the HC of WT is given as the sum of the seven helix segments, the contribution of one segment to the HC might be approximately 5% in average. The difference in the HCs of the variants of group A–C from WT are 0–4% and those of variants of group D are 6–11%, suggesting that one of the α-helices might be unfolded in the former variants and one or two may be unfolded in the latter variants. As Val315 is only manipulated to prepare variants, the unfolded α-helices might be those at

the C-terminal region of thermolysin. It should be noteworthy that partially unfolded variants maintain the steric structure avoiding catastrophic unfolding and exhibiting considerably high activities (Tables 2 and 3). The unfolding processes (Fig. 5) represent some microscopic irregular changes including autolysis, and thus the processes might not obey a simple two-phase transition model. Especially, the process of V315W obviously has two inflection points, suggesting at least two steps in the unfolding. The partial unfolding of the α-helices does not bring severe damages to the activity, and this is consistent with the suggestion that the partially unfolded helices might be located at the C-terminal region far enough from the active site.

A possibility can be raised that a variant with low HC might be an equilibrium mixture of the extensively unfolded form and intact form of thermolysin, although this possibility might not be probable. The variants were purified homogeneously by affinity chromatography in which the affinity ligand (Gly-D-Phe) is designed so to bind with the substrate binding site and enzyme preparations thus purified might have enzyme activities as high as that of WT. If any extensively unfolded form was present with the intact enzyme, the former might be degraded easily by autolysis and the resulting fragments might be observed in SDS-PAGE, though no such fragments were detected and the protein giving 34.6 kDa in SDS-PAGE did not disappear even in a long incubation of the variant solution.

Roles of the Residue at Position 315 in the Thermostability of Thermolysin – If the unfolding of the α-helices of thermolysin was reversible, the unfolding was considered to obey two-state denaturation model, and the thermodynamic parameters, such as the changes in Gibbs energy, enthalpy, and entropy (ΔG^{o}, ΔH^{o}, and ΔS^{o}) under the standard

conditions can be calculated. However, the reversibility was not observed in the CD signal at 222 nm and the thermolysin protein was degraded into small fragments when WT was cooled to 60^{o}C after heated up to 100^{o}C, and this observation is consistent with that previously reported (*71, 87, 88*). Therefore, thermal inactivation of thermolysin is given by the combined effects of unfolding and autolysis, and the preferential autolysis site was identified as Leu155–Ile156 (*68*). Considerably high enzyme activities of all variants suggest that the autolysis would be occurred in elevating temperature in the denaturation study (Fig. 5). Thus, the $T_{m,\ app}$ values must be reflected by not only unfolding but also autolysis (Table 2) (*71, 73*). As the enzyme activities of the variants are almost the same, the contribution of autolysis in $T_{m,\ app}$ should be almost the same, with all variants, and so the variation in $T_{m,\ app}$ may be mainly connected with the stability of thermolysin, more precisely the α-helices at the C-terminal region.

The plot of $T_{m,\ app}$ of the Val315 variant against the hydrophathy index of the amino acid at position 315 gives a positive correlation with a CC of 0.84 (Fig. 8B). The slope of the plot is 1.1, indicating that $T_{m,\ app}$ increases by 1.1^{o}C as the increase in hydropathy index of 1.0 unit. The order of WT, V315I, V315T, and V315R for T_{50} values is also in good agreement with that of hydropathy index of the amino acid introduced at position 315. It is considered that a hydrophobic cluster formed around Val315 stabilizes the connection of two α-helix segments (residues 282–296 and 301–313) at the C-terminal region (*25*). V315 interacts with Phe218 and Ile237 through the hydrophobic effect. Phe218 and Ile237 also interact with hydrophobic Ala163 and Ala167 on α-helix structure. Therefore, there is a possibility that the hydrophobic properties of the residues at 315 might influence the coordination geometry around the zinc ion and the enzyme activity.

Correlation between the Expression Amounts and $T_{m, app}$ Values of Val315 Variants – A positive correlation was observed in the plot of the $T_{m, app}$ of the V315 variant against the REA with a CC of 0.94 (Fig. 8C). The slope of the plot is 0.094, indicating that the $T_{m, app}$ increases by 0.94°C as REA increases by 10%. The higher the stability of the variant is, the higher the amount of the variant produced in the culture supernatant is. It has been reported that proteins destabilized by mutagenesis are more susceptible to intracellular degradation (*74*). The result in Fig. 8C suggests that the variant with $T_{m, app}$ of 78°C would not be produced in the *E. coli* culture and that increasing the stability is a key factor to produce higher amount of thermolysin using the *E. coli* system.

Roles of the Residue at Position 315 in Casein- and FAGLA-Hydrolytic Activity of Thermolysin – The enzyme activities of the Val315 variant for casein and FAGLA were plotted against hydropathy index of the amino acid incorporated into position 315 (data not shown). A slight correlation was observed showing that the activities of variants having hydrophilic amino acids. The amino acid at position 315 not only affects the stability of the C-terminal cluster and thus the gross structure of thermolysin but also affects the catalytic events executed at the active site.

Recombinant enzymes are used industrially for clinical diagnoses (*89*) and synthesis of intermediates of medicine and pesticide (*90*). The EA of recombinant enzyme is an important issue because the cost of enzyme is fairly high and determines the cost of the products. Our results demonstrate that Val315, which locates surrounded by C-terminal α-helices, is important for the stability of thermolysin. Results of single-amino-acid-substitution showed that there are good correlations among the thermostability ($T_{m, app}$) of thermolysin, stability of C-teminal α-helices, the EA, and the

hydropathy index of the amino acid incorporated into position 315. The variants having hydrophobic residues at position 315 (such as WT, V315I, and V315L) show higher thermostability and HCs probably by stabilizing the C-terminal hydrophobic cluster and show higher EAs in the *E. coli* culture. On the other hand, the variants having hydrophilic, bulky, or small residues (such as V315R, V315E, V315W, and V315G) show lower thermostability and HCs probably by destabilizing the C-terminal hydrophobic cluster and give the lower EAs. All variants exhibit considerably high enzyme activity. Thus, the stability of the gross structure and HC are not directly related with the activity. The decrease in the HC observed with the low-stability variants from that with the high-stability variants might be due to destabilization of the C-terminal hydrophobic cluster. This suggests that stability in the C-terminal region has a significant effect on production of the variants in *E. coli* culture and that the variants with lower stability would be degraded during the folding and/or secretion processes. It is reminded that WT is the best as well as V315I and V315L in the thermostability, EA, and even in enzyme activity, and that the Val residue is most optimally selected at position 315 by nature.

Table 1. Nucleic acid sequences of primers used for constructing thermolysin variants.

Thermolysin variants	Primer sequence
All truncated variants (forward)	5’-TAAAGTGGTATCTCATCAGTGGGG-3’
Δ316 (reverse)	5’-CACCCCTACCGCATCAAAG-3’
Δ315–316 (reverse)	5’-CCCTACCGCATCAAAGGCC-3’
Δ314–316 (reverse)	5’-TACCGCATCAAAGGCCTGC-3’
Δ313–316 (reverse)	5’-CGCATCAAAGGCCTGCTTC-3’
Δ298–316 (reverse)	5’-ACCGTACAAGTCAGTGGCTGATTG-3’
V315G (forward)	5’-GATGCGGTAGGGGGGAAATAAAGTGG-3’
V315A (forward)	5’-GATGCGGTAGGGGCGAAATAAAGTGG-3’
V315L (forward)	5’-GATGCGGTAGGGCTGAAATAAAGTGG-3’
V315I (forward)	5’-GATGCGGTAGGGATTAAATAAAGTGG-3’
V315F (forward)	5’-GATGCGGTAGGGTTCAAATAAAGTGG-3’
V315Y (forward)	5’-GATGCGGTAGGGTATAAATAAAGTGG-3’
V315W (forward)	5’-GATGCGGTAGGGTGGAAATAAAGTGG-3’
V315S (forward)	5’-GATGCGGTAGGGTCGAAATAAAGTGG-3’
V315T (forward)	5’-GATGCGGTAGGGACGAAATAAAGTGG-3’
V315Q (forward)	5’-GATGCGGTAGGGCAGAAATAAAGTGG-3’
V315D (forward)	5’-GATGCGGTAGGGGACAAATAAAGTGG-3’
V315E (forward)	5’-GATGCGGTAGGGGAGAAATAAAGTGG-3’
V315R (forward)	5’-GATGCGGTAGGGCGTAAATAAAGTGG-3’
V315K (forward)	5’-GATGCGGTAGGGAAGAAATAAAGTGG-3’

“Forward” or “reverse” in parentheses shows that the primer was used as a forward primer or as a reverse primer, respectively. Underlined nucleic acid sequences in primers for Val315 variants indicate mutation sites. Reverse primers for Val315 variants (not shown in this table) have nucleic acid sequence complementary to respective forward primers.

Table 2. Casein-hydrolysis activities and expression amounts of WT and thermolysin variants in the culture supernatants of *E. coli* transformed with their expression plasmids, and α-helix contents and $T_{m, app}$ values of the variants.

Thermolysin	[a]Casein-hydrolysis activity in culture supernatant (PU/ml-supernatant)	[b]Casein-hydrolysis activity of purified thermolysin (PU/mg)	[c]Expression amount in culture supernatant (mg/ml-supernatant)	$T_{m, app}$ (^oC)	α-Helix content (%)	Hydropathy index of the residue at position 315
WT	121 ± 1 (1.0)	13 ± 1 (1.0)	9.3 ± 0.7 (1.0)	88.8	36 (1.0)	4.2
Δ316	126 ± 1 (1.0)	13 ± 1 (1.0)	9.7 ± 0.8 (1.0)	87.8 (–1.0)	34 (1.0)	4.2
Δ315–316	ND	11 ± 1 (0.8)	ND	76.0 (–12.8)	25 (0.7)	–
Δ314–316	ND	ND	ND	ND	ND	–
Δ313–316	ND	ND	ND	ND	ND	–
Δ312–316	ND	ND	ND	ND	ND	–
Δ298–316	ND	ND	ND	ND	ND	–
V315G	10 ± 1 (0.1)	11 ± 1 (0.8)	0.9 ± 0.1 (0.1)	80.5 (–8.3)	29 (0.8)	–0.4
V315A	86 ± 1 (0.7)	12 ± 1 (0.9)	7.2 ± 0.6 (0.8)	86.6 (–2.2)	32 (0.9)	1.8
V315L	110 ± 1 (0.9)	12 ± 1 (0.9)	9.2 ± 0.8 (1.0)	86.6 (–2.2)	36 (1.0)	3.8
V315I	120 ± 1 (1.0)	11 ± 1 (0.8)	10.9 ± 1.0 (1.2)	87.8 (–1.0)	31 (0.9)	4.5
V315F	80 ± 1 (0.7)	10 ± 1 (0.8)	8.0 ± 0.8 (0.9)	85.3 (–3.5)	31 (0.9)	2.8
V315Y	25 ± 1 (0.2)	12 ± 1 (0.9)	2.1 ± 0.2 (0.2)	80.8 (–8.0)	34 (1.0)	–1.3
V315W	3 ± 1 (0.02)	8 ± 1 (0.6)	0.4 ± 0.1 (0.04)	77.3 (–11.5)	24 (0.7)	–0.9
V315S	47 ± 1 (0.4)	12 ± 1 (0.9)	3.9 ± 0.3 (0.4)	84.8 (–4.0)	34 (0.9)	–0.8
V315T	93 ± 1 (0.8)	13 ± 1 (1.0)	7.2 ± 0.6 (0.8)	86.6 (–2.2)	36 (1.0)	–0.7
V315Q	27 ± 1 (0.2)	10 ± 1 (0.8)	2.7 ± 0.3 (0.3)	81.6 (–7.2)	27 (0.8)	–3.5
V315D	4 ± 1 (0.03)	10 ± 1 (0.8)	0.4 ± 0.1 (0.04)	80.8 (–8.0)	22 (0.6)	–3.5
V315E	4 ± 1 (0.03)	11 ± 1 (0.8)	0.4 ± 0.1 (0.04)	77.7 (–11.1)	25 (0.7)	–3.5
V315R	5 ± 1 (0.04)	9 ± 1 (0.7)	0.6 ± 0.1 (0.1)	76.7 (–12.1)	28 (0.8)	–4.5
V315K	5 ± 1 (0.04)	7 ± 1 (0.5)	0.7 ± 0.1 (0.1)	77.6 (–11.2)	22 (0.6)	–3.9

ND, not detected (detection limit was 2 PU/ml); Hydrolysis of casein was carried out in 40 mM Tris-HCl buffer (pH 7.5) at 25^{o}C. Numbers in parentheses indicate values relative to WT. The average of triplicate determination with SD value is shown. [a]Culture supernatants (500 ml) collected by the cultivation at 37^{o}C for 48 h were analyzed for casein-hydrolysis activities. [c]Expression amount (mg/ml-supernatant) of thermolysin variants was calculated in dividing the value of the column a by that of the column b.

Table 3. FAGLA-hydrolysis activities of purified thermolysin in the absence and presence of 4 M NaCl.

Thermolysin	$(k_{cat}/K_m) \times 10^{-4}$ (M^{-1} s^{-1})		Degree of activation (B)/(A)
	0 M NaCl (A)	4 M NaCl (B)	
WT	2.3 ± 0.2 (1.0)	39 ± 1 (1.0)	17 (1.0)
Δ316	2.1 ± 0.1 (0.9)	38 ± 3 (1.0)	18 (1.1)
Δ315–316	1.5 ± 0.1 (0.7)	22 ± 1 (0.6)	15 (0.9)
V315G	1.7 ± 0.1 (0.7)	29 ± 1 (0.7)	17 (1.0)
V315A	2.3 ± 0.1 (1.0)	40 ± 3 (1.0)	17 (1.0)
V315L	2.0 ± 0.1 (0.9)	36 ± 1 (0.9)	18 (1.1)
V315I	1.9 ± 0.2 (0.8)	36 ± 1 (0.9)	18 (1.1)
V315F	2.0 ± 0.2 (0.9)	33 ± 1 (0.8)	17 (1.0)
V315Y	2.1 ± 0.1 (0.9)	36 ± 2 (0.9)	17 (1.0)
V315W	1.0 ± 0.1 (0.4)	18 ± 1 (0.5)	18 (1.1)
V315S	2.5 ± 0.1 (1.1)	41 ± 1 (1.1)	16 (0.9)
V315T	2.5 ± 0.1 (1.1)	40 ± 2 (1.0)	16 (0.9)
V315Q	2.1 ± 0.1 (0.9)	36 ± 3 (0.9)	17 (1.0)
V315D	1.5 ± 0.1 (0.7)	22 ± 1 (0.6)	15 (0.9)
V315E	1.5 ± 0.1 (0.7)	26 ± 1 (0.7)	17 (1.0)
V315R	2.1 ± 0.1 (0.9)	37 ± 1 (0.9)	18 (1.1)
V315K	1.8 ± 0.1 (0.8)	31 ± 1 (0.8)	17 (1.0)

FAGLA-hydrolysis activities were measured at 25°C in 40 mM Tris-HCl buffer (pH 7.5) containing 10 mM $CaCl_2$ (buffer B*) in the absence and presence of NaCl. The average of triplicate determination with SD value is shown. Numbers in parenthesis indicate values relative to WT.

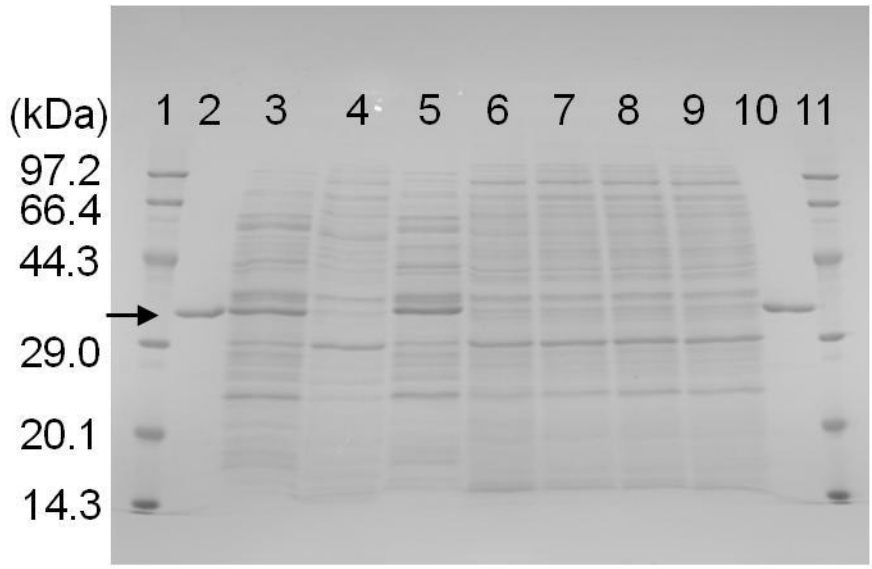

Fig. 1. SDS-PAGE analysis of culture supernatants of *E. coli* transformed with expression plasmids for the C-terminal deletion variants of thermolysin. The culture supernatants of the *E. coli* cultured in LB medium at 37^{o}C for 48 h were analyzed by SDS-PAGE. A 12.5% SDS-polyacrylamide gel was used and stained by CBB R-250. An arrow labeled with TLN indicates the position of 34.6 kDa corresponding to the molecular mass of thermolysin. Marker proteins (lanes 1 and 11); native thermolysin from *B. thermoproteolyticus* (lanes 2 and 10); the supernatants of *E. coli* transformed with the expression plasmids for wild-type (lane 3), pUC19 (lane 4), Δ316 (lane 5), Δ315–316 (lane 6), Δ314–316 (lane 7), Δ313–316 (lane 8), and Δ298–316 (lane 9).

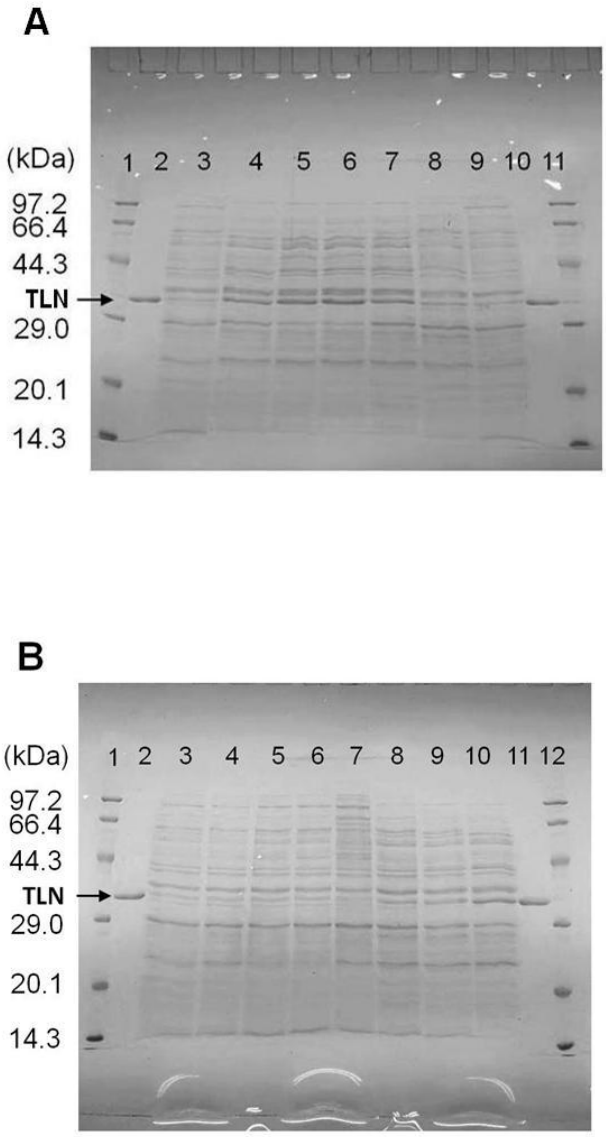

Fig. 2. SDS-PAGE analysis of culture supernatants of *E. coli* transformed with expression plasmids for Val315 variants of thermolysin. The culture supernatants of the *E. coli* cultured in LB medium at 37°C for 48 h were analyzed by SDS-PAGE. A 12.5% SDS-polyacrylamide gel was used and stained by CBB R-250. An arrow labeled with TLN indicates the position of 34.6 kDa corresponding to the molecular mass of thermolysin. (A) Marker proteins (lanes 1 and 11); native thermolysin from *B. thermoproteolyticus* (lanes 2 and 10); the supernatants of *E. coli* transformed with the expression plasmids for V315G (lane 3), V315A (lane 4), V315L (lane 5), V315I (lane 6), V315F (lane 7), V315Y (lane 8), and V315W (lane 9). (B) Marker proteins (lanes 1 and 12); native thermolysin from *B. thermoproteolyticus* (lanes 2 and 11); the supernatants of *E. coli* transformed with the expression plasmids for V315K (lane 3), V315R (lane 4), V315D (lane 5), V315E (lane 6), V315N (lane 7), V315Q (lane 8), V315S (lane 9), and V315T (lane 10).

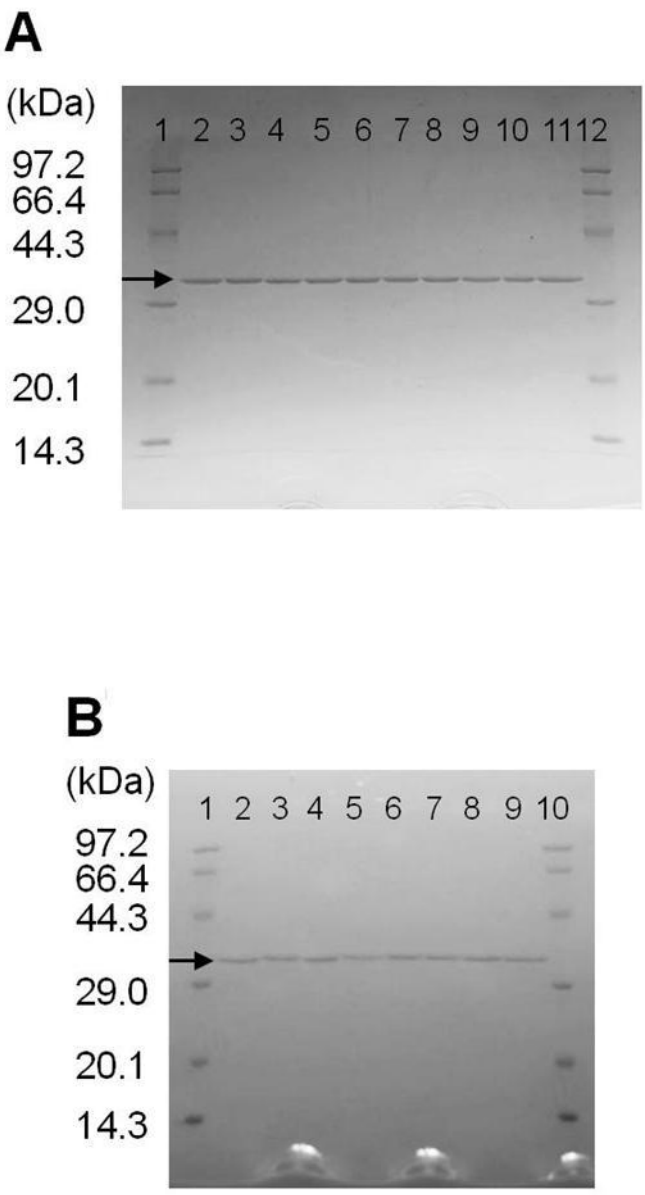

Fig. 3. SDS-PAGE analysis of purified wild-type (WT) thermolysin and thermolysin variants. One micro-gram each of WT and the variants was loaded onto the gel. A 12.5% SDS-polyacrylamide gel was used and stained by CBB R-250. An arrow at the left of the gel indicates the position of 34.6 kDa corresponding to the molecular mass of thermolysin. (A) Marker proteins (lanes 1 and 12), WT (lane 2), Δ316 (lane 3), V315A (lane 4), V315L (lane 5), V315I (lane 6), V315F (lane 7), V315Y (lane 8), V315Q (lane 9), V315S (lane 10), and V315T (lane 11). (B) Marker proteins (lanes 1 and 10), WT (lane 2), Δ315–316 (lane 3), V315G (lane 4), V315W (lane 5), V315D (lane 6), V315E (lane 7), V315K (lane 8), and V315R (lane 9).

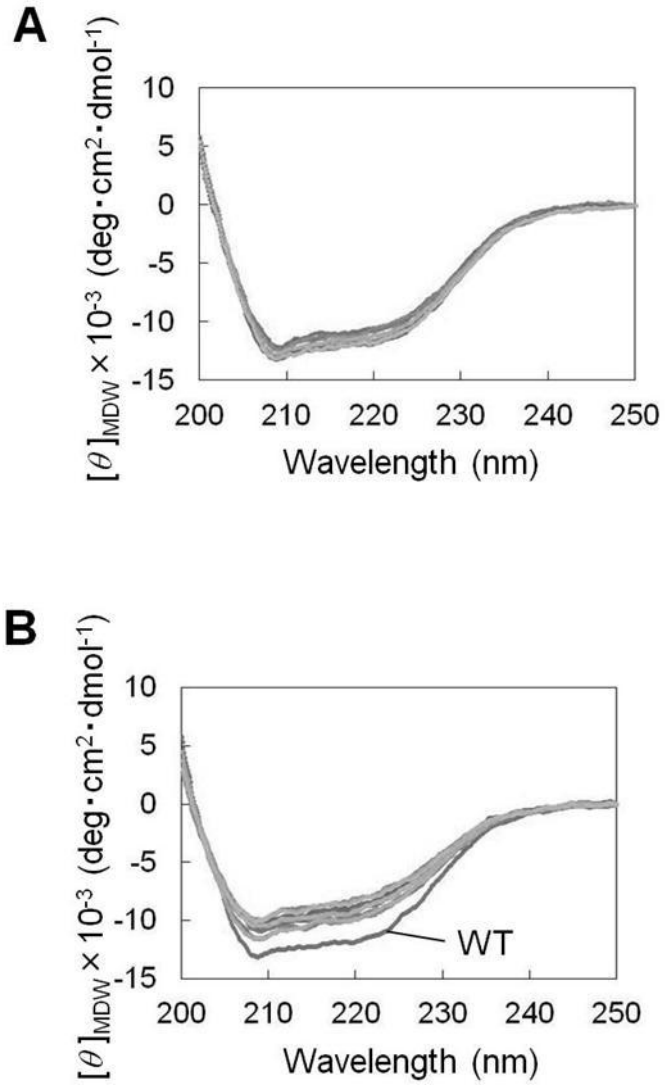

Fig. 4. CD spectra of wild-type (WT) thermolysin and thermolysin variants. CD spectra of WT and the variants (1 μM) in 40 mM Tris-HCl buffer (pH 7.5) containing 10 mM $CaCl_2$ (buffer B*) were recorded at 25°C. CD spectra. (A) WT, Δ316, V315A, V315L, V315I, V315F, V315Y, V315S, and V315T from the bottom to the top. (B) WT, V315Q, Δ315–316, V315G, V315W, V315D, V315E, V315K, and V315R from the bottom to the top.

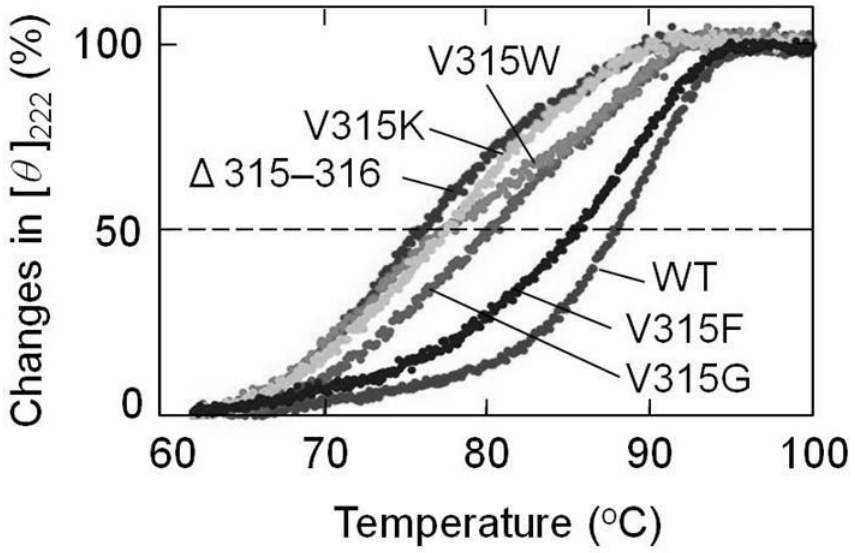

Fig. 5. Thermal denaturation of wild-type (WT) thermolysin and thermolysin variants. WT and the variants (2.5 μM) in buffer B* (pH 7.5) were heated from 60°C to 100°C at a rate of 0.5°C/min, and the changes in $[\theta]_{222}$ were recorded continuously. The denaturation curves of WT and 16 variants were measured and those of WT, Δ315–316, V315G, V315F, V315W, and V315K were shown as representatives.

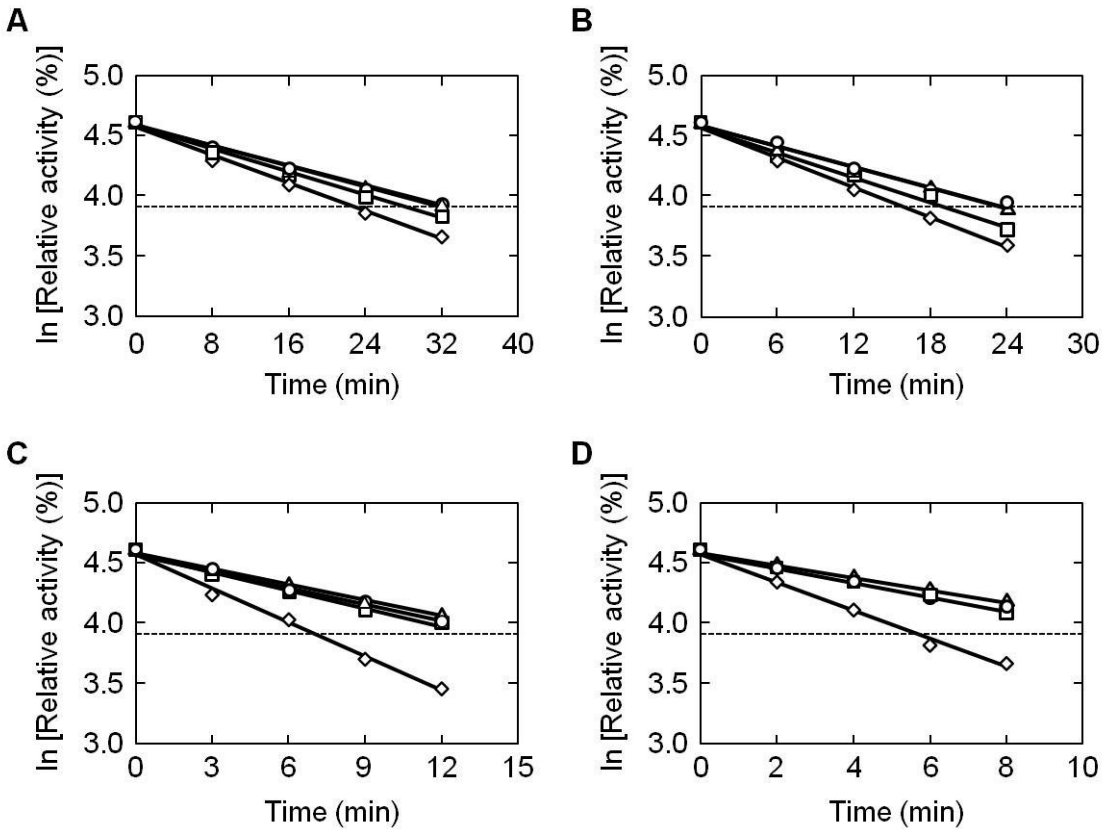

Fig. 6. Thermal denaturation of wild-type (WT) thermolysin and thermolysin variants at various temperatures. FAGLA-hydrolysis activities of WT and the variants were measured at 25°C after thermal incubation at 60°C (panel A), 65°C (panel B), 70°C (panel C), and 75°C (panel D) for specified time. The relative activity (k_{cat}/K_m) was expressed as the ratio of the activity observed after thermal incubation to that before the incubation. The natural logarithms of relative activities of WT and variants were plotted against incubation time at the specified temperature. The horizontal dotted line shows ln [Relative activity] given when the relative activity is 50%. Symbols: WT, ○; V315I, △; V315T, □; and V315R, ◇.

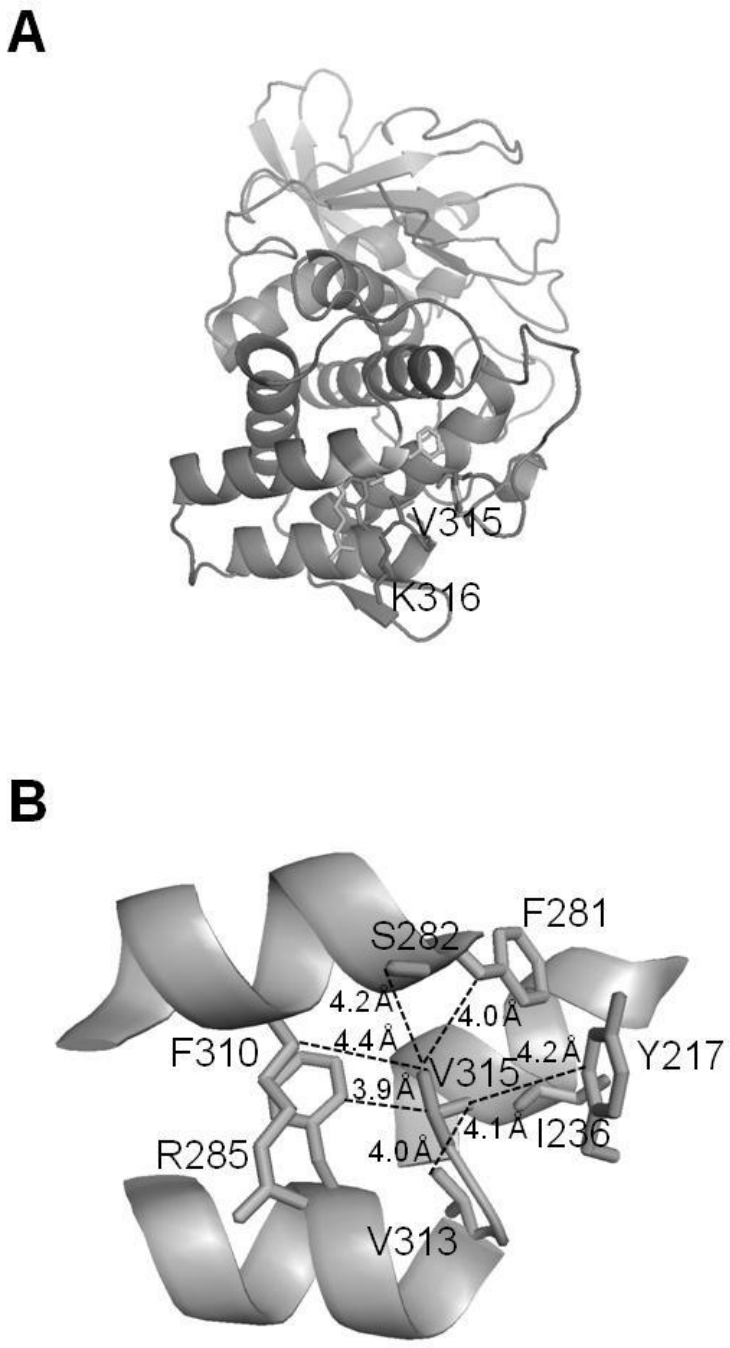

Fig. 7. Structute of thermolysin. The thermolysin structure is illustrated based on Protein Data Bank PDB number 8TLN [*59*]. (A) Overall structure of thermolsysin. (B) Close-up view of the C-terminal region of thermolysin.

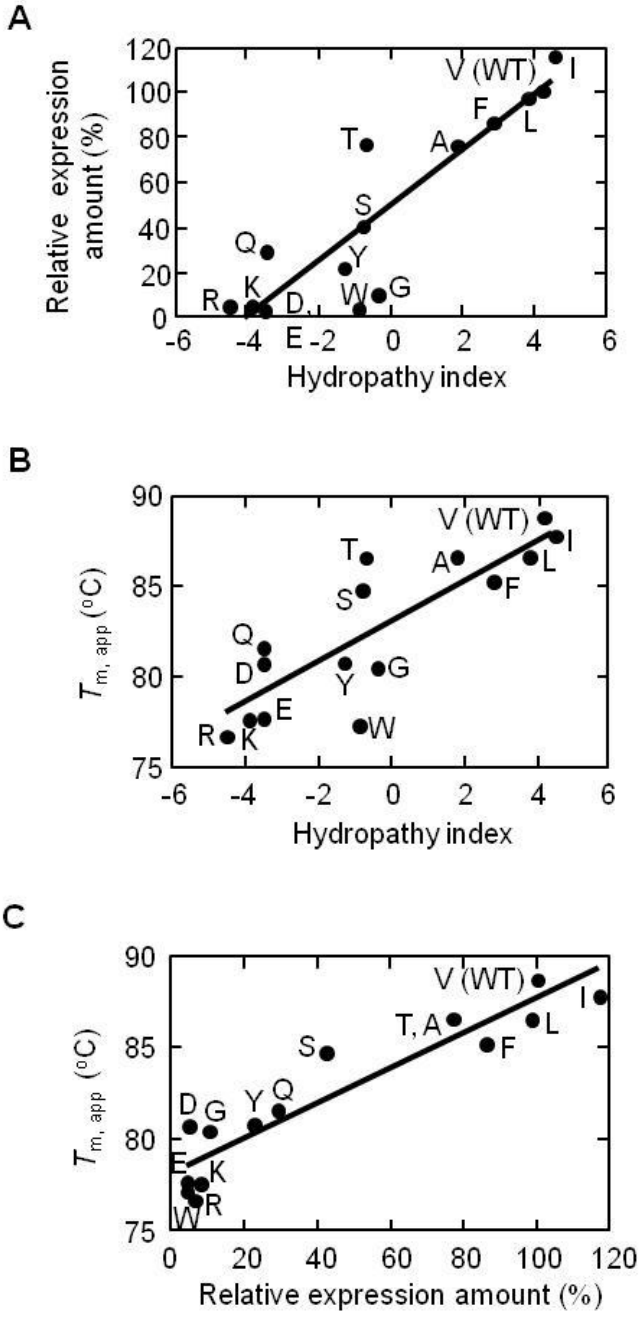

Fig. 8. Correlation between the relative expression amounts (REAs) and observed melting temperatures ($T_{m, app}$) of thermolysin variants and hydropathy indexes of the amino acid residues at position 315. (A) Correlation between the REAs and hydropathy indexes. The REA (%) is the ratio of the amount of the variants expressed in the culture supernatants incubated at 37°C for 48 h to that of WT (9.3±0.7 mg/l-supernatant). The amino acid residue at position 315 is shown as a single-letter amino acid code. The data were fitted by the least-squares regression (LSR) to a linear line given by y = 12x + 50 and *r* (correlation coefficient) = 0.90. (B) Correlation between the $T_{m, app}$ values and hydropathy indexes. The data were fitted by LSR to a linear line given by y = 1.1x + 83 and *r* = 0.84. (C) Correlation between the $T_{m, app}$ values and their REAs. The data were fitted by LSR to a linear line given by y = 0.094x + 78 and *r* = 0.94.

Chapter 4

Role of Leu202, a Residue Located at the S_1' Subsite of Thermolysin, on Its Substrate Specificity

Introduction

Thermolysin is widely used in industry for the peptide bond formation through reverse reaction of hydrolysis. The most extensive use is the synthesis of *N*-carbobenzoxy-L-aspartyl-L-phenylalanine methyl ester (ZDFM), a precursor of an artificial sweetener, aspartame, from *N*-carbobenzoxy-L-aspartic acid (ZD) and L-phenylalanine methyl ester (FM) (*23, 91*). Therefore, improvement of the activity and stability of thermolysin is an important subject.

Thermolysin catalyzes specifically the hydrolysis of peptide bonds containing bulky hydrophobic amino acid residues such as Phe and Leu at the P_1' position and also at the P_1 position [the subsites and the corresponding residues in the substrates were designated based on the nomenclature of Schechter, I. and Berger, A. (*92*)] (*80, 93*). Therefore, acetyl-D-Phe, succinyl-D-Leu, and Gly-D-Phe have been used as ligands in the affinity purification of thermolysin (*94–96*). It is reported that alcohols with 3 and 4 carbon atoms (such as 1-propanol, 2-propanol, 1-butanol or 2-butanol) strongly inhibit thermolysin activity (*97*). Crystallographic analysis has revealed that 2-propanol, the structure of which corresponds to the side chain of Leu, binds to the S_1' subsite of thermolysin (*98*). These findings support that Leu is the best residue fitted to the S_1' pocket.

The substrate-binding site of thermolysin is generally considered to be separated into four subsites; S_2, S_1, S_1', and S_2' (*22*). The S_1 subsite of thermolysin is formed by Phe114, and the S_1' subsite is by Phe130, Leu133, Val139, and Leu202 (*25–27*). In substrate recognition, the S_1 and S_1' bind with hydrophobic side chains of the P_1 and P_1' residues of substrate, while the main chain of the active-site sheet region (Asn112–Trp115) binds with the main chain of the substrate. Crystallographic analysis of thermolysin has shown the substrate-unbound open form and substrate-bound closed form, suggesting the possible intrinsic movement between the two forms during catalysis (*25–27*). Figure 1 shows the overall structure of thermolysin with four residues in the S_1' subsite highlighted. Of these residues, Leu202 is thought to be the most important for substrate recognition because the interaction of Cδ of Leu202 with the P_1' side chain is always observed in thermolysin-inhibitor complexes (*99*). Kreiji *et al*. reported the site-directed mutagenesis study of Leu202 of thermolysin-like protease (TLP) from *B. stearothermophilus* (TLP-ste; [EC 3.4.24.4]) (*99*). TLP-ste is a well characterized TLP. It consists of 319 amino acid residues and differs at 44 residues among its 319 residues from thermolysin, which is composed of 316 residues, including a three-residue insertion. The numbering of the amino acid residues in thermolysin is applied to TLP-ste. They produced five single Leu202 variants and found that not only variants incorporated with less-bulky residues (Leu202→Gly, Ala, or Val) but also those with more bulky residues (Leu202→Phe or Tyr) decreased the activity (k_{cat}/K_m) for a substrate *N*-[3-(2-furyl)acryloyl]-glycyl-L-leucine amide (FAGLA), in which the P_1' residue is Leu, while increased the k_{cat}/K_m value for a substrate *N*-[3-(2-furyl)acryloyl]-glycyl-L-phenyalanine amide (FAGFA), in which the P_1' residue is Phe (*99*). This suggests that the S_1' subsite is suitable for recognizing Leu rather than

Phe of the P_1' position in substrate.

In this chapter, to clarify further the role of Leu202 in the catalytic activity and substrate specificity of thermolysin, 19 single variants by introducing mutations at position 202 were produced and characterized their hydrolysis activities for casein, neutral substrates FAGLA and *N*-[3-(2-furyl)acryloyl]-L-alanyl-L-phenylalanine amide (FAAFA), and a negatively charged substrate ZDFM. The results indicate that all Leu202 variants retain hydrolysis activity for the substrates examined and that the correlations between the activities for different substrates are even weak, suggesting that Leu202 is not much critical for catalytic activity but plays an important role in substrate specificity of thermolysin.

Materials and Methods

Materials – Casein (Lot WKL1761) was purchased from Wako Pure Chemical (Osaka, Japan). FAGLA (Lot 57H5800) and FAAFA (Lot 093K1396) were from Sigma (St. Louis, MO). The concentrations of FAGLA and FAAFA were determined spectrophotometrically using the molar absorption coefficient, ε_{345} = 766 M^{-1} cm^{-1} (*23*, *75*). ZDFM was prepared as described previously (*23*), and its concentration was determined using the molar absorption coefficient ε_{257} = 387 M^{-1} cm^{-1} (*23*). All other chemicals were of reagent grade and purchased from Nacalai Tesque (Kyoto, Japan). All spectrophotometric measurements were done with a Shimadzu UV-visible recording spectrophotometer UVmini-1240 (Kyoto, Japan).

Production of Thermolysin Variants – Thermolysin variants were produced and

purified as described in chapter 3.

SDS-PAGE – SDS-PAGE was performed as described in Chapter 3.

Hydrolysis of Casein – Casein-hydrolysis activity of thermolysin was measured as described in Chapter 3.

Hydrolysis of FAGLA and FAAFA – The thermolysin-catalyzed hydrolysis of FAGLA and FAAFA was measured by following the decrease in absorbance at 345 nm, and the amount of furylacryloyl (FA)-dipeptide amides hydrolyzed was calculated using the difference of molar absorption coefficient due to hydrolysis, $\Delta\varepsilon_{345} = -310\ M^{-1}\ cm^{-1}$, at 25°C (*23, 75*). The FAGLA-hydrolysis was carried out in 40 mM Tris–HCl buffer (pH 7.5) containing 10 mM $CaCl_2$. The FAAFA-hydrolysis was done in 40 mM Tris–HCl buffer (pH 7.5) containing 10 mM $CaCl_2$ and 5% (v/v) DMSO. The hydrolysis was carried out under pseudo-first-order conditions, where the substrate concentration is much lower than the Michaelis constant (K_m) (> 30 mM) (*23*) because of the sparing solubility (< 6 mM) of FAGLA and FAAFA (*23, 75*). Under the conditions, the enzyme activity was evaluated by the specificity constant (k_{cat}/K_m).

Hydrolysis of ZDFM – The thermolysin-catalyzed hydrolysis of ZDFM was measured by following the decrease in absorbance at 224 nm, the amount of ZDFM hydrolyzed was calculated using the difference of molar absorption coefficient due to hydrolysis, $\Delta\varepsilon_{224} = -493\ M^{-1}\ cm^{-1}$, at 25°C (*23*). The reaction was carried out in 40 mM Tris–HCl buffer (pH 7.5) containing 10 mM $CaCl_2$. Under this condition, the k_{cat} and K_m

values were separately determined with Kaleida Graph Version 4.0 (Hulinks, Tokyo, Japan) based on the Michaelis-Menten equation by the non-linear least-squares regression (LSR) method.

Results

Purification of the Leu202 Variants – Leu202 of thermolysin was changed into either one of the 19 amino acids. Wild-type (WT) thermolysin and the thermolysin variants were expressed in the *E. coli* expression system (*76*), in which the mature- and pro-domains were expressed as independent polypeptides. Figure 2 shows SDS-PAGE of the purified preparations of WT thermolysin and the variants. They yielded a single band with a molecular mass of 34 kDa. From 500 ml of culture supernatants, 0.5–1.0 mg of purified preparations were obtained. CD spectra of the variants at 200–250 nm were essentially the same as that of WT (data not shown), suggesting that significant conformational change was not induced in thermolysin by mutation.

Casein-hydrolysis Activities of the Leu202 Variants – Table 1 shows the casein-hydrolysis activities of WT and the variants at pH 7.5 at 25^{o}C. All variants exhibited the activity. Their specific activities were in the range of 10–130% of that of WT (12,000 units/mg). The L202M variant, in which Leu202 is substituted with Met, exhibited the highest (130% of that of WT), while the L202K, L202R, L202D, and L202E variants, containing a positive or negative charge in the residue introduced at position 202, exhibited considerably lower activity (10–20% of that of WT).

FAGLA-hydrolysis Activities of the Leu202 Variants – Table 2 shows the FAGLA-hydrolysis activities of WT and Leu202 variants at pH 7.5 at 25°C. All variants exhibited the activity. At 0 M NaCl, the k_{cat}/K_m values were in the range of 4–260% of that of WT (20,000 M^{-1} s^{-1}). The L202Y variant exhibited the highest (260% of that of WT), while the L202N, L202Q, L202D, and L202E variants, containing a carboxyl or amide group in the residue introduced at position 202 exhibited much lower activities (4–10% of that of WT).

Table 2 also shows the k_{cat}/K_m value at 4 M NaCl and the degree of the NaCl-induced activation, which is defined as the ratio of the k_{cat}/K_m value at 4 M NaCl to that at 0 M NaCl, of WT and the variants at pH 7.5 at 25°C. All variants were activated by NaCl. The degree of activation by 4 M NaCl of WT is 17 as has been reported previously (*60, 100*) and those of the 19 variants were in the range of 7–40, being 40–240 % of that of WT.

ZDFM-hydrolysis Activities of the Leu202 Variants – Table 3 shows the ZDFM-hydrolysis activities of WT thermolysin and the Leu202 variants at pH 7.5 at 25°C. The L202W variant lacked activity. The K_m, k_{cat}, and k_{cat}/K_m values of the other 18 variants were in the range of 10–1,000, 20–410, and 10–370%, respectively, of those of WT (0.7 mM, 4.0 s^{-1}, and 5.7 mM^{-1} s^{-1}, respectively). The L202D and L202E variants, containing a negatively-charged side-chain in a residue introduced at position 202, exhibited fairly high K_m values (360–690% of that of WT) indicating that the interaction with the substrate ZDFM is much reduced in these variants. On the other hand, the L202F and L202Y, containing an aromatic group in a residue at position 202, exhibited much lower K_m values (10% of that of WT) indicating that the interaction with the substrate is

enhanced in these variants. It is noted that the variants (L202K and L202R) containing a positive charge introduced at position 202 showed almost the same K_m values as WT but exhibited fairly higher k_{cat} values (310–410% of that of WT). This suggests that these variants have almost the same ability as WT in the interaction with the ZDFM, although they are much preferable in formation of the transition state in comparison with WT. Consequently, L202D and L202E exhibited lower, and L202F, L202Y, L202K and L202R exhibited higher k_{cat}/K_m values (30–80 and 120–370% of that of WT, respectively) than those of WT.

FAAFA-hydrolysis Activities of the Leu202 Variants – Table 4 shows the FAAFA-hydrolysis activities of WT thermolysin and the Leu202 variants at pH 7.5 at 25^{o}C. The k_{cat}/K_m values of the variants were in the range of 10–950% of WT (79,000 M^{-1} s^{-1}). Like the case with FAGLA (Table 2), the L202Y variant exhibited the highest value (950% of that of WT). Interestingly, unlike the case with FAGLA, the L202K and L202R variants exhibited higher values (170–330%) than that of WT.

Discussion

Insights into the Role of Leu202 on Thermolysin Activity – Casein, FAGLA, and ZDFM are frequently used as substrates of thermolysin (*22, 60, 91, 99*). In this study, all variants except the L202W exhibited activities for these substrates, suggesting that Leu202 is not critical for the activity. This is in contrast to previous results with 70 active-site single variants, in which one of the twelve active-site residues (Ala113, Phe114, Trp115, Asp150, Tyr157, Gly162, Ile168, Ser169, Asp170, Asn227, Val230,

and Ser234) were mutated, that 41 variants lacked activity (*60*). In thermolysin, the zinc-binding motif sequence $H^{142}ELTH^{146}$ is located in a central α-helix (residues 137−152), and Glu166 which chelates the active-site zinc ion is located in another α-helix (residues 163−176). Leu202 is not contained in any α-helix, although Asp150, Tyr157, Gly162, Ile168, Ser169, and Asp170 are in α-helices. A possibility could be considered that mutation of a residue contained in an α-helix may affect the states of the residues in the same helix.

It has been suggested that the salt-induced activation of thermolysin results from combination of two effects of salt, namely, the effect on the structure of bulk-water and that on the enzyme structure. By adding high concentration of the neutral salt to the protein solution, the ions are shielded so that the electrostatic interactions are weakened and the water structure might be destroyed and thus the dielectric constant of the medium is decreased to enhance the hydrophobic interaction. These effects of salts on the water properties might affect the protein properties. On the other hand, there must be direct interactions of ions of salts with the protein surface to change the protein structure (*23, 81, 101, 102*). A conformation change induced in the active site is observed in the presence of 4 M NaCl by crystallographic analysis (*103*). Thermolysin exists in two conformers in a common buffer with low salt concentration, whereas it is in a conformer in the presence of 4 M NaCl. Presently, there is no evidence if this conformation change is related with the salt-induced activation or if this conformation change is resulted from the change in water structure or the interaction of the thermolysin surface with Na^+ and/or Cl^- ions.

The k_{cat}/K_m values of the Leu202 variants in the FAGLA hydrolysis at 0 M NaCl were compared with their degrees of activation by 4 M NaCl (Fig. 3). The correlation

coefficient, *r*, was −0.35, indicating weak negative correlation. This is in agreement with our previous results using the active-site single variants above described that the *r* was −0.54 (*60*).

Insights into the Role of Leu202 on the Substrate Specificity of Thermolysin – The k_{cat}/K_m values of the Leu202 variants for different substrates were compared (Fig. 4). The *r* value of the comparison between the k_{cat}/K_m values for FAGLA and the specific activities of casein was 0.21 (Fig. 4A), that between the k_{cat}/K_m values for ZDFM and the specific activities of casein was –0.45 (Fig. 4B), and that between the k_{cat}/K_m values for ZDFM and FAGLA was 0.40 (Fig. 4C). These *r* values indicate that all correlations are weak suggesting that Leu202 plays an important role in controlling the substrate specificity of thermolysin. This is in contrast to previous results obtained with the 70 active-site single variants that the *r* value for the comparison between the k_{cat}/K_m values for ZDFM and FAGLA is 0.84 (*60*). Only the L202Y exhibited higher activity in FAGLA-hydrolysis than WT (Table 2), while nine variants (L202A, L202V, L202F, L202Y, L202P, L202S, L202T, L202K, and L202R) exhibited higher activity (k_{cat}/K_m) in ZDFM-hydrolysis than WT (Table 3). All variants except the L202W, L202I, L202M, and L202H exhibited higher ratios of the k_{cat}/K_m values for ZDFM to those for FAGLA (Fig. 4D). ZDFM has a negatively-charged P_1 residue, Asp. The S_1 subsite is formed only by Phe114 (*25–27*). Accordingly, mutation at position 202 may affect the state of the S_1 subsite. It is noted that Trp115 located in the S_2 subsite could be replaced only to Phe and Tyr to exert activity, although the variants replaced with non-aromatic amino acids at this position never showed the activity (*104*) suggesting that an aromatic residue is indispensable at the S_2 subsite for thermolysin activity.

The k_{cat}/K_m values in the hydrolysis of two neutral substrates, FAGLA and FAAFA, by the Leu202 variants were compared (Fig. 5A). The *r* value was 0.84, indicating fairly good correlation. Unlike the case with FAGLA (Table 2), eight variants (L202V, L202F, L202Y, L202T, L202K, L202R, L202H, and L202E) exhibited higher FAAFA-hydrolysis activity than WT (Table 4). All variants except L202I, L202M, and L202P exhibited higher ratios of the k_{cat}/K_m values for FAAFA to those for FAGLA (Fig. 5B).

Streptomyces caespitosus neutral protease (ScNP), one of a zinc metalloproteinase with a molecular mass of 14 kDa, catalyzes specifically the hydrolysis of peptide bonds with aromatic amino acid residues at the P_1' position (*105, 106*): it cleaves FAAFA and does not FAGLA. It was reported that the S_1' subsite of this enzyme is composed of Gln71, Tyr75, Asp76, Val80, Gly105, Gly106, and Gly107 (*107*), and Val80 seems to correspond with Leu202 in thermolysin. These results suggest that mutations of Leu202 to other amino acids mostly make the S_1' subsite more preferable for the substrate with aromatic residues at the P_1' position. In other words, Leu202 may give an attribute to the S_1' to preferably accommodate the aliphatic residue Leu of the P_1' position. It should be reminded that the degrees of hydrophobicity of Leu and Phe are similar (*80, 108*). Therefore, the selection of Leu rather than Phe might be performed not only by hydrophobicity but by steric limitation of the S_1' subsite.

In this study, the mutation at position 202 was shown to confer various effects on substrate specificity depending on the characteristics of the introduced residue. However, the L202K and L202R variants with a positively-charged residue introduced at position 202 exhibited similar characteristics: the k_{cat}/K_m values of L202K and L202R for FAGLA were 60 and 30%, respectively, of that of WT, while those for ZDFM were 370

and 360% of that of WT, and those for FAAFA were 330 and 170%. The increased activity for ZDFM may be explained by the enforced electrostatic attraction between position 202 and the substrate. The decreased activity for FAGLA and increased one for FAAFA cannot be explained by the electrostatic interaction. It should be noted that the increased activity was observed with ZDFM and FAAFA, both of which have Phe as the P_1' residue. FAGLA has Leu as the P_1'. This suggests that the sizes of Lys and Arg introduced into position 202 of the S_1' subsite may be suitable to accommodate Phe rather than Leu of the P_1' position of substrate probably due to steric preference.

Thermodynamic Analysis of the ZDFM-hydrolysis Activities of the Leu202 Variants – To further examine the role of Leu202, thermodynamic analysis was carried out in the hydrolysis of ZDFM, a substrate to which the Michaelis-Menten treatment is applicable to determine k_{cat} and K_m, separately. The Gibbs energy for the binding between enzyme and substrate, ΔG^o, is the energy difference between free enzyme plus substrate and the enzyme-substrate complex. The activation Gibbs energy, $\Delta G^‡$, is the energy difference between free enzyme plus substrate and the transition state. ΔG^o and $\Delta G^‡$ were calculated according to Eq. 1 and 2, respectively (*109*).

$$\Delta G^o = -RT\,[\ln(1/K_m)] \qquad \text{(Eq. 1)}$$

$$\Delta G^‡ = -RT\,[\ln(k_{cat}/K_m) - \ln(RT/Nh)] \qquad \text{(Eq. 2)}$$

where R, T, N, and h are the gas constant (= 8.314 J K^{-1} mol^{-1}), absolute temperature, Avogadro number (= 6.022×10^{23} mol^{-1}), and Planck constant (= 6.626×10^{-34} J s), respectively. $\Delta\Delta G^o$ and $\Delta\Delta G^‡$ are defined as the changes in ΔG^o and $\Delta G^‡$, respectively,

induced by the mutation of Leu202 of WT thermolysin. The $\Delta\Delta G^{o}$ and $\Delta\Delta G^{\ddagger}$ values were compared (Fig. 6). The *r* was calculated to be 0.61 indicating relatively weak correlation. The more the ES complex is stabilized, the more the transition state is stabilized. However, some exceptional cases were also observed. The mutation of Leu202 into Lys or Arg did not change ΔG^{o}, however, with considerably decreasing $\Delta G^{\ddagger}$, suggesting that introduction of a positive charge might affect formation of the ES complex and transition state in a different manner from other mutations.

Relationship of Activities for Casein, FAGLA, FAAFA, and ZDFM against Hydropathy Index of the Residues Introduced at Position 202 – In Chapter 3, it was reported that the residue(s) in the C-terminal region of thermolysin, are strongly connected with the gross stability of the enzyme. They also affect the enzyme activity and substrate specificity suggesting that there might be a long-range interaction between the C-terminal region and active site. It is obvious that the substrate specificity is determined by various factors. Correlations between the hydrolytic activities of the variants for the respective substrates and hydropathy indexes of the amino acid residues at position 202 were examined (Fig. 7). Hydropathy index proposed by Kyte and Doolittle was exploited (*86*). The *r* values of the correlation with hydropathy index were: 0.66 for the casein-hydrolysis activity (Fig. 7A); 0.19 for the FAGLA-hydrolysis activity (Fig. 7B); –0.0047 for the FAAFA-hydrolysis activity and the index was –0.047 (Fig. 7C); –0.25 for the ZDFM-hydrolysis activity (Fig. 7D). These *r* values indicate a weak correlation for casein-hydrolysis activity and no correlation for the hydrolytic activities against the other dipeptide substrates. This may be caused by that casein has multiple cleavable sites by thermolysin as compared with the other dipeptide substrates

to suppress the effects of change in the substrate specificity by mutation. These low *r* values also suggests that preference for P_1' residue of substrates are determined not only by hydrophobicity of the S_1' pocket.

In conclusion, it has demonstrated that Leu202 located at the S_1' subsite of thermolysin plays an important role in its substrate specificity and that the substrate specificity could be modified by single mutation of Leu202.

Table 1. Casein-hydrolysis activities of the Leu202 thermolysin variants.

Thermolysin	Specific activity (units/mg)
WT	12,000 ± 200 (1.0)
L202G	3,200 ± 100 (0.3)
L202A	4,200 ± 100 (0.4)
L202V	3,500 ± 200 (0.3)
L202I	11,000 ± 100 (0.9)
L202M	15,300 ± 100 (1.3)
L202F	12,000 ± 200 (1.0)
L202Y	5,300 ± 100 (0.4)
L202W	3,400 ± 100 (0.3)
L202P	3,200 ± 100 (0.3)
L202S	4,600 ± 200 (0.4)
L202T	5,300 ± 100 (0.4)
L202C	5,800 ± 200 (0.5)
L202N	4,000 ± 200 (0.3)
L202Q	5,700 ± 100 (0.5)
L202K	1,500 ± 100 (0.1)
L202R	1,400 ± 100 (0.1)
L202H	5,200 ± 200 (0.4)
L202D	2,500 ± 100 (0.2)
L202E	2,500 ± 100 (0.2)

Hydrolysis of casein was carried out in 40 mM Tris-HCl buffer (pH 7.5) at 25^{o}C. Numbers in parentheses indicate the relative values by comparing the value for wild-type (WT) thermolysin. The mean value of triplicate determination and standard-deviation (SD) value are shown.

Table 2. FAGLA-hydrolysis activities at 0 or 4 M NaCl of the Leu202 thermolysin variants.

Thermolysin	$(k_{cat}/K_m)\times10^{-4}$ ($M^{-1}s^{-1}$)		
	0 M NaCl (A)	4 M NaCl (B)	(B) / (A)
WT	2.0 ± 0.2 (1.0)	34 ± 2 (1.0)	17 (1.0)
L202G	0.10 ± 0.03 (0.05)	1.5 ± 0.1 (0.04)	15 (0.9)
L202A	0.76 ± 0.01 (0.4)	19 ± 1 (0.6)	25 (1.5)
L202V	1.3 ± 0.1 (0.7)	28 ± 3 (0.8)	22 (1.3)
L202I	0.50 ± 0.02 (0.3)	11 ± 1 (0.3)	22 (1.3)
L202M	0.91 ± 0.01 (0.5)	14 ± 1 (0.4)	15 (0.9)
L202F	2.0 ± 0.1 (1.0)	28 ± 2 (0.8)	14 (0.8)
L202Y	5.1 ± 0.1 (2.6)	37 ± 5 (1.1)	7 (0.4)
L202W	0.90 ± 0.1 (0.5)	16 ± 1 (0.5)	18 (1.1)
L202P	1.2 ± 0.2 (0.6)	22 ± 1 (0.7)	18 (1.1)
L202S	0.90 ± 0.1 (0.5)	14 ± 1 (0.4)	16 (0.9)
L202T	1.3 ± 0.2 (0.7)	16 ± 1 (0.5)	12 (0.7)
L202C	0.50 ± 0.1 (0.3)	10 ± 1 (0.3)	20 (1.2)
L202N	0.08 ± 0.01 (0.04)	3.2 ± 0.2 (0.1)	40 (2.4)
L202Q	0.10 ± 0.01 (0.05)	1.5 ± 0.3 (0.04)	15 (0.9)
L202K	1.1 ± 0.0 (0.6)	36 ± 3 (1.1)	33 (1.9)
L202R	0.50 ± 0.0 (0.3)	8.7 ± 1 (0.3)	17 (1.0)
L202H	1.4 ± 0.1 (0.7)	49 ± 2 (1.4)	35 (2.1)
L202D	0.07 ± 0.02 (0.04)	1.3 ± 0.1 (0.04)	19 (1.1)
L202E	0.13 ± 0.01 (0.1)	1.9 ± 0.2 (0.06)	15 (0.9)

FAGLA-hydrolysis activity was measured in 40 mM Tris-HCl buffer (pH 7.5) containing 10 mM $CaCl_2$ and 0 or 4 M NaCl at 25°C. Numbers in parentheses indicate the relative values by comparing the value for WT thermolysin. The mean value of triplicate determination and SD value are shown.

Table 3. Kinetic parameters of the Leu202 thermolysin variants in the hydrolysis of ZDFM.

Thermolysin	K_m (mM)	k_{cat} (s^{-1})	k_{cat}/K_m ($mM^{-1}\ s^{-1}$)
WT	0.7 ± 0.1 (1.0)	4.0 ± 0.2 (1.0)	5.7 ± 0.6 (1.0)
L202G	0.3 ± 0.0 (0.4)	0.8 ± 0.0 (0.2)	2.7 ± 0.2 (0.5)
L202A	0.2 ± 0.0 (0.3)	1.7 ± 0.1 (0.4)	8.5 ± 0.7 (1.5)
L202V	0.2 ± 0.0 (0.3)	2.4 ± 0.1 (0.6)	12.0 ± 0.1 (2.1)
L202I	0.7 ± 0.1 (1.0)	0.7 ± 0.1 (0.2)	1.0 ± 0.1 (0.2)
L202M	2.2 ± 0.7 (3.1)	1.7 ± 0.4 (0.4)	0.8 ± 0.3 (0.1)
L202F	0.1 ± 0.0 (0.1)	0.7 ± 0.0 (0.2)	7.0 ± 0.3 (1.2)
L202Y	0.1 ± 0.0 (0.1)	1.5 ± 0.0 (0.4)	15.0 ± 0.7 (2.6)
L202W	–	–	< 0.01
L202P	0.1 ± 0.0 (0.1)	1.2 ± 0.0 (0.3)	12.0 ± 0.0 (2.1)
L202S	0.3 ± 0.0 (0.4)	2.3 ± 0.1 (0.6)	7.7 ± 0.7 (1.4)
L202T	0.3 ± 0.0 (0.4)	1.8 ± 0.1 (0.5)	6.0 ± 0.5 (1.1)
L202C	1.8 ± 0.4 (2.6)	5.6 ± 0.9 (1.4)	3.1 ± 0.9 (0.5)
L202N	0.9 ± 0.1 (1.3)	2.3 ± 0.2 (0.6)	2.6 ± 0.4 (0.5)
L202Q	7.1 ± 2.3 (10)	9.7 ± 2.8 (2.4)	1.4 ± 0.6 (0.3)
L202K	0.6 ± 0.0 (0.9)	12.5 ± 0.3 (3.1)	20.8 ± 1.5 (3.7)
L202R	0.8 ± 0.1 (1.1)	16.5 ± 0.8 (4.1)	20.6 ± 2.4 (3.6)
L202H	0.3 ± 0.0 (0.4)	1.0 ± 0.1 (0.3)	3.3 ± 0.5 (0.6)
L202D	4.8 ± 1.2 (6.9)	8.5 ± 1.3 (2.1)	1.8 ± 0.6 (0.3)
L202E	2.5 ± 0.2 (3.6)	11.2 ± 0.5 (2.8)	4.5 ± 0.4 (0.8)

ZDFM-hydrolysis activity was measured in 40 mM Tris-HCl buffer (pH 7.5) containing 10 mM $CaCl_2$ at 25°C. Numbers in parentheses indicate the relative values by comparing the value for WT thermolysin. The mean value of triplicate determination and SD value are shown. The k_{cat}/K_m value of L202W was less than 0.01 $mM^{-1}\ s^{-1}$, and the K_m and k_{cat} values could not be determined.

Table 4. FAAFA-hydrolysis activities of the Leu202 thermolysin variants.

Thermolysin	FAAFA
	$(k_{cat}/K_m)\times10^{-4}$ (M^{-1} s^{-1})
WT	7.9 ± 0.3 (1.0)
L202G	0.4 ± 0.2 (0.1)
L202A	6.3 ± 0.5 (0.8)
L202V	9.9 ± 1.0 (1.3)
L202I	1.4 ± 0.1 (0.2)
L202M	1.3 ± 0.1 (0.2)
L202F	43 ± 1 (5.4)
L202Y	75 ± 10 (9.5)
L202W	4.0 ± 0.2 (0.5)
L202P	0.9 ± 0.1 (0.1)
L202S	7.4 ± 0.1 (0.9)
L202T	8.0 ± 0.3 (1.0)
L202C	3.0 ± 0.2 (0.4)
L202N	4.5 ± 1.5 (0.6)
L202Q	4.0 ± 0.4 (0.5)
L202K	26 ± 1 (3.3)
L202R	13 ± 1 (1.7)
L202H	13 ± 1 (1.7)
L202D	2.7 ± 0.2 (0.3)
L202E	8.4 ± 0.2 (1.1)

FAAFA-hydrolysis activity was measured in 40 mM Tris-HCl buffer (pH 7.5) containing 10 mM $CaCl_2$ and 5% DMSO at 25^{o}C. Numbers in parentheses indicate the relative values by comparing the value for WT thermolysin. The mean value of triplicate determination and SD value are shown.

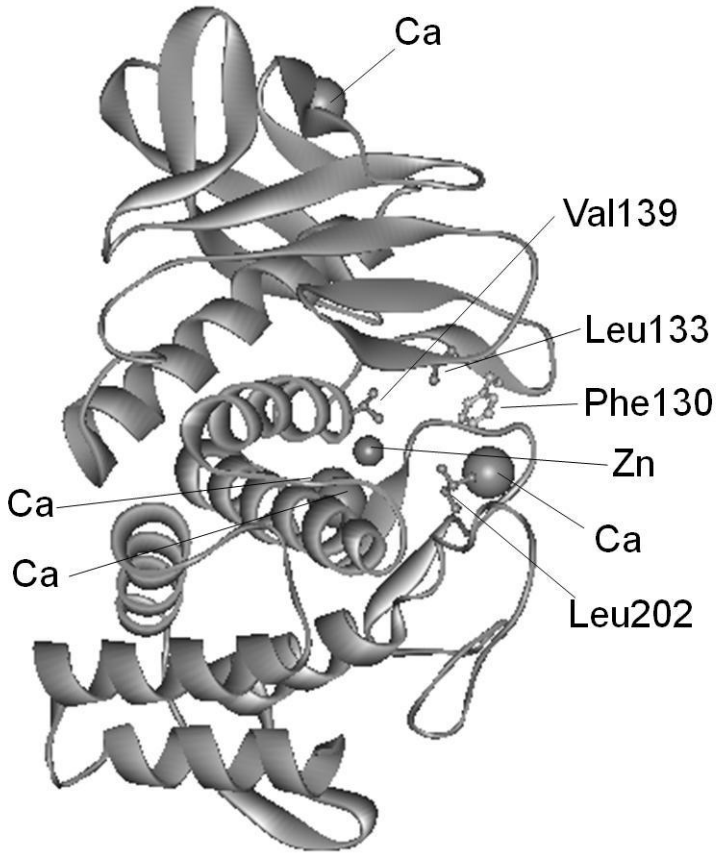

Fig. 1. Overall protein structure of thermolysin. The structure is based on Protein Data Bank accession number 8TLN. The main chain is represented by a ribbon model. Side chains of Phe130, Leu133, Val139, and Leu202 are represented by a ball-and-stick model. Zinc and calcium ions are shown as spheres.

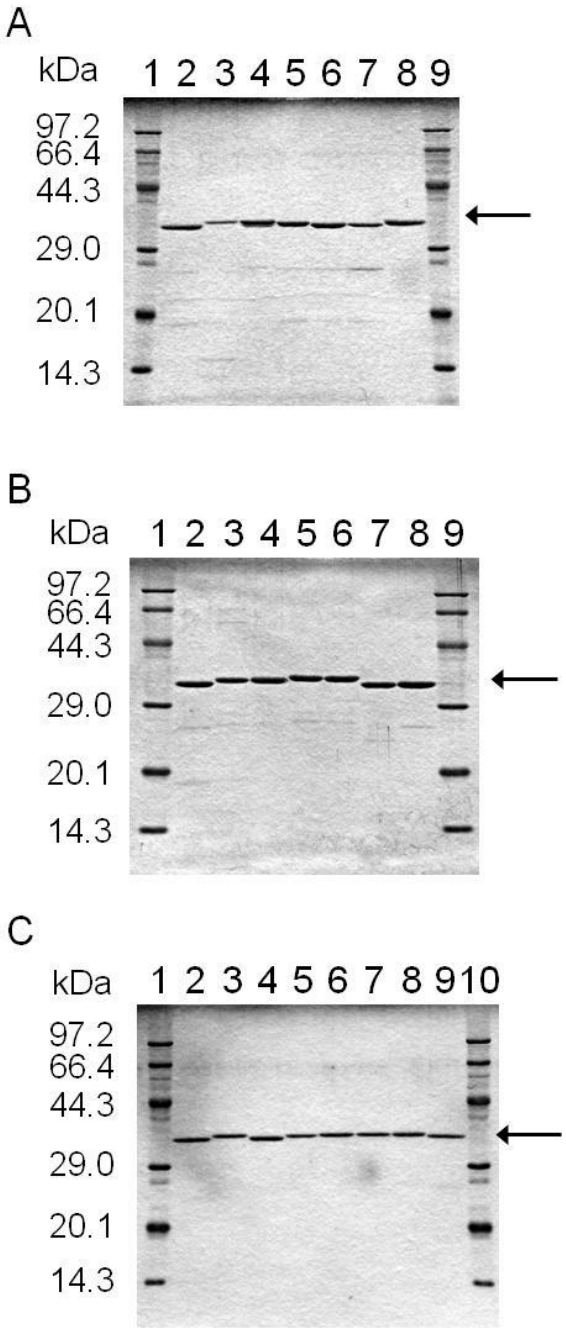

Fig. 2. SDS-PAGE analysis of purified preparations of the Leu202 variants. Coomassie Brilliant Blue-stained 12.5% SDS-polyacrylamide gel is shown. (A) Molecular-weight marker proteins (lanes 1 and 9), WT (lane 2), L202G (lane 3), L202A (lane 4), L202V (lane 5), L202I (lane 6), L202F (lane 7), and L202Y (lane 8). (B) Molecular-weight marker proteins (lanes 1 and 9), WT (lane 2), L202N (lane 3), L202Q (lane 4), L202D (lane 5), L202E (lane 6), L202R (lane 7), and L202K (lane 8). (C) Molecular-weight marker proteins (lanes 1 and 10), WT (lane 2), L202H (lane 3), L202W (lane 4), L202P (lane 5), L202T (lane 6), L202S (lane 7), L202C (lane 8), and L202M (lane 9). The arrow indicates the band corresponding to thermolysin.

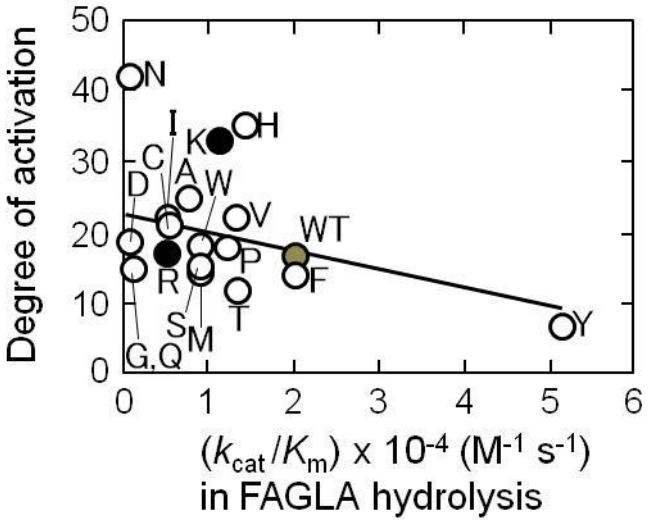

Fig. 3. Relationship between the FAGLA-hydrolysis activity at 0 M NaCl and the degree of activation by 4 M NaCl of the Leu202 variants. The degree of activation is calculated by dividing the FAGLA-hydrolysis activity (k_{cat}/K_m) at 4 M NaCl by that at 0 M NaCl. The values of the FAGLA-hydrolysis activity are cited from Tables 2. The line is drawn by linear least-squares-regression (LSR) method. The regression coefficient, r, is −0.35. WT is marked in gray; L202K and L202R are in black; and other 17 variants in white.

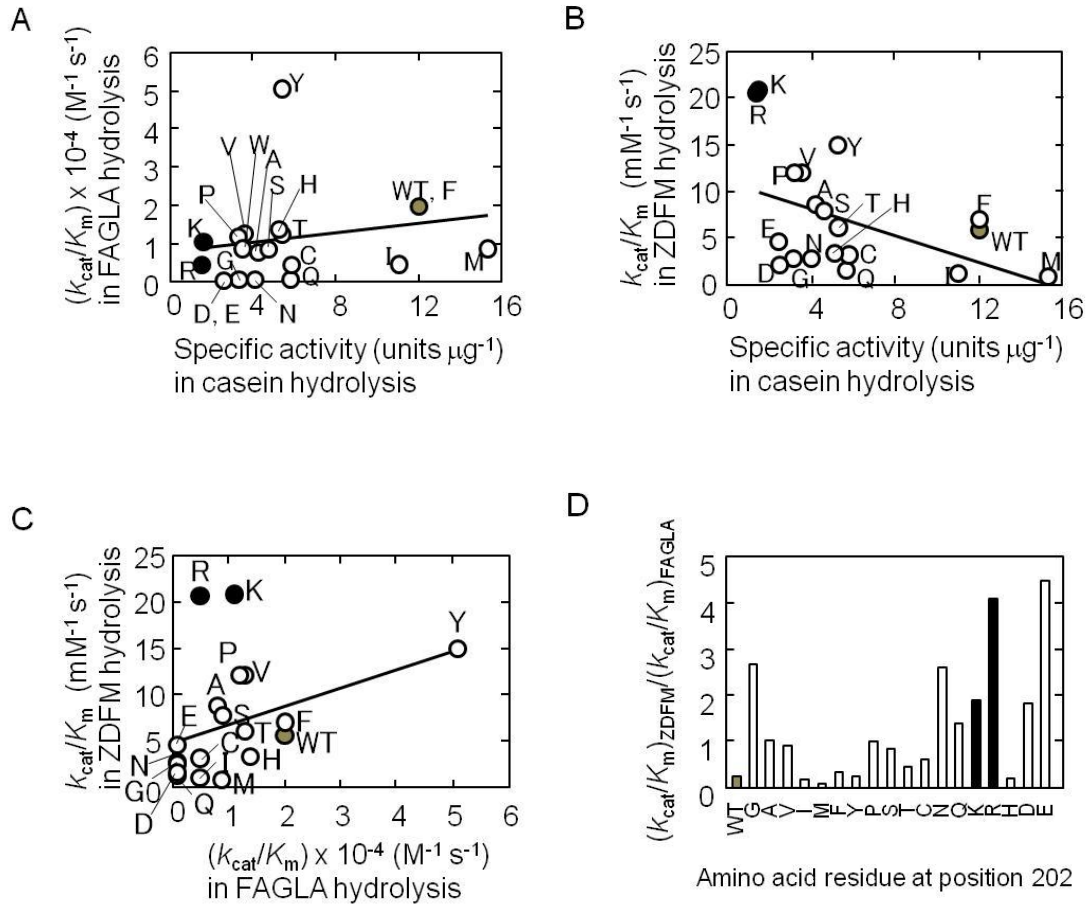

Fig. 4. Comparison of Casein-, FAGLA-, and ZDFM-hydrolysis activities of the Leu202 variants. (A) Casein- and FAGLA-hydrolysis activities. (B) Casein- and ZDFM-hydrolysis activities. (C) FAGLA- and ZDFM-hydrolysis activities. The values of the activities are cited from Tables 1, 2, and 3, respectively. The lines are drawn by linear LSR method. The regression coefficients (r) are: A, 0.21; B, –0.45; and C, 0.40. (D) Ratios of the k_{cat}/K_m value for ZDFM hydrolysis to that for FAGLA hydrolysis. WT is marked in gray; L202K and L202R are in black; and other 17 variants in white.

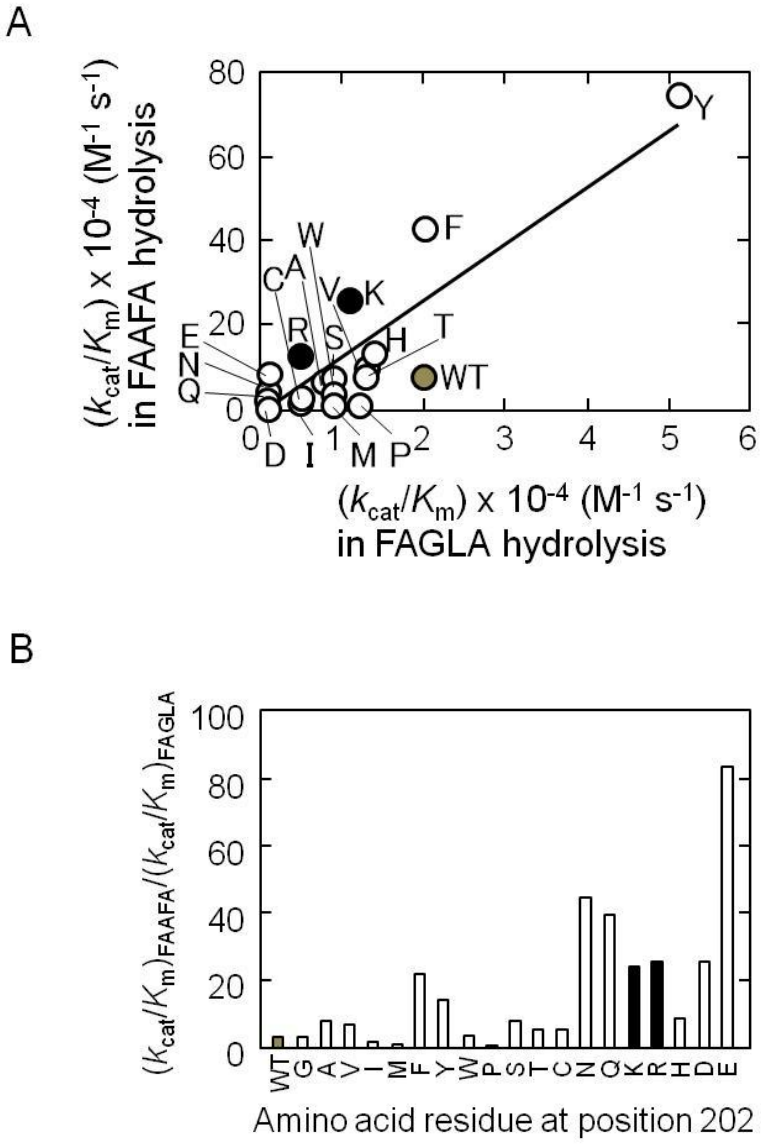

Fig. 5. Comparison of FAGLA- and FAAFA-hydrolysis activities of the Leu202 variants. The k_{cat}/K_m values of the FAGLA- and FAAFA-hydrolysis activities are cited from Tables 2 and 4, respectively. (A) FAAFA- and FAGLA-hydrolysis activities. The line is drawn by linear LSR method. The regression coefficient, *r*, is 0.84. (B) Ratios of the k_{cat}/K_m value for FAAFA hydrolysis to that for FAGLA hydrolysis. WT is marked in gray; L202K and L202R are in black; and other 17 variants in white.

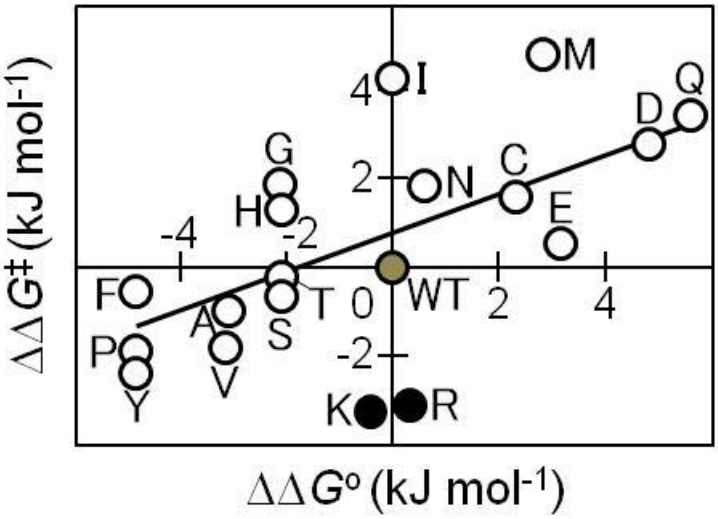

Fig. 6. Comparison of the mutation-mediated changes in the binding Gibbs energy and activation Gibbs energy for the ZDFM hydrolysis catalyzed by the Leu202 variants. The values for the binding Gibbs energy and activation Gibbs energy are calculated by Eq. 1 and 2 using the values in Table 3. $\Delta\Delta G^{o}$ and $\Delta\Delta G^{\ddagger}$ are the changes in ΔG^{o} and $\Delta G^{\ddagger}$, respectively, induced by the mutation of Leu202 in WT thermolysin. ΔG^{o} and $\Delta G^{\ddagger}$ of WT thermolysin are –18.0 and 51.6 kJ mol^{-1}, respectively. The line is drawn by linear LRS method. The regression coefficient, *r*, is 0.61. WT is marked in gray; L202K and L202R are in black; and other 16 variants in white.

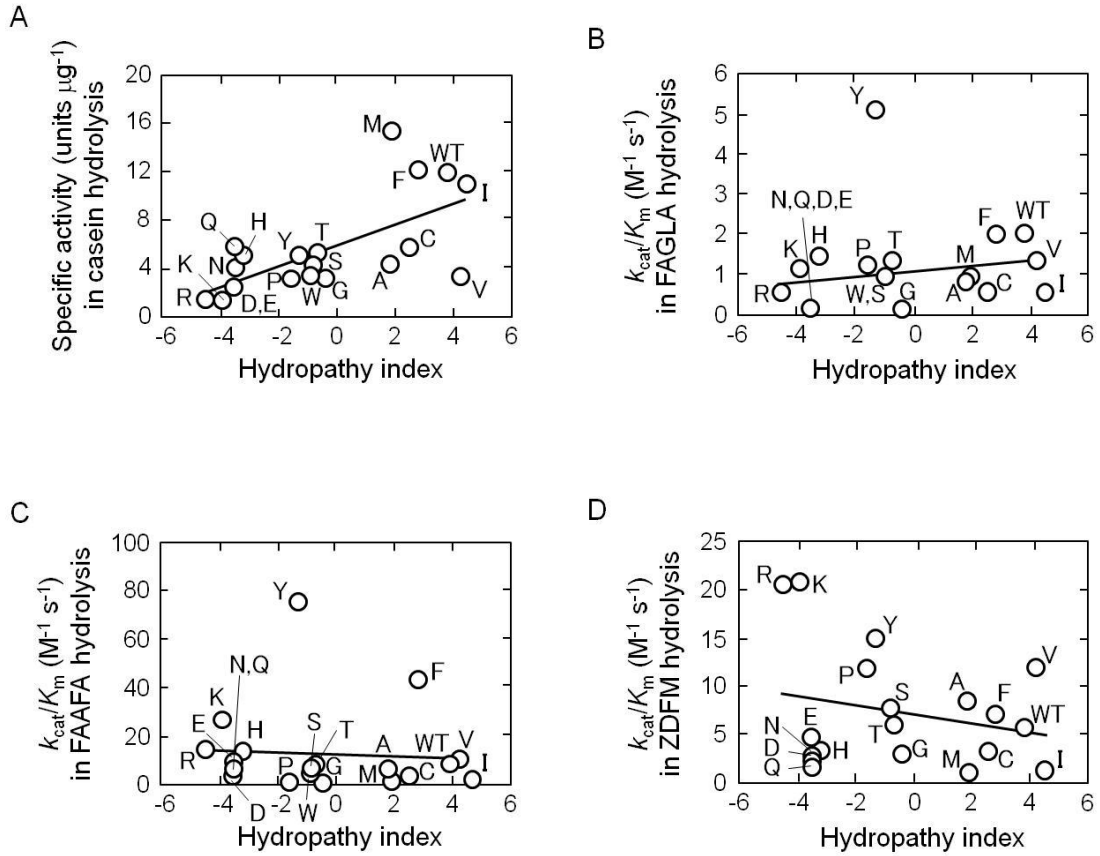

Fig. 7. Correlation between hydropathy indexes of the residues at position 202 and the catalytic activities of thermolysin variants. (A) Correlation between casein-hydrolysis activities and hydropathy indexes. Correlation coefficient (r) = 0.66. (B) Correlation between FAGLA-hydrolysis activities and hydropathy indexes. r = 0.19. (C) Correlation between FAAFA-hydrolysis activities and hydropathy indexes. r = –0.047. (D) Correlation between ZDFM-hydrolysis activities and hydropathy indexes. r = –0.25.

Summary

Chapter 1

Hepatocyte growth factor activator inhibitor type 1 (HAI-1) is a membrane-bound, Kunitz-type serine protease inhibitor. HAI-1 inhibits serine proteases that have potent pro-hepatocyte growth factor-converting activity, such as the membrane-type serine protease, matriptase. HAI-1 comprises an N-terminal domain, followed by an internal domain, first protease inhibitory domain (Kunitz domain I), low-density lipoprotein receptor A module (LDLRA) domain, and a second Kunitz domain (Kunitz domain II) in the extracellular region. The roles of these domains in the inhibition of matriptase were assessed. Soluble forms of recombinant rat HAI-1 mutants made up with various combinations of domains were produced, and their inhibitory activities toward the hydrolysis of a chromogenic substrate were analyzed using a soluble recombinant rat matriptase. Kunitz domain I exhibited inhibitory activity against matriptase, but Kunitz domain II did not. The N-terminal domain and Kunitz domain II decreased the association rate between Kunitz domain I and matriptase, whereas the internal domain increased this rate. The LDLRA domain suppressed the dissociation of the Kunitz domain I-matriptase complex. Surprisingly, an HAI-1 mutant lacking the N-terminal domain and Kunitz domain II showed an inhibitor constant of 1.6 pM, and the inhibitory activity was 400 times higher in this HAI-1mutant than in the mutant with all domains. These findings, together with the known occurrence of an HAI-1 species lacking the N-terminal domain and Kunitz domain II in *vivo*, suggest that the domain structure of HAI-1 is organized in a way that allows HAI-1 to flexibly control matriptase activity.

Chapter 2

Matriptase contains the non-catalytic domains (stem domain) and catalytic domain in the extracellular region. The role of the stem domain in the interaction between matriptase and HAI-1 was addressed. Secreted variants of recombinant matriptase containing the entire extracellular domain (HL-matriptase) or only the catalytic domain (L-matriptase) were prepared, and the inhibition activities of a cell membrane-anchored form of recombinant HAI-1 (maHAI-1) against the matriptase variants in the hydrolysis of peptidyl-4-methyl-coumaryl-7-amide (MCA) substrates were compared. HL-matriptase and L-matriptase were inhibited by purified maHAI-1 with a similar extent when *t*-butyloxycarbonyl (Boc)-Gln-Ala-Arg-MCA (1) and acetyl-Lys-Thr-Lys-Gln-Leu-Arg-MCA (2) were used as substrates. However, HL-matriptase was inhibited more strongly than L-matriptase by maHAI-1 in the hydrolysis of Boc-[(2*S*)-2-amino-3-(benzyloxycarbonyl)propionyl]-Pro-Arg-MCA (3). These results show that the stem domain of matriptase facilitates the inhibitory interaction of this protease with maHAI-1 in the hydrolysis of substrate 3, although it has no effect in the hydrolysis of substrates 1 and 2. To my knowledge, this is the first evidence that the stem domain of matriptase can affect the interaction between this protease and HAI-1.

Chapter 3

Thermolysin is a thermophilic and halophilic zinc metalloproteinase that consists of β-rich N-terminal (residues 1–157) and α-rich C-terminal (residues 158–316) domains. Expression of thermolysin variants truncated from the C-terminus was examined in *E. coli* culture. The C-terminal Lys316 residue was not significant in the expression, but Val315 was critical. Variants in which Val315 was substituted with fourteen amino acids

were prepared. The variants substituted with hydrophobic amino acids such as Leu and Ile were almost the same as wild-type thermolysin (WT) in the expression amount, α-helix content, and stability. Variants with charged (Asp, Glu, Lys, and Arg), bulky (Trp), or small (Gly) amino acids were lower in these characteristics than WT. All variants exhibited considerably high activities (50–100% of WT) in hydrolyzing protein and peptide substrates. The expression amount, helix content, and stability of variants showed good correlation with hydropathy indexes of the amino acids substituted for Val315. Crystallographic study of thermolysin has indicated that Val315 is a member of the C-terminal hydrophobic cluster. The results obtained in this study indicate that stabilization of the cluster increases thermolysin stability and that the variants with higher stability are expressed more in the culture. Although thermolysin activity was not severely affected by the variation at position 315, the stability and specificity were modified significantly, suggesting the long-range interaction between the C-terminal region and active site.

Chapter 4

The role of Leu202 in thermolysin, a residue located in the S_1' subsite, was examined using 19 single variants at position 202 and measuring their hydrolysis activities for casein, *N*-[3-(2-furyl)acryloyl]-glycyl-L-leucine amide (FAGLA), *N*-carbobenzoxy-L-aspartyl-L-phenylalanine methyl ester (ZDFM), and *N*-[3-(2-furyl)acryloyl]-L-alanyl-L-phenylalanine amide (FAAFA) at pH 7.5 at 25°C. All variants except for the variant L202W, in which Leu202 was replaced to Trp, retained activities for all substrates. The L202W variant lacked the activity for ZDFM and retained for the other three. The correlation between the activities of variants for FAGLA and ZDFM was weak with the

correlation coefficient (r) of 0.40, whereas that between the activities for FAGLA and FAAFA was fairly good (r = 0.87). These correlations were marked in the variants L202K and L202R: the k_{cat}/K_m values of L202K and L202R for FAGLA were 60 and 30%, respectively, of that of wild-type thermolysin, while those for ZDFM were 370 and 360%, and those for FAAFA were 330 and 170%. These results suggest that Leu202 is not much critical for catalytic activity but plays an important role in substrate specificity of thermolysin.

References

1. Lin, C.Y., Tseng, I.C., Chou, F.P., Su, S.F., Chen, Y.W., Johnson, M.D., and Dickson R.B. (2008) Zymogen activation, inhibition, and ectodomain shedding of matriptase. *Front. Biosci*. **13**, 621–635
2. Darragh, M.R., Bhatt, A.S., and Craik, C.S. (2008) MT-SP1 proteolysis and regulation of cell-microenvironment interactions. *Front. Biosci*. **13**, 528–539
3. Bugge, T.H., List, K., and Szabo, R. (2007) Matriptase-dependent cell surface proteolysis in epithelial development and pathogenesis. *Front. Biosci*. **12**, 5060–5070
4. Kim, M.G., Chen, C., Lyu, M.S., Cho, E.G., Park, D., Kozak, C., and Schwartz, R.H. (1999) Cloning and chromosomal mapping of a gene isolated from thymic stromal cells encoding a new mouse type II membrane serine protease, epithin, containing four LDL receptor modules and two CUB domains. *Immunogenetics*, **49**, 420–428
5. Zhang, T., Cai, X, Schlegelberger, B., and Zheng, S. (1998) Assignment of human putative tumor suppressor genes ST13 (alias SNC6) and ST14 (alias SNC19) to human chromosome bands 22q13 and 11q24→q25 by in situ hybridization. *Cytogenet. Cell Genet*. **83**, 56–57
6. Takeuchi, T., Harris, J.L., Huang, W., Yan, K.W., Coughlin, S.R., and Craik, C.S. (2000) Cellular localization of membrane-type serine protease 1 and identification of protease-activated receptor-2 and single-chain urokinase-type plasminogen activator as substrates. *J. Biol. Chem.* **275**, 26333–26342
7. Lee, S.L., Dickson, R.B., and Lin, C.Y. (2000) Activation of hepatocyte growth

factor and urokinase/plasminogen activator by matriptase, an epithelial membrane serine protease. *J. Biol. Chem.* **275**, 36720–36725

8. Satomi, S., Yamasaki, Y., Tsuzuki, S., Hitomi, Y., Iwanaga, T., and Fushiki, T. (2001) A role for membrane-type serine protease (MT-SP1) in intestinal epithelial turnover. *Biochem. Biophys. Res. Commun.* **287**, 995–1002
9. Kirchhofer, D., Peek, M., Li, W., Stamos, J., Eigenbrot, C., Kadkhodayan, S., Elliott, J.M., Corpuz, R.T., Lazarus, R.A., and Moran, P. (2003) Tissue expression, protease specificity, and Kunitz domain functions of hepatocyte growth factor activator inhibitor-1B (HAI-1B), a new splice variant of HAI-1. *J. Biol. Chem.* **278**, 36341–36349
10. Netzel-Armett, S., Currie, B.M., Szabo, R., Lin, C.Y., Chen, L.M., Chai, K.X., Antalis, T.M., Bugge, T.H., and List, K. (2006) Evidence for a matriptase-prostasin proteolytic cascade regulating terminal epidermal differentiation. *J. Biol. Chem.* **281**, 32941–32945
11. Oberst, M.D., Singh, B., Ozdemirli, M., Dickson, R.B., Johnson, M.D., and Lin, C.Y. (2003) Characterization of matriptase expression in normal human tissues. *J. Histochem. Cytochem.* **51**, 1017–1025
12. Shimomura, T., Denda, K., Kitamura, A., Kawaguchi, T., Kito, M., Kondo, J., Kagaya, S., Qin, L., Takata, H., Miyazawa, K., and Kitamura, N. (1997) Hepatocyte growth factor activator inhibitor, a novel Kunitz-type serine protease inhibitor. *J. Biol. Chem.* **272**, 6370–6376
13. Kataoka, H., Suganuma, T., Shimomura, T., Itoh, H., Kitamura, N., Nabeshima, K., and Koono, M. (1999) Distribution of hepatocyte growth factor activator inhibitor type 1 (HAI-1) in human tissues. Cellular surface localization of HAI-1 in simple

columnar epithelium and its modulated expression in injured and regenerative tissues. *J. Histochem. Cytochem.* **47**, 673–682

14. Miyazawa, K., Shimomura, T., Kitamura, A., Kondo, J., Morimoto, Y., and Kitamura, N. (1993) Molecular cloning and sequence analysis of the cDNA for a human serine protease responsible for activation of hepatocyte growth factor. *J. Biol. Chem.* **268**, 10024–10028
15. Itoh, H., Kataoka, H., Tomita, M., Hamasuna, R., Nawa, Y., Kitamura, N., and Koono, M. (2000) Upregulation of HGF activator inhibitor type 1 but not type 2 along with regeneration of intestinal mucosa. *Am. J. Physiol. Gastrointest. Liver Physiol.* **278**, G635–G643
16. Shimomura, T., Denda, K., Kawaguchi, T., Matsumoto, K., Miyazawa, K., and Kitamura, N. (1999) Multiple sites of proteolytic cleavage to release soluble forms of hepatocyte growth factor activator inhibitor type 1 from a transmembrane form. *J. Biochem.* (Tokyo) **126**, 821–828
17. Tsuzuki, S., Murai, N., Miyake, Y., Inouye, K., Hirayasu, H., Iwanaga, T., and Fushiki, T. (2005) Evidence for the occurrence of membrane-type serine protease 1/matriptase on the basolateral sides of enterocytes. *Biochem. J.* **388**, 679–687
18. Denda, K., Shimomura, T., Kawaguchi, T., Miyazawa, K., and Kitamura, N. (2002) Functional characterization of Kunitz domains in hepatocyte growth factor activator inhibitor type 1. *J. Biol. Chem.* **277**, 14053–14059
19. Oberst, M.D., Johnson, M.D., Dickson, R.B., Lin, C.Y., Singh, B., Stewart, M., Williams, A., al-Nafussi, A., Smyth, J.F., Gabra, H., and Sellar, G.C. (2002) Expression of the serine protease matriptase and its inhibitor HAI-1 in epithelial ovarian cancer: correlation with clinical outcome and tumor clinicopathological

parameters. *Clin. Cancer Res.* **8**, 1101–1107

20. Vogel, L.K., Sæbø., M., Skjelbred, C.F., Abell, K., Pedersen, E.D., Vogel, U., and Kure, E.H. (2006) The ratio of Matriptase/HAI-1 mRNA is higher in colorectal cancer adenomas and carcinomas than corresponding tissue from control individuals. *BMC Cancer* **4**, 176
21. Endo, S. (1962) Studies on protease produced by thermophilic bacteria, *J. Ferment. Technol*. **40**, 346–353
22. Inouye, K. (2003) Thermolysin, in: J. R. Whitaker, A. G. J. Voragen, D. W. S. Wong (Eds.), Handbook of Food Enzymology, Marcel Dekker, New York, pp. 1019–1028
23. Inouye, K. (1992) Effects of salts on thermolysin: activation of hydrolysis and synthesis of *N*-carbobenzoxy-L-aspartyl-L-phenylalanine methyl ester, and a unique change in the absorption spectrum of thermolysin, *J. Biochem.* **112**, 335–340
24. Titani, K., Hermodson, M.A., Ericsson, L.H., Walsh, K.A., and Neurath, H. (1972) Amino-acid sequence of thermolysin. *Nature* **238**, 35–37
25. Holmes, M. A and Matthews, B.W. (1982) Structure of thermolysin refined at 1.6 Å resolution. *J. Mol. Biol.* **160**, 623–639
26. Hangauer, D.G., Monzingo, A.F., and Matthews, B.W. (1984) An interactive computer graphics study of thermolysin-catalyzed peptide cleavage and inhibition by *N*-carboxymethyl dipeptides. *Biochemistry* **23**, 5730–5741
27. Mock, W.L. and Aksamawati, M. (1994) Binding to thermolysin of phenolate-containing inhibitors necessitates a revised mechanism of catalysis. *Biochem. J.* **302**, 57–68

28. Lin, C.Y., Anders, J., Johnson, M., and Dickson, R.B. (1999) Purification and characterization of a complex containing matriptase and a Kunitz-type serine protease inhibitor from human milk. *J. Biol. Chem.* **274**, 18237–18242

29. Hooper, J.D., Clements, J.A., Quigley, J.P., and Antalis, T.M. (2001) Type II transmembrane serine proteases. Insights into an emerging class of cell surface proteolytic enzymes. *J. Biol. Chem.* **276**, 857–860

30. Takeuchi, T., Shuman, M.A., and Craik, C.S. (1999) Reverse biochemistry: use of macromolecular protease inhibitors to dissect complex biological processes and identify a membrane-type serine protease in epithelial cancer and normal tissue. *Proc. Natl. Acad. Sci. U. S. A.* **96**, 11054–11061

31. Benaud, C., Dickson, R.B., and Lin, C.Y. (2001) Regulation of the activity of matriptase on epithelial cell surfaces by a blood-derived factor. *Eur. J. Biochem.* **268**, 1439–1447

32. Yamasaki, Y., Satomi, S., Murai, N., Tsuzuki, S., and Fushiki, T. (2003) Inhibition of membrane-type serine protease 1/matriptase by natural and synthetic protease inhibitors. *J. Nutr. Sci. Vitaminol. (Tokyo)* **49**, 27–32

33. Mazzone, M. and Comoglio, P. M. (2006) The Met pathway: master switch and drug target in cancer progression. *FASEB J.* **20**, 1611–1621

34. Nozaki, S., Endo, Y., Nakahara, H., Yoshizawa, K., Ohara, T., and Yamamoto, E. (2006) Targeting urokinase-type plasminogen activator and its receptor for cancer therapy. *Anticancer Drugs* **17**, 1109–1117

35. Deryugina, E.I. and Quigley, J.P. (2006) Matrix metalloproteinases and tumor metastasis. *Cancer Metastasis Rev.* **25**, 9–34

36. Rosmann, S., Hahn, D., Lottaz, D., Kruse, M.N., Stöcker, W., and Sterchi, E.E.

(2002) Activation of human meprin-alpha in a cell culture model of colorectal cancer is triggered by the plasminogen-activating system. *J. Biol. Chem.* **277**, 40650–40658

37. Bond, J.S., Matters, G.L., Banerjee, S., and Dusheck, R.E. (2005) Meprin metalloprotease expression and regulation in kidney, intestine, urinary tract infections and cancer. *FEBS Lett.* **579**, 3317–3322
38. Oberst, M.D., Williams, C.A., Dickson, R.B., Johnson, M.D., and Lin, C.Y. (2003) The activation of matriptase requires its noncatalytic domains, serine protease domain, and its cognate inhibitor. *J. Biol. Chem.* **278**, 26773–26779
39. Morrison, J.F. and Walsh, C.T. (1988) The behavior and significance of slow-binding enzyme inhibitors. *Adv. Enzymol. Relat. Areas Mol. Biol.* **61**, 201–203
40. Dharmasena, S.P., Wimalasena, D.S., and Wimalasena, K. (2002) A slow-tight binding inhibitor of dopamine beta-monooxygenase: a transition state analogue for the product release step. *Biochemistry* **41**, 12414–12420
41. Copeland, R.A. (2005) in Evaluation of Enzyme Inhibitors in Drug Discovery: A Guide for Medical Chemists and Pharmacologists, pp. 141–177, John Wiley & Sons, Inc., Hoboken, New Jersey
42. Lu, D., Yuan, X., Zheng, X., and Sadler, J.E. (1997) Bovine proenteropeptidase is activated by trypsin, and the specificity of enteropeptidase depends on the heavy chain. *J. Biol. Chem.* **272**, 31293–31300
43. Brown, M.S., Herz, J., and Goldstein, J.L. (1997) LDL-receptor structure. Calcium cages, acid baths and recycling receptors. *Nature* **388**, 629–630
44. Fass, D., Blacklow, S., Kim, P.S., and Berger, J.M. (1997) Molecular basis of

familial hypercholesterolaemia from structure of LDL receptor module. *Nature* **388**, 691–693

45. Esser, V., Limbird, L.E., Brown, M.S., Goldstein, J.L., and Russel, D.W. (1988) Mutational analysis of the ligand binding domain of the low density lipoprotein receptor. *J. Biol.Chem.* **263**, 13282–13290

46. Huang, Z.F., Wun, T.C., and Broze, G.J., Jr. (1993) Kinetics of factor Xa inhibition by tissue factor pathway inhibitor. *J. Biol. Chem.* **268**, 26950–26955

47. Scandura, J.M., Zhang, Y., Van Nostrand, W.E., and Walsh, P.N. (1997) Progress curve analysis of the kinetics with which blood coagulation factor XIa is inhibited by protease nexin-2. *Biochemistry* **36**, 412–420

48. Rezaie, A.R. (2004) Kinetics of factor Xa inhibition by recombinant tick anticoagulant peptide: both active site and exosite interactions are required for a slow- and tight-binding inhibition mechanism. *Biochemistry* **43**, 3368–3375

49. Oberst, M.D., Chen, L.Y., Kiyomiya, K., Williams, C.A., Lee, M.S., Johnson, M.D., Dickson, R.B., and Lin, C.Y. (2005) HAI-1 regulates activation and expression of matriptase, a membrane-bound serine protease. *Am. J. Physiol. Cell Physiol.* **289**, C462–C470

50. Moestrup, S.K. (1994) The alpha 2-macroglobulin receptor and epithelial glycoprotein-330: two giant receptors mediating endocytosis of multiple ligands. *Biochim. Biophys. Acta* **1197**, 197–213

51. Szabo, R. and Bugge, T.H. (2008) Type II transmembrane serine proteases in development and disease. *Int. J. Biochem. Cell Biol*. **40**, 1297–1316

52. Qiu, D., Owen, K., Gray, Bass, R., and Ellis, V. (2007) Roles and regulation of membrane-associated serine proteases. *Biochem. Soc. Trans*. **35**, 583–587

53. Mikhailova, A.G. and Rumsh, L.D. (1999) Autolysis of bovine enteropeptidase heavy chain: evidence of fragment 118–465 involvement in trypsinogen activation. *FEBS lett*. **442**, 226–230

54. Laemmli, U.K. (1970) Cleavage of structural proteins during the assembly of the head of bacteriophage T4. *Nature* **227**, 680–685

55. Moran, P., Li, W., Fan, B., Vij, R., Eigenbrot, C., and Kirchhofer, D. (2006) Pro-urokinase-type plasminogen activator is a substrate for hepsin. *J. Biol. Chem*. **281**, 30439–30446

56. Szabo, R., Hobson, J.P., List, K., Molinolo, A., Lin, C.Y., and Bugge, T.H. (2008) Potent inhibition and global co-localization implicate the transmembrane Kunitz-type serine protease inhibitor hepatocyte growth factor activator inhibitor-2 in the regulation of epithelial matriptase activity. *J. Biol. Chem*. **283**, 29495–20504

57. Feder, J., Garrett, L.R., and Wildi, B.S. (1971) Studies on the role of calcium in thermolysin. *Biochemistry* **10**, 4552–4556

58. Tajima, M., Urabe, I., Yutani, K., and Okada, H (1976) Role of calcium ions in the thermostability of thermolysin and *Bacillus subtilis* var. *amylosacchariticus* neutral protease. *Eur. J. Biochem.* **64**, 243–247

59. Holand, D.R., Tronrud, D.E., Pley, H.W., Flaherty, K.M., Stark, W., Jansonius, J.N., McKay, D.B., and Matthews, B.W. (1992) Structural comparison suggests that thermolysin and related neutral proteases undergo hinge-bending motion during catalysis. *Biochemistry* **31**, 11310–11316

60. Kusano, M., Yasukawa, K., and Inouye, K. (2009) Insights into the catalytic roles

of the polypeptide regions in the active site of thermolysin and generation of the thermolysin variants with high activity and stability. *J. Biochem.* **145**, 103–113

61. Kusano, M., Yasukawa, K., and Inouye, K. (2010) Effects of the mutational combination on the activity and stability of thermolysin. *J. Biotechnol.* **147**, 7–16
62. Yasukawa, K. and Inouye, K. (2007) Improving the activity and stability of thermolysin by site-directed mutagenesis. *Biochim. Biophys. Acta.* **1774**, 1281–1288
63. Kawasaki, Y., Yasukawa, K., and Inouye, K. (2013) Effects of site-directed mutagenesis in the N-terminal domain of thermolysin on its stabilization. *J. Biochem.* **153**, 85–92
64. Menach, E., Yasukawa, K., and Inouye, K. (2010) Effects of site-directed mutagenesis of the loop residue of the N-terminal domain Gly117 of thermolysin on its catalytic activity. *Biosci. Biotechnol. Biochem.* **74**, 2457–2462
65. de Kreij, A., van den Burg, B., Venema, G., Vriend, G., Eijsink, V.G., and Nielsen, J.E. (2002) The effects of modifying the surface charge on the catalytic activity of the thermolysin-like protease. *J. Biol. Chem.* **277**, 15432–15438
66. Mansfeld, J., Vriend, G., Dijkstra, B.W., Veltman, O.R., Van den Burg, B., Venema, G., Ulbrich-Hofmann, R., and Eijsink, V.G. (1997) Extreme stabilization of a thermolysin-like protease by an engineered disulfide bond. *J. Biol. Chem.* **272**, 11152–11156
67. Eijsink, V.G., Bjørk, A., Gåseidnes, S., Sirevåg, R., Synstad, B., van den Burg, B., and Vriend, G. (2004) Rational engineering of enzyme stability. *J. Biotechnol.* **113**, 105–120

68. Matsumiya, Y., Nishikawa, K., Aoshima, H., Inouye, K., and Kubo, M. (2004) Analysis of autodegradation sites of thermolysin and enhancement of its thermostability by modifying Leu^{155} at an autodegradation site. *J. Biochem.* **135**, 547–553.

69. Takita, T., Aono, T., Sakurama, H., Itoh, T., Wada, T., Minoda, M., Yasukawa, K., and Inouye, K. (2008) Effects of introducing negative charges into the molecular surface of thermolysin by site-directed mutagenesis on its activity and stability. *Biochim. Biophys. Acta.* **1784**, 481–488

70. Veltman, O.R., Vriend, G., Berendsen, H.J., Van den Burg, B., Venema, G., and Eijsink, V.G. (1998) A single calcium binding site is crucial for the calcium-dependent thermal stability of thermolysin-like proteases. *Biochemistry* **37**, 5312–5319

71. Vriend, G., Berendsen, H.J., van den Burg, B., Venema, G., and Eijsink, V.G. (1998) Early steps in the unfolding of thermolysin-like proteases. *J. Biol. Chem.* **273**, 35074–35077

72. Eijsink, V.G., Vriend, G., van den Burg, B., Venema, G., and Stulp, B.K. (1990) Contribution of the C-terminal amino acid to the stability of *Bacillus subtilis* neutral protease. *Protein Eng*. **4**, 99–104

73. Vriend, G. and Eijsink, V. (1993) Prediction and analysis of structures, stability and folding of thermolysin-like proteases. *J. Comput. Aided Mol. Des.* **7**, 367–396

74. Mauizi, M.R. (1992) Proteases and protein degradation in *Escherichia coli*. *Experientia* **48**, 178–201

75. Feder, J. (1968) A spectrophotometric assay for neutral protease. *Biochem. Biophys. Res. Commun.* **32**, 326–332

76. Yasukawa, K., Kusano, M., and Inouye, K (2007) A new method for the extracellular production of recombinant thermolysin by co-expressing the mature sequence and pro-sequence in *Escherichia coli*. *Protein Eng. Des. Sel.* **20**, 375–383.

77. Inouye, K., Minoda, M., Takita, T., Sakurama, H., Hashida, Y., Kusano, M., and Yasukawa, K. (2006) Extracellular production of recombinant thermolysin expressed in *Escherichia coli*, and its purification and enzymatic characterization. *Protein Expr. Purif.* **46**, 248–255

78. Chen, Y.H., Yang, J.T., and Chau, K.H. (1974) Dertermination of the helix and beta form of proteins in aqueous solution by circular dichroism. *Biochemistry* **13**, 3350–3359.

79. Johnson W.C. (1999) Analyzing protein circular dichroism spectra for accurate secondary structures. *Proteins* **35**, 307–312

80. Inouye, K., Lee, S.-B., and Tonomura, B (1996) Effect of amino acid residues at the cleavable site of substrates on the remarkable activation of thermolysin by salts. *Biochem. J.* **315**, 133–138

81. Inouye, K., Lee, S.-B., Nambu, K., and Tonomura, B. (1997) Effects of pH, temperature, and alcohols on the remarkable activation of thermolysin by salts, *J. Biochem.* **122**, 358–364

82. Inouye, K., Kuzuya, K., and Tonomura, B. (1994) A spectrophotometric study on the interaction of thermolysin with chloride and bromide ions, and the state of tryptophyl residue 115. *J. Biochem.* **116**, 530–535

83. Inouye, K. (1991) Chromatographic behaviors of proteins and amino acids on gel filtration matrix, TSK-GEL Toyopearl. *Agric. Biol. Chem.* **55**, 2129–2139

84. Sánchez-Ruiz, J.M., López-Lacomba, J.L., Cortijo, M., and Mateo, P.L. (1998) Differential scanning calorimetry of the irreversible thermal denaturation of thermolysin. *Biochemistry* **27**, 1648–1652

85. Eijsink, V.G., Vriend, G., van der Vinne, B., Hazes, B., van den Burg, B., and Venema G. (1992) Effects of changing the interaction between subdomains on the thermostability of *Bacillus* neutral proteases. *Proteins* **14**, 224–236

86. Kyte, J. and Doolittle, R.F. (1982) A simple method for displaying the hydropathic character of a protein. *J. Mol. Biol*. **157**, 105–132

87. Hashida, Y. and Inouye, K. (2007) Kinetic analysis of the activation-and-inhibition dual effects of cobalt ion on thermolysin activity. *J. Biochem*. **141**, 843–853

88. Hashida, Y. and Inouye, K (2007) Molecular mechanism of the inhibitory effect of cobalt ion on thermolysin activity and the suppressive effect of calcium ion on the cobalt ion-dependent inactivation of thermolysin. *J. Biochem.* **141**, 879–888

89. Kopetzki, E., Lehnert, K., and Buckel, P. (1994) Enzymes in diagnostics: achievements and possibilities of recombinant DNA technology. *Clin. Chem.* **40**, 688–704

90. Koeller, K.M. and Wong, C.-H. (2001) Enzymes for chemical synthesis. *Nature* **409**, 232–240

91. Kusano, M., Yasukawa, K., and Inouye, K. (2010) Synthesis of *N*-carbobenzoxy-L-aspartyl-L-phenylalanine methyl ester catalyzed by thermolysin variants with improved activity. *Enzyme Microb. Technol.* **46**, 320–325

92. Schechter, I. and Berger, A. (1967) On the size of the active site in proteases. I.

papain. *Biochem. Biophys. Res. Commun.* **27**, 157–162

93. Morihara, K. and Tsuzuki, H. (1970) Thermolysin: kinetic study with oligopeptides. *Eur. J. Biochem.* **15**, 374–380

94. Pangburn M.K., Burstein, Y., Morgan, P.H., Walsh, K.A., and Neurath, H. (1973) Affinity chromatography of thermolysin and of neutral proteases from *B. subtilis*. *Biochem. Biophys. Res. Commun.* **54**, 371–379

95. Walsh, K.A., Burstein, Y., and Pangburn, M.K. Thermolysin and other neutral metalloendopeptidases in *Methods in Enzymology* (Jakoby, W.B. and Wilchek, M. eds.) Vol. 34, pp. 435–440, Academic Press, New York

96. Inouye, K., Nakamura, K., Kusano, M., and Yasukawa, K. (2007) Improvement in performance of affinity gels containing Gly-D-Phe as a ligand to thermolysin due to increasing the spacer chain length. *Biosci. Biotechnol. Biochem.* **71**, 2083–2086

97. Muta, Y. and Inouye, K. (2002) Inhibitory effects of alcohols on thermolysin activity as examined using a fluorescent substrate. *J. Biochem.* **132**, 945–951

98. English, A.C., Done, S.H., Caves, L.S.D., Groom, C.R., and Hubbard, R.E. (1999) Locating interaction sites on proteins: the crystal structure of thermolysin soaked in 2% to 100% isopropanol. *Proteins* **37**, 628–640

99. de Kreij, A., van den Burg, B., Veltman O.R., Vriend, G., Venema, G., and Eijsink, V.G.H. (2001) The effect of changing the hydrophobic S_1' subsite of thermolysin-like proteases on substrate specificity. *Eur. J. Biochem.* **268**, 4985–4991

100. Inouye, K., Kuzuya, K., and Tonomura, B. (1998) Effect of salts on the solubility of thermolysin: a remarkable increase in the solubility as well as the activity by the addition of salts without aggregation or dispersion of thermolysin. *J. Biochem.*

123, 847–852

101. Inouye, K., Kuzuya, K., and Tonomura, B. (1998) Sodium chloride enhances markedly the thermal stability of thermolysin as well as its catalytic activity. *Biochim. Biophys. Acta* **1388**, 209–214
102. Menach, E., Yasukawa, K., and Inouye, K. (2013) Effects of mutations of thermolysin, Asn116 to Asp and Asp150 to Glu, on salt-induced activation and stabilization. *Biosci. Biotechnol. Biochem.* **77**, 741–746
103. Kamo, M., Inouye, K., Nagata, K., and Tanokura, M. (2005) Preliminary X-ray crystallographic analysis of thermolysin in the presence of 4 M NaCl. *Acta Cryst*. **D61**, 710–712
104. Inouye, K., Mazda, N., and Kubo, M. (1998) Need for aromatic residue at position 115 for proteolytic activity found by site-directed mutagenesis of tryptophan 115 in thermolysin. *Biosci. Biotechnol. Biochem.* **62**, 798–800
105. Kurisu, G., Sugimoto, A., Harada, S., Takagi, M., Imanaka, T., and Kai, Y. (1997) Characterization of a small metalloprotease from *Streptomyces caespitosus* with high specificity to aromatic residues. *J. Ferment. Bioeng.* **83**, 590–592
106. Inouye, K., Shimada, T., and Yasukawa, K. (2007) Effects of neutral salts and alcohols on the activity of *Streptomyces caespitosus* neutral protease. *J. Biochem.* **142**, 317–324
107. Kurisu, G., Kinoshita, T., Sugimoto, A., Nagara, A., Kai, Y., Kasai, N., and Harada, S. (1997) Structure of the zinc endoprotease from *Streptomyces caespitosus*. *J. Biochem.* **121**, 304–308
108. Nozaki, Y. and Tanford, C. (1971) The solubility of amino acids and two glycine peptides in aqueous ethanol and dioxane solutions. Establishment of a

hydrophobicity scale. *J. Biol. Chem.* **246**, 2211–2217

109. Fersht, A. (1985) *Enzyme Structure and Mechanism, 2nd edn.*, pp. 311–346, Freeman, New York

Acknowledgements

Firstly, I would like to express my sincere gratitude to Dr. Kuniyo Inouye, Professor Emeritus of Kyoto University, for his highly credible and excellent guidance in my study.

I would like to thank Dr. Kiyoshi Yasukawa, Professor of Kyoto University, for his guidance, help, and encouragement.

I would like to thank Dr. Teisuke Takita, Assistant Professor of Kyoto University, for his helpful discussion, and encouragement.

I would like to thank Dr. Tohru Fushiki, Professor of Kyoto University, for giving me an excellent opportunity to research.

I would like to thank Dr. Satoshi Tsuzuki, Assistant Professor of Kyoto University, for his technical advice and polite guidance.

I would also like to thank all members of Laboratory of Enzyme Chemistry for their helpful advice, support, and encouragement.

Lastly, I am deeply grateful to my family for their continuous support and encouragement.

August 2014

KENJI KOJIMA

List of publications

Original papers

1. Kojima, K., Tsuzuki, S., Fushiki, T., and Inouye, K. (2008) Roles of functional and structural domains of hepatocyte growth factor activator inhibitor type 1 in the inhibition of matriptase. *J. Biol. Chem.* **283**, 2478–2487
2. Kojima, K., Tsuzuki, S., Fushiki, T., and Inouye, K. (2009) Role of the stem domain of matriptase in the interaction with its physiological inhibitor, hepatocyte growth factor activator inhibitor type 1. *J. Biochem.* **145**, 783–790
3. Kojima, K., Tsuzuki, S., Fushiki, T., and Inouye, K. (2009) The activity of a type II transmembrane serine protease, matirptase, is dependent solely on the catalytic domain. *Biosci. Biotechnol. Biochem.* **73**, 454–456
4. Kojima, K., Nakata, H., and Inouye, K. (2014) Involvement of Val315 located in the C-terminal region of thermolysin in its expression in *Escherichia coli* and its thermal stability. *Biochim. Biophys. Acta* **1844**, 330–338
5. Kojima, K., Date, A., and Inouye, K. Role of Leu202, a residue located at the S_1' subsite of thermolysin, on its substrate specificity. *J. Biochem., in revision*

Related papers and review

1. Kojima, K. and Inouye, K. (2011) Activation of matriptase zymogen. *J. Biochem.* **150**, 123–125
2. Inouye, K., Tsuzuki, S., Yasumoto, M., Kojima, K., Mochida, S., and Fushiki, T. (2010) Identification of the matriptase second CUB domain as the secondary site for interaction with hepatocyte growth factor activator inhibitor type-1. *J. Biol.*

Chem. **285**, 33394–33403

3. Inouye, K., Tomoishi, M., Yasumoto, M., Miyake, Y., Kojima, K., Tsuzuki, S., and Fushiki, T. (2013) Roles of CUB and LDL receptor class A domain repeats of a transmembrane serine protease matriptase in its zymogen activation. *J. Biochem.* **153**, 51–61

Other publications

1. Daba, T., Kojima, K., and Inouye, K. (2012) Characterization and solvent engineering of wheat β-amylase for enhancing its activity and stability. *Enzyme Microb. Technol.* **51**, 245–251
2. Daba, T., Kojima, K., and Inouye, K. (2013) Kinetic and thermodynamic analysis of the inhibitory effects of maltose, glucose, and related carbohydrates on wheat β-amylase. *Enzyme Microb. Technol.* **52**, 251–257
3. Daba, T., Kojima, K., and Inouye, K. (2013) Interaction of wheat β-amylase with maltose and glucose as examined by fluorescence. *J. Biochem.* **154**, 85–92
4. Daba, T., Kojima, K., and Inouye, K. (2013) Chemical modification of wheat β-amylase by trinitrobenzensulfonic acid, methoxypolyethylene glycol, and glutaraldehyde to improve its thermal stability and activity. *Enzyme Microb. Technol.* **53**, 420–426